POLITECNICO DI TORINO

Master's Degree Program in Environmental and Land Engineering

Specialization: Climate Change

Master's Thesis

Ecological and hydromorphological analyses supporting the restoration of the Sot river, Valencian Community, Spain

Supervisors:
prof. Paolo Vezza
prof. Guillermo Palau Salvador
prof. Ignacio Díez Torrijos

Candidate:
Ginevra Apis

Academic Year 2025-2026

Summary

Mediterranean river systems are highly dynamic environments subjected to multiple anthropogenic pressures and an increasing frequency of extreme hydrological events, making river restoration a key component of contemporary water management strategies. This study focuses on the Río Sot (Sot de Chera, Spain) following the 2024 DANA flood event, with the aim of providing technical and scientific information to support future restoration actions and participatory decision-making processes.

The research is structured around three main components: (I) water quality assessment based on historical datasets and field campaigns conducted before and after the event; (II) analysis of riparian vegetation recolonisation patterns through spatial mapping; and (III) hydrological and spatial assessment integrating 2D hydraulic modelling with an evaluation of the interaction between the updated floodplain extent and agricultural land use.

Water quality analysis indicates overall stability in the long-term historical dataset. Localised anthropogenic pressures within the urban area are associated with increased concentrations of ammonium and nitrites, suggesting the influence of wastewater inputs on local water quality conditions. A background nutrient load, particularly in terms of nitrates, is also present and is likely related to agricultural activities within the catchment. Although the absence of summer field measurements limits a robust assessment of seasonal variability, historical data suggest minor seasonal fluctuations in selected parameters, particularly total coliform concentrations.

Riparian vegetation shows a progressive but heterogeneous recolonisation of the river corridor following the flood event. Native species are gradually re-establishing along the channel, although their distribution is spatially uneven, partly influenced by ongoing post-flood infrastructural works in the upstream sector. In this context, *Arundo donax* represents a key ecological concern: although already present prior to the event, it is currently more abundant in the downstream reaches, while in upstream areas it remains less dominant but locally competitive with native vegetation, potentially limiting their establishment.

The hydrological and spatial analysis shows a significant enlargement of the public river domain compared to previous delineations, resulting in increased exposure of agricultural parcels and a consequent redefinition of land-use constraints within the floodplain. The 2D hydraulic modelling further indicates that the low-level ford crossings are hydraulically critical already under the 60 m^3/s MCO scenario, where overtopping occurs and a relevant part of the discharge is conveyed over the road surface. Under the extreme 358 m^3/s scenario, maximum simulated water depths and velocities reach 5.49 m and 7.70 m/s, respectively. All ford crossings are overtopped, and the two pedestrian footbridges are exceeded by the

computed maximum water levels, whereas the main road bridge remains above the simulated water surface.

Overall, the results highlight how extreme flood events reshape fluvial environments by triggering complex ecological recovery processes and modifying hydrological space, often in tension with local socio-economic activities.

Within this context, the study contributes to the EU project RIVIVE, which promotes the integration of riverscape conviviality concepts into inclusive and socially equitable river restoration strategies. The datasets and methodologies developed provide a robust scientific basis to support participatory governance processes, including Riparian Assemblies.

Table of Contents

List of Figures 5

List of Tables 9

1 Introduction 10

2 Study area 13
2.1 Physical setting . . . 13
2.2 Hydrological setting . . . 14
2.3 Ecological Context . . . 19
2.4 Socioeconomic Context . . . 21
2.5 The 2024 DANA Event . . . 25

3 Materials and Methods 33
3.1 Water Quality Analyses . . . 33
3.1.1 Historical Data . . . 33
3.1.2 Field Data . . . 39
3.2 Riparian Vegetation . . . 45
3.2.1 Survey methodology and considered species . . . 45
3.2.2 GIS processing and spatial analysis . . . 48
3.3 Hydrodynamic simulation and spatial exposure . . . 49
3.3.1 2D Hydraulic modelling . . . 49
3.3.2 Spatial analysis of agricultural parcels . . . 54

4 Results 58
4.1 Water Quality Results . . . 58
4.1.1 Annual historical analysis . . . 58
4.1.2 Field Monitoring data . . . 64
4.1.3 Comparison between field monitoring data and historical data 73
4.2 Riparian Vegetation . . . 77
4.2.1 Arboreal vegetation: Populus spp. . . . 77

4.2.2 Shrub layer: Nerium oleander and Tamarix spp. 79
4.2.3 Arundo donax distribution 82
4.2.4 Summary of spatial patterns 86
4.3 Hydrodynamic simulation and spatial exposure 88
4.3.1 2D Hydraulic modelling 88
4.3.2 Spatial analysis of agricultural parcels 97

5 Discussion 103
5.1 Water quality dynamics and anthropogenic pressures 103
5.2 Riparian vegetation recovery and invasive species dynamics 105
5.3 Hydraulic risk and river corridor management 109
5.4 The role of technical-scientific data in participatory processes 110

6 Conclusion 114
6.1 Concluding remarks 114
6.2 Limitations and future perspectives 115

Appendices 116

A Annual historical water quality data 118

B Seasonal Water Quality Plots 126

C Field monitoring data 131

D Comparison between field monitoring data and historical data 138

E Riparian Vegetation 141

Bibliography 145

List of Figures

2.1 Overview of Las Toscas spring 14
2.2 Rio Sot valley-Topography 14
2.3 Regional geographic and hydrological setting of the study area . . . 15
2.4 Overview of the Buseo dam 16
2.5 Detailed map of the studied Río Sot river reach 17
2.6 Boundaries of the Chera–Sot de Chera Natural Park 19
2.7 Overview of Sot de Chera.-Autumn 2025. 22
2.8 Recreational use and river bathing activities at Charco Gruñidor . . 23
2.9 Agricultural land use and parcel distribution along the river channel 24
2.10 Spatial distribution of cumulative rainfall during the DANA event . 26
2.11 Geographical overview of the main municipalities affected by the DANA 27
2.12 Hydrological and macro-geomorphological response of the Río Sot catchment 31
2.13 Fluvial impacts and systemic environmental damage in Sot de Chera 32

3.1 Temporal availability of water quality data. 36
3.2 Spatial distribution of sampling points. 40
3.3 Instrumentation used for field data collection 43
3.4 Details of multi-parameters test strip bottle. 44
3.5 Ammonia liquid kit. 44
3.6 Use of binoculars for remote observation of riparian vegetation. . . 46
3.7 First steel pedestrian bridge: field condition and DTM integration. . 51
3.8 Road bridge: field condition and DTM integration. 51
3.9 Main ford: field condition and 2D model implementation. 52
3.10 Second steel pedestrian bridge: field condition and DTM integration. 52
3.11 Spatial distribution of the regulatory zones in Sot de Chera. 56

4.1 Microbiological parameter concentrations at the Río Sot 59
4.2 Annual historical boxplots of Nitrities and Total Chlorine. 60

4.3 Interannual evolution and historical trends of Water Temperature, COD, and BOD_5 . . . 62
4.4 Seasonal boxplots of hydrochemical and microbiological parameters exhibiting statistically significant differences between cold and hot periods- water T and pH. . . . 65
4.4 Seasonal boxplots of hydrochemical and microbiological parameters exhibiting statistically significant differences between cold and hot periods-Total coliforms. . . . 66
4.5 Longitudinal trends of Nitrates in Autumn and Spring. . . . 69
4.6 Longitudinal trends of Nitrites in Autumn and Spring . . . 70
4.7 Longitudinal trends of Ammonia in Autumn and Spring. . . . 71
4.8 Longitudinal trends of Electrical Conductivity (EC) in Autumn and Spring. . . . 72
4.9 Longitudinal trends of nitrate concentrations during autumn and spring compared with the respective seasonal boxplots. . . . 74
4.10 Longitudinal trends of Total Chlorine concentrations during autumn and spring compared with the respective seasonal boxplots. . . . 75
4.11 Longitudinal trends of Electrical Conductivity during autumn and spring compared with the respective seasonal boxplots. . . . 76
4.12 Examples of Poplars dynamics along the Río Sot. . . . 78
4.13 Spatial distribution of Poplars along the Rio Sot, November-December 2025. . . . 79
4.14 Examples of shrub dynamics along the Río Sot . . . 80
4.15 Spatial distribution of emergent aquatic vegetation along the Rio Sot, November-December 2025. . . . 81
4.16 Examples of emergent aquatic vegetation along the Río Sot . . . 82
4.17 Example of co-occurrence and spatial segregation of *Phragmites australis* and *Arundo donax* on a fluvial bar. . . . 83
4.18 Examples of *Arundo donax* distribution along the Río Sot. . . . 84
4.19 Mapping of *Arundo donax* along the Rio Sot, November-December 2025. . . . 85
4.20 Road restoration works-Sot de Chera. . . . 87
4.21 Hydrodynamic simulation results for the base flow scenario (1 m^3/s). Depth and flow velocity maps. . . . 89
4.22 Hydrodynamic simulation results for the ordinary high flow scenario (60 m^3/s): depth and flow velocity maps. . . . 90
4.23 Detailed views of the flow velocity field during the 60 m^3/s scenario. 91
4.24 Stage and flow hydrographs for the three ford structures during the 60 m^3/s ordinary high flow scenario. . . . 92
4.25 Hydrodynamic simulation results for the extreme flood scenario (358 m^3/s): depth and flow velocity maps. . . . 94

4.26 Detailed views of the maximum water depth during the 358 m^3/s extreme flood scenario. 95
4.27 Stage and flow hydrographs for the three ford structures during the 358 m^3/s extreme flow scenario. 96
4.28 Pre vs post DANA HPD boundaries. 97
4.29 Cadastral parcels exposure inside current DPH. 99
4.30 Cadastral parcels exposure inside current Easement zone. 100
4.31 Cadastral parcels exposure inside current Police zone. 101
4.32 Cadastral parcels exposure inside total current regulatory framework. 102

5.1 Invasion mechanics and localised management of *Arundo donax* . . 108
5.2 Participatory assemblies in Sot de Chera: collaborative mapping and expert-guided community dialogue. 112
5.3 Participatory assemblies in Sot de Chera: data presentation and community rehabilitation sketch. 113

6.1 Recent post-flood recovery interventions and nature-based bioengineering works implemented within the urban reach of Sot de Chera. 117

A.1 Annual distributions of core physical and chemical baseline parameters. 119
A.2 Annual trends for chlorine compounds and dissolved oxygen saturation. 120
A.3 Annual concentrations of nitrogen-based nutrient parameters. 121
A.4 Annual concentrations of phosphates and macro-indicators of organic pollution. 122
A.5 Annual trends for microbiological indicators and water colouration. 123
A.6 Annual concentrations of total suspended solids, iron, and copper. . 124
A.7 Annual concentrations of specific trace pollutants and agrochemicals. 125

B.1 Seasonal distributions of physical and chemical baseline parameters. 126
B.2 Seasonal concentrations of nutrient parameters. 127
B.3 Seasonal concentrations of organic pollution indicators. 128
B.4 Seasonal trends for microbiological parameters, suspended solids, and colour. 129
B.5 Seasonal concentrations of heavy metals, trace elements, and specific pollutants. 130

C.1 Seasonal longitudinal concentrations of nutrients (nitrogen species) along the river sector: comparison between Autumn 2025 and Spring 2026 campaigns. 132
C.2 Seasonal longitudinal data of pH and carbonate system parameters (KH and Total Alkalinity) along the river sector: comparison between Autumn 2025 and Spring 2026 campaigns. 133

C.3 Seasonal longitudinal data for physical and mineralization parameters: Electrical Conductivity (EC), Total Dissolved Solids (TDS), Total Hardness (GH), and Water Temperature (T) across Autumn 2025 and Spring 2026 campaigns. 134
C.4 Longitudinal concentration trends of heavy metals (Chromium VI, Iron, and Copper) along the river sector: comparison between Autumn 2025 and Spring 2026 campaigns. 135
C.5 Longitudinal concentration datasets for halogen species (Part 1: Free and Total Chlorine) along the river sector: comparison between Autumn 2025 and Spring 2026 campaigns. 136
C.6 Longitudinal concentration datasets for halogen species (Part 2: Fluoride and Bromine) along the river sector: comparison between Autumn 2025 and Spring 2026 campaigns. 137

D.1 Seasonal longitudinal trends of primary nutrient indicators (Nitrites and Ammonium) along the river sector, Autumn vs Spring. 139
D.2 Seasonal longitudinal trends of secondary hydrochemical indicators (pH, Water Temperature, and Total Chlorine) along the river sector, Autumn vs Spring 140

E.1 Spatial distribution of riparian poplar species (*Populus* spp.) along the Rio Sot in the municipal area of Sot de Chera, November-December 2025. 142
E.2 Spatial distribution of shrub riparian species along the Rio Sot in the municipal area of Sot de Chera, November-December 2025. . . . 143
E.3 Spatial distribution of *Phragmites australis* along the Rio Sot in the municipal area of Sot de Chera, November-December 2025. 144

List of Tables

2.1 Anthropogenic pressures and impacts identified for the Río Sot water body 23

3.1 Water quailty parameters-Rio sot 34
3.2 Summary of water quality data characteristics 35
3.3 Regulatory water quality thresholds and sources. 37
3.4 Temporal subdivision of the data. 38
3.5 Summary of measured water quality parameters, field instrumentation and resolution. 42
3.6 Target riparian species. 46

4.1 Seasonal Mann-Kendall trend analysis results for Temperature, COD, and BOD_5. 61
4.2 Summary of CHJ JUH403 monitoring parameters showing statistically significant seasonal differences- Mann–Whitney U test. 66
4.3 Cadastral metrics for the current hydraulic regulation zones. 98
4.4 Comparative distribution of DPH exposure classes (Pre vs Post-DANA) 98

Chapter 1

Introduction

River ecosystems rank among the most vulnerable environments worldwide, being heavily exposed to anthropogenic activities that fundamentally alter their structural integrity, ecological functioning, and capacity to deliver essential ecosystem services [1].

Within this global framework, the European continent represents a highly pressured region. According to the latest "State of Water" report by the European Environment Agency [2], only approximately 40% of European surface waters currently achieve the "good" or "high" ecological status required by the Water Framework Directive (WFD). The primary stressors compromising river networks include diffuse pollution, driven by agricultural runoff, and point-source discharges, originating from industrial facilities and urban wastewater treatment plants. Furthermore, structural interventions such as dam construction, channelization, and land drainage heavily disrupt natural hydromorphology, while water abstraction for irrigation and municipal supply severely depletes baseline flows. Cumulatively, these anthropogenic drivers degrade physical habitats, depress local biodiversity, and impair the overall provision of ecosystem services across European catchments [3, 4]).

In the European landscape, Mediterranean river basins are exceptionally susceptible to these dynamics. The combination of long-term human pressures, natural water scarcity, and strong hydro-climatic variability makes these systems particularly vulnerable to hydrological stress and ecological degradation [5]. (This inherent vulnerability is further exacerbated by anthropogenic climate change. According to the Intergovernmental Panel on Climate Change (IPCC), the Mediterranean region is expected to undergo significant climatic changes, including shifts in precipitation patterns, rising temperatures, and changes in runoff regimes. These changes are likely to intensify existing environmental pressures and enhance the mobilization and transport of pollutants within river catchments [6]. These trends are already materializing across Mediterranean catchments through an increasing frequency of

extreme hydrometeorological events, as demonstrated by the October 2024 DANA that severely impacted eastern Spain.

In this context, river restoration has emerged as a fundamental strategy to rehabilitate watercourses and enhance their resilience. The European Union's Biodiversity Strategy for 2030 identifies the restoration of freshwater ecosystems as a key objective for reversing biodiversity loss, while the Nature Restoration Law establishes legally binding targets for the recovery of degraded ecosystems, including rivers and floodplains [7, 8]. Rather than relying on isolated and localised interventions, river restoration increasingly adopts a holistic perspective that acknowledges the complexity of river systems. Its efforts aim to recover the overall functioning of the fluvial system by simultaneously addressing channel morphology, flow regimes, water quality, and longitudinal and lateral ecological connectivity [9, 10]. While historically river restoration has been guided primarily by engineering-based and top-down approaches, contemporary water management recognizes that sustainable ecological recovery cannot be achieved without integrating the human dimension[11, 12, 13]. This paradigm shift is reflected in the concept of riverscape conviviality, a socio-ecological framework developed within the RIVIVE project [14]. The concept envisions river corridors not only as functional hydraulic infrastructure or strictly segregated conservation zones, but also as dynamic socio-ecological landscapes where human and natural processes interweave.

RIVIVE (Restoring riverscapes in the Mediterranean) is a research project supported by the European Biodiversity Partnership (Biodiversa+ [15]), specifically designed to address the severe degradation of Mediterranean river ecosystems. By bridging the gap between natural and social sciences, the project combines physical and ecological rehabilitation with social innovation, holding the concept of riverscape conviviality at its core.

To put this vision into practice, RIVIVE works closely with local communities through citizen science activities and participatory governance processes. The project has established a series of Living Labs across the Mediterranean, that provide spaces for collaboration among researchers, public authorities, and local stakeholders in the design and evaluation of river restoration strategies. One of the places involved in this project is Sot de Chera, a small municipality in the Valencian Community that was heavily impacted by the DANA in October 2024. A core mechanism of RIVIVE's participatory approach is the establishment of River Assemblies (*Asambleas del Río*).

In the municipality of Sot de Chera, these assemblies act as horizontal governance platforms that bring together different stakeholders, including local residents, agricultural landowners, public administrators, and academic researchers. These forums provide a collaborative space to discuss the state of the Río Sot, address land-use conflicts, and co-design sustainable management strategies.

However, for these participatory processes to succeed, they must be grounded

in reliable technical and scientific data that are translated into accessible formats to support decision-making and a shared understanding of the river system and its management challenges.

Recognizing this need, the primary objective of this thesis is to generate and synthesize multidisciplinary data to support and inform the *Asambleas del Río* in Sot de Chera. By turning complex eco-hydrological and spatial information into accessible knowledge, this work aims to provide a common evidence base for decision-making in the post-DANA recovery phase.

To achieve this goal, the research is structured around three specific sub-objectives, addressing key challenges of the Río Sot corridor:

- Water quality assessment: This objective focuses on evaluating the spatial and seasonal hydrochemical dynamics of the river by integrating long-term historical basin datasets with high-resolution field monitoring campaigns conducted between Autumn 2025 and Spring 2026. The aim is to identify potential anthropogenic pressures, point-source pollution inputs, and post-flood disturbances.

- Riparian vegetation mapping: This objective examines the early stages of post-flood ecological succession along the active channel, focusing on the recolonization patterns of native pioneer species and on the spatial expansion of the invasive giant reed (*Arundo donax*).

- Hydrodynamic modelling: This objective aims to characterize the kinematic and spatial behaviour of the river through high-resolution two-dimensional simulations. By routing different flow scenarios ranging from ordinary flows up to the extreme 358 m^3/s peak. The analysis assesses flood dynamics, inundation extents, and the hydraulic resilience of the new river crossing infrastructures.

- Spatial analysis of hydraulic and land-use conflicts: This objective assesses the impact of post-DANA geomorphological changes on the local cadastral framework. By intersecting the updated boundaries of the Hydraulic Public Domain (DPH) and its protection zones with agricultural parcels in Sot de Chera, it provides a spatial basis for understanding new regulatory constraints and supporting land-use conflict resolution.

Chapter 2

Study area

2.1 Physical Setting

Sot de Chera is a Spanish municipality located in the inland northern sector of the Valencia province, within the comarca of Los Serranos [16].

The local climate is classified as continental Mediterranean to semi-arid, characterized by hot, dry summers and highly concentrated, torrential precipitation events during autumn and spring [17]. Total annual rainfall ranges between approximately 500 mm and 600 mm [18].

From a geological perspective, the regional framework is mainly composed of Jurassic and Cretaceous carbonate formations, predominantly limestones and dolostones. The alternation between permeable carbonate units and less permeable marly layers controls the hydrogeological behaviour of the area, favouring rapid infiltration and subsurface flow. Groundwater circulation is largely guided by fractures and faults, leading to the emergence of numerous springs along structural discontinuities. In some cases, these discharges give rise to travertine-forming springs, such as Las Toscas, a vauclusian-type spring located around seven kilometres downstream from the village of Sot de Chera. These features reflect the complex interaction between karst groundwater circulation and surface water dynamics within the Río Sot catchment [19].

The topography of the area is rugged and steep, defined by sharp mountain ridges with elevations ranging between 500 m and 1000 m above sea level, interspersed with narrow valleys and deep gorges (*gargantas* or *barrancos*). This structural setting forms a 400 m deep canyon inside which the urban settlement of Sot de Chera is situated [20]. This steep geomorphological conformation induces high hydraulic gradients, significantly accelerating catchment concentration times (t_c) and enhancing flash-flood vulnerability along the valley floor.

Figure 2.1: Overview of Las Toscas spring. Picture taken in Autumn 2025.

Figure 2.2: Overview of the Río Sot (Río Reatillo) valley, showing the steep mountain topography and the natural confinement of the river channel. Picture taken in Summer 2025.

2.2 Hydrological setting

From a macro-regional perspective, the study area is located within the Júcar River Basin District (*Demarcación Hidrográfica del Júcar* - DHJ), under the administrative jurisdiction of the *Confederación Hidrográfica del Júcar* (CHJ). The local hydrographic network ultimately drains toward the Turia River system (see Figure 2.3).

The main drainage element of the study area is the Río Sot (also referred to as Río Reatillo) sub-basin, which covers approximately 252.49 km^2 and is enclosed within the mountainous framework of the Chera–Sot de Chera Natural Park. Runoff generated within the catchment is conveyed along the main valley floor into the

Buseo reservoir (*Embalse de Buseo*) and subsequently toward the confluence with the Turia River [21].

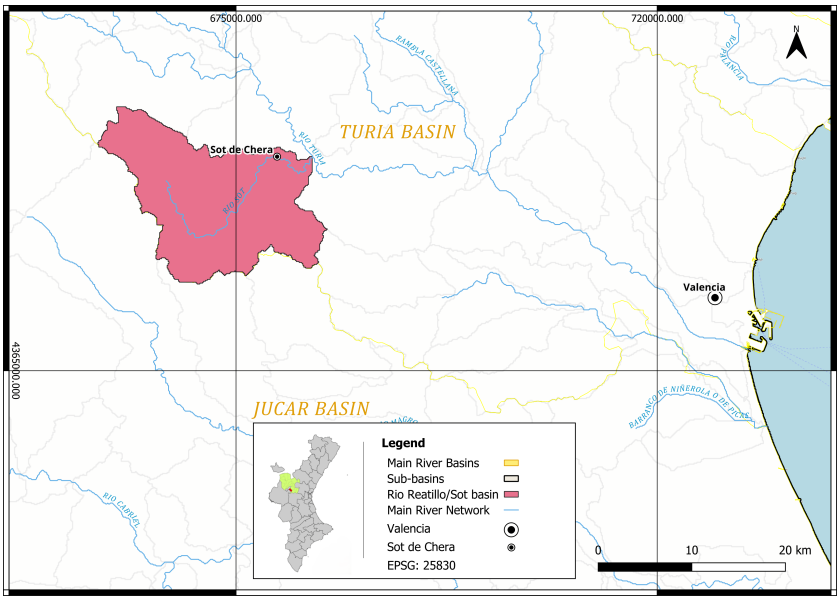

Figure 2.3: Geographical and hydrological setting of the study area. The map illustrates the location of Sot de Chera and the Río Reatillo/Sot sub-basin (highlighted in pink) relative to the macro-regional Turia and Júcar river basins. The main river network is defined according to Article 3 of the Water Framework Directive (WFD). Coordinate system: ETRS89 / UTM zone 30N.

The analysed river reach, approximately 13 km in length, extends from the Buseo dam upstream to the confluence with the Turia River downstream (see Figure 2.5). The Buseo dam (Figure 2.4) is a gravity structure with a storage capacity of 8 hm^3 [22], located within a narrow limestone gorge. It is the oldest dam built in the Turia basin and was originally designed for flow regulation, although its current operational role is limited. Following the extreme meteoric event of the October 2024 DANA, strict precautionary operational restrictions were implemented due to structural safety concerns; consequently, the reservoir is currently maintained at significantly reduced storage levels as a passive risk mitigation measure [23].

The hydrological regime of the study reach is strongly controlled by this upstream reservoir. In addition to flow regulation, the Buseo impoundment influence sediment continuity and downstream water quality through trapping processes and internal biogeochemical cycling. As a result, both discharge dynamics and physicochemical conditions in the Río Sot are structurally dependent on reservoir operations and upstream catchment transport dynamics.

The catchment is characterized by a dense network of ephemeral tributaries

Figure 2.4: Overview of the Buseo dam, a gravity structure located within a narrow limestone gorge upstream of the studied reach. It represents the upstream regulation element of the Río Sot hydrographic system. Photo taken prior to the 2024 DANA event [24].

(*barrancos*). These channels enhance hydrological connectivity by rapidly conveying high volumes of runoff and hillslope sediment toward the main channel, increasing the flash-flood responsiveness of the entire fluvial system.

According to the regional River Basin Management Plan [18], the water body is classified as a permanent natural river belonging to the ecotype *"ríos mineralizados de baja montaña mediterránea"* (Low-altitude Mediterranean mineralized rivers). Historical records from the Spanish National Flow Gauging Yearbook indicate a mean discharge of 0.35 m^3/s for the baseline period 1945–1966 [25], while the minimum ecological flow is currently established by administrative regulations at 0.01 m^3/s.

The hydromorphological and physical-chemical statuses are officially classified as Good and Very Good respectively, both assigned with a low level of confidence due to data scarcity in the secondary monitoring network. The main pressures impacting the channel network can be summarized as follows:

- **Hydromorphological alterations:** presence of small anthropogenic structures (weirs, culverts, and bridges inducing local backwater effects) and localised channelization, combined with the historical occupation and reduction of riparian margins.
- **Flow regulation:** altered discharge and hydrograph regime due to the presence of the Buseo reservoir and its associated hydraulic management.
- **Water abstractions:** seasonal irrigation withdrawals for agricultural use, which deplete low-flow conditions during summer months.

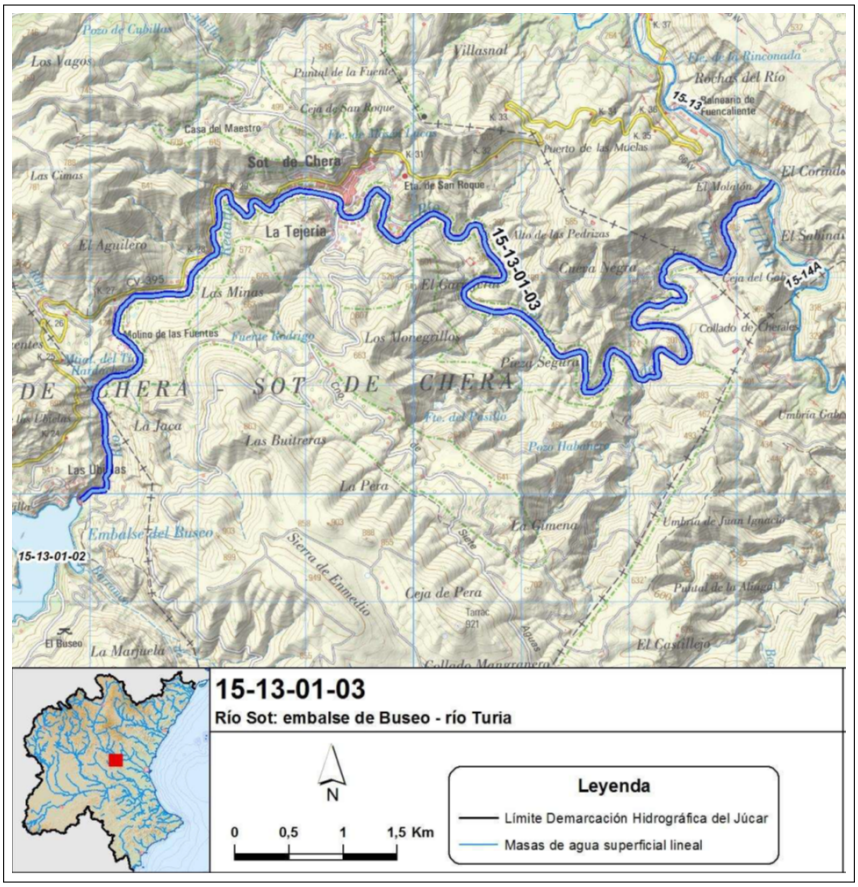

Figure 2.5: Detailed view of the studied river reach (Water Body ID: ES080MSPF15130103, "Río Sot: embalse de Buseo - río Turia"). The map highlights the approximately 13 km fluvial corridor extending from the Buseo dam upstream, passing through the urban settlement of Sot de Chera, down to the confluence with the Turia River downstream. Topographic relief and official hydrographic boundaries are shown (source: Plan hidrológico cuenca. Ciclo 2022-2027 [18]).

- **Diffuse and point-source pollution:** nutrient inputs (mainly nitrogen compounds) derived from agricultural land use and occasional unauthorized wastewater discharges. Consequently, the area has been officially designated as a Nitrate Vulnerable Zone (NVZ) for surface and groundwater bodies under regional environmental legislation [26].

To address these environmental pressures, the Basin authority's (CHJ) 2022–2027 programme of measures includes: (i) strict monitoring of environmental flow compliance downstream of hydraulic structures, (ii) ecomorphological restoration

of riparian and fluvial spaces, focusing on native vegetation recovery and channel substrate stabilization, (iii) legal regulation and metering of water abstractions to ensure strict compliance with existing concessions, and (iv) periodic biological and chemical monitoring of recreational bathing waters within the municipal reach.

2.3 Ecological Context

The study area is located within the Chera–Sot de Chera Natural Park, a protected area covering approximately 6,451 ha. The park is part of the Natura 2000 Network and includes the Special Area of Conservation (SAC) Sierra Negrete and the associated Special Protection Area (SPA), designated for the conservation of habitats and species of Community interest [19] (Figure 2.6). The park is characterized by a high diversity of habitats resulting from the interaction between its complex topography, Mediterranean climate, and fluvial systems.

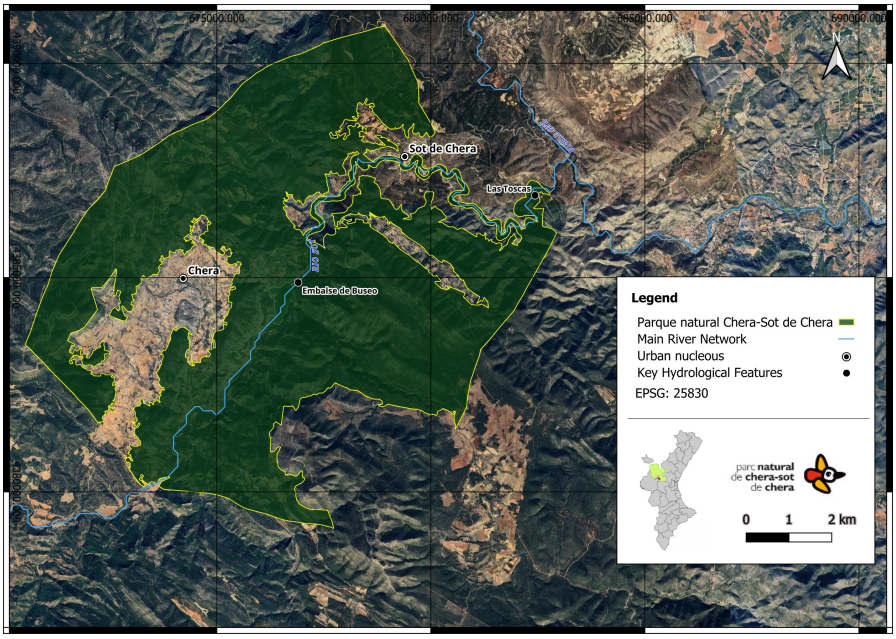

Figure 2.6: Geographical boundaries and extension of the Chera–Sot de Chera Natural Park (shaded in green). The map contextualizes the protected area within the rugged regional topography, highlighting the main river network, the location of the urban nuclei, and key hydrological landmarks including the Buseo dam and Las Toscas spring (source: boundary data from Generalitat Valenciana; basemap: Google Satellite; elaborated by the author). Coordinate system: ETRS89 / UTM zone 30N.

From a faunal perspective, the official management data for the protected area registers a total of 20 species of Community interest within the combined SAC and SPA framework [19]. Among these, cliff-dwelling raptors are of particular management importance, including the vulnerable Bonelli's eagle (*Aquila fasciata*), as well as fauna closely associated with the Río Sot riparian corridor, which provides suitable habitat for endemic amphibians and protected mammals such as

the Eurasian otter (*Lutra lutra*).

With respect to flora, terrestrial ecosystems are dominated by Mediterranean forests and scrublands, including holm oak (*Quercus ilex*) woodlands, Portuguese oak (*Quercus faginea*) stands, juniper formations (*Juniperus* spp.), and boxwood communities (*Buxus sempervirens*) occurring on rocky slopes and limestone outcrops. The floristic value of the area is further enhanced by the presence of several Iberian endemic species and plant communities characteristic of eastern Spain.

Among the habitats of Community interest listed under the Habitats Directive (92/43/EEC) [27], the park hosts well-preserved riparian gallery forests dominated by white poplar (*Populus alba*), black poplar (*Populus nigra*), willow species (*Salix* spp.), and elm (*Ulmus minor*). Other notable habitats include oleander galleries (*Nerium oleander*), yew forests (*Taxus baccata*), juniper woodlands, and petrifying springs associated with carbonate-rich groundwater emergence. These habitats contribute significantly to the ecological integrity of the protected area and support a wide range of plant and animal species.

The Río Sot and its associated riparian corridor represent a key ecological component of the study area, due to the concentration of hydrophilic habitats and the close interaction between fluvial processes and vegetation dynamics. Along the riverbanks and within narrow ravines, riparian gallery forests composed of *Populus alba*, *Populus nigra*, *Salix alba*, and *Ulmus minor* are present, together with shrub communities including oleander (*Nerium oleander*), hawthorn (*Crataegus monogyna*), and other species adapted to periodically disturbed and flood-prone environments. Emergent aquatic vegetation, such as cattails (*Typha latifolia*) and common reed (*Phragmites australis*), occupies shallow, slow-flowing, and low-energy sections of the channel.

Beyond their ecological role, these riparian communities provide important eco-hydrological functions. Root systems contribute to bank stabilization and reduce erosion processes, while vegetation increases channel roughness and influences flow resistance, particularly during ordinary and moderate flood events [28]. Riparian forests also enhance landscape connectivity by acting as biological corridors between different habitats. Aquatic and emergent vegetation further contribute to sediment trapping and nutrient uptake, while providing habitat, shelter, and food resources for a wide range of aquatic and semi-aquatic organisms.

The structure and dynamics of these native communities are closely linked to the natural disturbance regime of Mediterranean flash-flood rivers. High-magnitude flood events periodically reshape channel morphology, removing parts of the established riparian vegetation and creating new depositional surfaces available for recolonization ([28, 29]). Different riparian communities exhibit distinct responses to flood disturbance. Woody pioneer species such as *Populus* and *Salix* are associated with rapid colonization of newly formed alluvial surfaces [30, 31], while emergent macrophytes and shrub communities are able to persist or recover through

vegetative regeneration following physical disturbance [32, 5].

According to the regional River Basin Management Plan [18], the overall ecological status of the Río Sot water body is classified as Good with a high level of confidence. Nevertheless, the CHJ explicitly inventories significant pressures linked to the presence of allochthonous species, warning of an objective risk of morphological alterations affecting riverbanks caused by exotic biological invasions.

Within the study area, the giant reed (*Arundo donax*) represents the most aggressive and pervasive invasive alien species affecting the riparian zone. Listed among the top 100 worst invasive organisms globally [33], *A. donax* outcompetes native vegetation, leading to severe ecological and water resource management challenges. The species alters the physical, chemical, and biological properties of the colonized fluvial habitats, inducing biodiversity loss, altering natural sediment regimes, and modifying the local river microclimate [34, 29]. Furthermore, due to its exceptionally high evapotranspiration rates, *A. donax* consumes significantly more water per unit of surface area than native poplars and willows [35], severely impacting the local hydrological balance during low-flow periods.

Among the additional hazards associated with the presence of *A. donax* is the increase in wildfire risk, as it produces large amounts of biomass that, when dried, can burn easily. This represents a critical issue for a territory characterized by widespread "High" and "Very High" fire risk classifications according to the official fire prevention plan of the Natural Park [36].

While this structural inventory represents the baseline condition reported by regional authorities, the mechanical disturbance and structural destruction caused by the October 2024 DANA event have radically altered these dynamics, as discussed in detail in the following sections.

2.4 Socioeconomic Context

Sot de Chera is a small rural municipality with a permanent population of 427 inhabitants [37], characterized by strong seasonal variability due to ecotourism activities. Tourism is closely linked to the geological and hydrological features of the Natural Park, as well as to recreational river bathing areas such as the *Charco Gruñidor*. The population exhibits an aging structure, with a prominent concentration of permanent residents within the 65–74 age range [38].

The municipality is not equipped with a fully centralized wastewater treatment plant. Wastewater is managed through a simplified municipal sewerage network, with final discharge ultimately affecting the Río Sot corridor. This infrastructure was partially disrupted by the 2024 DANA event, which damaged sections of the sewer network and reduced system functionality.

Although tourism is now the main economic sector, historically, the local

Figure 2.7: Overview of Sot de Chera. Picture taken in Autumn 2025.

economy has been based on Mediterranean agriculture, which remains an important component of land use. The agricultural system includes dryland olive, almond, and carob cultivation on surrounding slopes, small irrigated orchards (*huertas*) near the urban core, and citrus plantations and citrus plantations, especially in the downstream alluvial areas, where extensive citrus cultivation is present (see Figure 2.9). The community maintains a direct dependence on the river for irrigation purposes.

This close interaction between human activities and the fluvial corridor generates a high level of spatial overlap between private land and the active river channel. Agricultural parcels frequently border the channel margins, creating a direct interface between productive land and public hydraulic space.

This strong connection with the river is not only economic but also cultural and social. In this context, the Río Sot functions as a shared space where environmental, agricultural, and social interests intersect (Figure 2.8).

The following table (Table 2.1) summarizes the main anthropogenic pressures documented along the studied river reach [39].

Figure 2.8: Recreational use and river bathing activities at the *Charco Gruñidor* pool (Sot de Chera) before the 2024 flood event. Source: *Valencia Bonita* [40].

Table 2.1: Anthropogenic pressures, drivers, and environmental impacts identified by the CHJ for the Río Sot water body [39].

Pressure Group	**Main Drivers & Activities**	**Identified Environmental Risk & Impact**
Hydromorphological Pressures	Flood protection infrastructure, check dams, bridges, and piped crossings	Alteration of habitats due to hydrological changes and longitudinal connectivity obstacles.
Biological / Ecological Pressures	Exotic biological invasions	Morphological alterations and structural degradation affecting the riverbanks.
Diffuse / Point-source Pollution	Upstream agricultural runoff and unauthorized wastewater discharges	Decline in chemical and physicochemical water quality parameters (surface nitrogen inputs).
Water Extractions / Land Use	Agricultural irrigation and urban development demands	Hydrological alterations due to water extraction and physical land occupation of the riparian margins.

(a)

(b)

Figure 2.9: Agricultural land use in Sot de Chera: (a) overview of the urban nucleus and the traditional irrigated orchards (*huertas*) directly bordering the Río Sot channel following the 2024 DANA flood; (b) satellite view of the extensive citrus plantations arranged in regular geometric patterns within the river bends downstream of the village (source: Google Satellite).

2.5 The 2024 DANA

Between 28 October and 4 November 2024, the Iberian Peninsula was affected by an episode of intense, locally torrential and persistent rainfall, associated with the presence of a Depresión Aislada en Niveles Altos (DANA) located near the Strait of Gibraltar. This configuration favoured the development of low-level pressure systems and the channeling of a strong easterly flow of moist air from the Mediterranean Sea towards the eastern part of the peninsula. The combination of these factors led to the formation of organized and quasi-stationary convective systems that particularly affected the provinces of Valencia, Cuenca, Albacete and Murcia.

The most critical day of the event was 29 October, when exceptionally intense rainfall was recorded over large areas of the Valencian inland, particularly in the Plana de Utiel-Requena, Hoya de Buñol, Ribera Alta and Los Serranos regions. According to analyses by AEMET and the Confederación Hidrográfica del Júcar (CHJ), return periods exceeding 1,000–2,000 years were reached in some areas. Daily maximum values widely exceeded 300 mm, with extreme accumulations recorded in Turís of 771.24 mm in 14 hours and maximum hourly intensities of 184.6 mm/h [41, 42].

The exceptional nature of the event is also reflected in the precipitation volumes recorded across the entire Júcar River Basin District. On 29 October alone, approximately 2400 hm^3 of water were recorded, of which more than 700 hm^3 were concentrated in the most affected sub-basins: the Barranco del Poyo (around 150 hm^3), the Magro River (over 400 hm^3), the Turia River (over 130 hm^3) and the Barranco de Picassent (around 17 hm^3). Considering the entire period from 28 October to 5 November, the total precipitation volume reached approximately 4100 hm^3, a value exceeding the total storage capacity of all reservoirs in the basin [43].

The extreme rainfall generated widespread flooding across numerous watercourses within the Júcar basin, particularly affecting the Magro, Júcar and Turia rivers, as well as the Rambla del Poyo and several smaller ravines. In many cases, discharge values reached extremely high levels, causing extensive overbank flooding and inundations over large parts of the province of Valencia.

According to the Plan para la Recuperación y Mejora de la Resiliencia frente a las Inundaciones en el Territorio Afectado por la DANA en la Comunitat Valenciana (MITECO) [43], the event had a multidimensional impact on the territory. From a human perspective, the DANA affected more than 306,000 people and caused 237 fatalities, in addition to numerous injuries and evacuations. Infrastructural damage affected road and railway networks, hydraulic infrastructure, bridges, river crossings, drainage systems and flood protection structures, in many cases compromising territorial connectivity and accessibility to settlements.

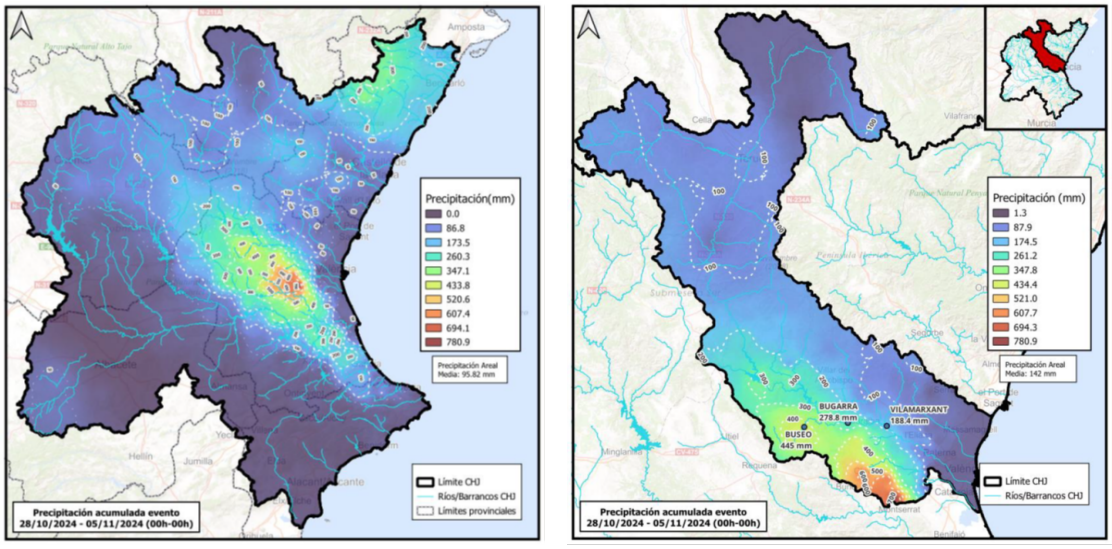

(a) **(b)**

Figure 2.10: Spatial distribution of cumulative rainfall during the DANA event from 28 October to 5 November 2024 (00:00–00:00 UTC): (a) interpolated rainfall map across the entire Júcar River Basin District (CHJ), showing an areal average precipitation (*Precipitación Areal Media*) of 95.82 mm; (b) detailed hydrological focus on the Turia River basin, indicating an areal average of 142 mm and highlighting the exceptional local accumulation recorded at the Buseo reservoir gauge station (445 mm) upstream of Sot de Chera. The colour-coded legends represent cumulative precipitation (*Precipitación*) in millimeters. Map features include the CHJ administrative boundary (*Límite CHJ*), watercourses and ravines (*Ríos/Barrancos CHJ*), and provincial limits (*Límites provinciales*) (source: Confederación Hidrográfica del Júcar [42]).

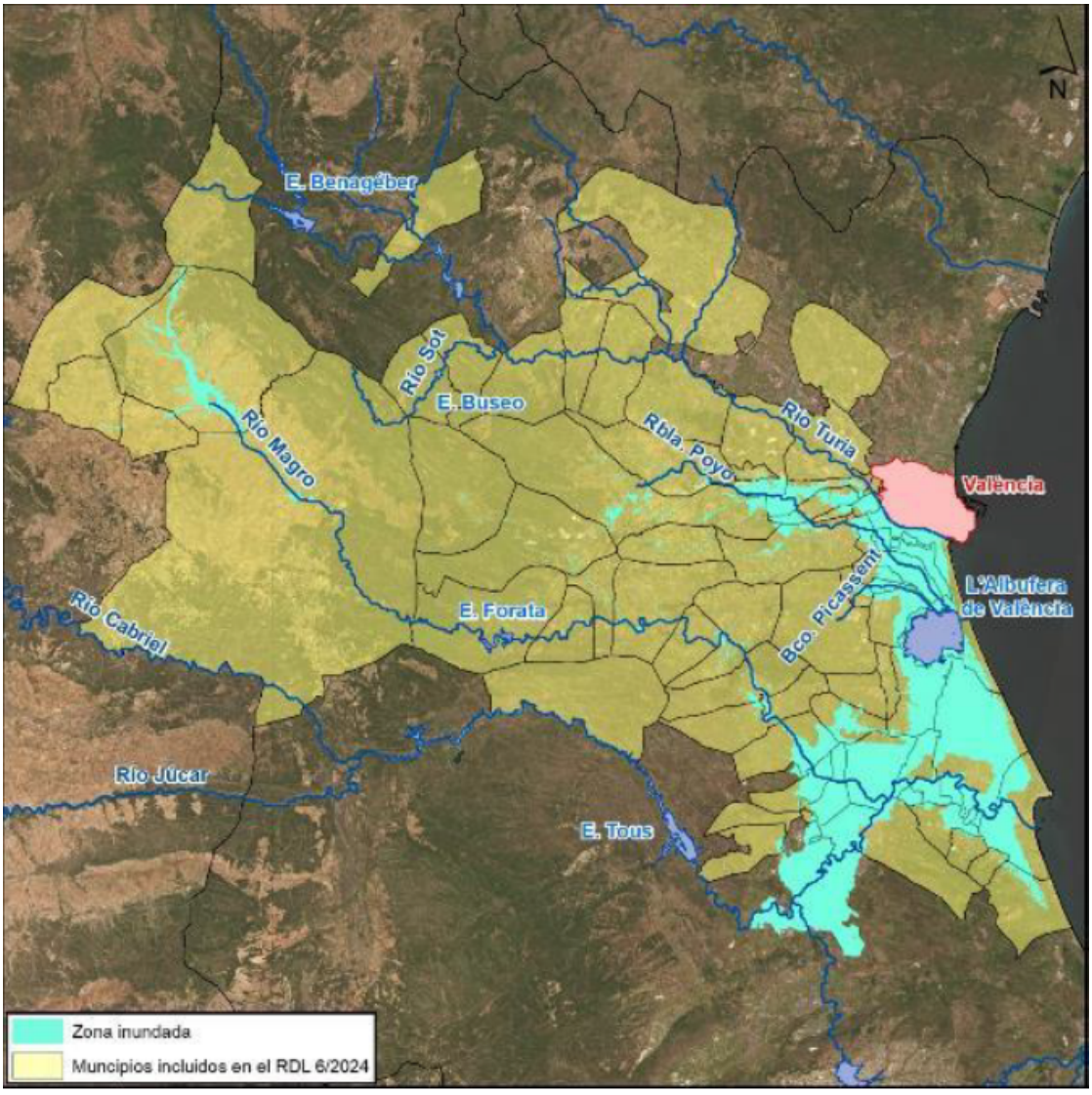

Figure 2.11: Geographical overview of the main municipalities affected by the October 2024 DANA and the delimited flooded areas within the Júcar River Basin District. The legend identifies the flooded zones (Zona inundada, highlighted in cyan) and the municipalities officially recognized as affected by the event and included in the emergency response decree (Municipios incluidos en el RDL 6/2024, highlighted in yellow). Source: Ministerio para la Transición Ecológica y el Reto Demográfico (MITECO) [43].

From an economic perspective, the event generated significant losses in the agricultural, industrial and service sectors, as well as widespread damage to residential and commercial buildings. According to the Cámara de Comercio de Valencia, estimated direct economic losses in the affected municipalities exceed 13 billion euros [44].

From an environmental and territorial perspective, the DANA caused severe alterations to the affected fluvial systems. High discharges and flow energy triggered widespread bank erosion, extreme sediment transport, channel reshaping and deposition of large quantities of sediment across floodplain areas. These processes were also associated with impacts on aquatic and riparian ecosystems, alongside diffuse pollution phenomena due to the mobilization of solid waste, including construction debris, plastics and other anthropogenic materials transported by floodwaters.

Overall, the event is considered one of the most significant floods recorded in Spain in recent decades, both in terms of rainfall intensity and persistence, as well as spatial extent and diversity of impacts.

Although media and institutional attention was primarily concentrated on the metropolitan areas of the province of Valencia, significant hydrological and geomorphological impacts were also observed in the inland mountainous basins of the Serranía region, including the area of Sot de Chera.

The 2024 DANA in Sot de Chera

Among the locations most severely affected by the 29–30 October 2024 event in the Los Serranos region, Sot de Chera stands out. During the most intense phase of the episode, the convective system that had initially affected the central-southern sector of the province of Valencia progressively shifted northwards, reaching the Turia basin in the evening hours of 29 October. According to AEMET from 20:00 onwards inland Valencian regions recorded exceptionally intense rainfall, with accumulations exceeding 200 mm in three hours in the area of the Embalse de Buseo [41].

Persistent rainfall between the evening of 29 October and the night of 30 October generated a second and more intense flood wave in the Turia basin. Particularly significant was the hydrological response of the Reatillo–Río Sot sub-basin, where inflows exceeded 7.5 hm^3/h between 20:00 and 23:00, associated with average rainfall intensities above 30 mm/h [45].

According to hydrological reconstructions by the Confederación Hidrográfica del Júcar (CHJ) [43], this contribution led to the rapid filling of the Embalse de Buseo, causing a malfunction of the monitoring instrumentation when flow values of approximately 646 m^3/s were recorded. The peak discharge remains unknown, as the sensors failed during the most critical phase of the event.

The Embalse de Buseo, managed by the Generalitat Valenciana, reached its spillway level around 22:00 on 29 October. The overtopping flow triggered erosion and instability processes on the slope immediately downstream of the right abutment, resulting in the loss of superficial confinement of the slope and damage to several intake structures. Damage was also reported on the left abutment, and Emergency Scenario 2 of the dam Emergency Action Plan was activated.

In the downstream valley section below the reservoir, the response of the Río Sot exhibited a rapid rise in water levels and overbank flooding affecting the urban area of Sot de Chera. Among the most affected locations in the lower Turia basin, the CHJ report identifies Sot de Chera, Gestalgar and Pedralba, highlighting that the most severe damage occurred in Sot de Chera (Figure 2.12).

The event caused the death of two people, a four-year-old child and his father. From an infrastructural perspective, widespread damage was recorded in the road network, river crossings and essential services (Figure 2.13). Particularly significant was the interruption of the road connection between Chera and Sot de Chera, which contributed to the temporary isolation of the municipality. Water supply networks and sewage systems were also severely affected; full service restoration required several days, and intermittent disruptions continued in the following months due to slope instability and damage to water conveyance infrastructure [46].

Beyond damage to buildings and infrastructure, the flood caused profound transformations of the fluvial environment. High flow energy generated widespread bank erosion, extreme sediment transport and channel reshaping, with the removal of sediments and substantial portions of soil, exposing the underlying bedrock. This process also had significant consequences for agricultural activities due to the loss of the most fertile soil layers. In addition, the intensity of the flow led to the removal of large portions of riparian vegetation along the river corridor (see Figure 2.13a). In several reaches, the Río Sot exhibited marked morphological changes compared to its pre-event configuration, highlighting the role of the DANA not only as a flood event but also as a major geomorphological driver of transformation within the fluvial system.

The geomorphological evolution of the Río Sot did not cease with the recession of the floodwaters. During the following months, the river corridor became a highly active recovery zone, undergoing widespread physical modifications associated with emergency reconstruction works. At the Buseo dam, the extreme inflows compromised the abutments, prompting the Dirección General del Agua (MITECO) to order an extraordinary review of the infrastructure's structural and hydraulic safety and to initiate urgent stabilization works [43].

Further downstream, extensive earthmoving works were undertaken to re-establish severed territorial connections. These interventions focused primarily on reconstructing the road link between Chera and Sot de Chera in the northern

sector of the municipality, together with a broader programme to restore vehicular and pedestrian river crossings destroyed by the flood. As the summer season approached, additional in-channel works were carried out within the urban reach to rehabilitate the traditional river bathing areas and restore recreational access.

The reconstruction process involved several administrative bodies, including the Ayuntamiento de Sot de Chera, the Generalitat Valenciana and the Confederación Hidrográfica del Júcar (CHJ).

(a)

(b)

Figure 2.12: Hydrological and macro-geomorphological response of the Río Sot catchment during the October 2024 DANA event: (a) structural damage and slope instability on the right abutment of the Buseo dam (*Embalse de Buseo*) induced by the peak overtopping flow (source: *Levante-EMV* [23]); (b) oblique aerial overview of the active river corridor within the urban boundary of Sot de Chera (source: *El País* [47]).

(a)

(b)

(c)

Figure 2.13: Fluvial impacts and systemic environmental damage in Sot de Chera: (a) diachronic orthophoto comparison tracking the river corridor before the event (top) and immediately after (bottom), demonstrating the near-complete stripping of riparian vegetation patches and severe structural alterations (source: elaborated by the author); (b) localised cross-sectional scouring with complete flushing of alluvial soil layers and clear exposure of the underlying geological bedrock (source: local photographer); (c) structural failure of an urban river crossing caused by combined hydrodynamic pressure and organic debris clogging, with severed critical municipal lifeline networks (water supply and sewage) visible in the foreground (source: *Levante-EMV* [48]).

Chapter 3

Materials and Methods

3.1 Water Quality Analyses

Two complementary analyses were carried out to assess the water quality of the Río Sot: a spatial analysis, aimed at evaluating longitudinal variations along the river reach, and a temporal analysis, designed to identify potential seasonal trends. Both historical datasets and field data collected during two sampling campaigns were used.

3.1.1 Historical Data

Dataset selection

To characterize the baseline water quality conditions of the river, extracted from the Water Information System of the Júcar River Basin (SIA Júcar, 2025) [49], were analysed.

Within the study area, four monitoring stations were available: two located upstream near the urban area (JUH420 and JUH409), and two located further downstream after Las Toscas (JUH403 and JUH412). Following an initial evaluation of data availability, temporal coverage, and parameter completeness, station JUH403 was selected for further analysis. This station provided the most complete and continuous dataset, enabling robust statistical analysis, and included recent measurements relevant to the objectives of the study.

The dataset covers the period from 1992 to May 2025 and includes a wide range of physico-chemical, biological, and microbiological parameters, as well as selected pesticides and fungicides.

Given the large number of available parameters, a subset was selected based on their representativeness for the study area and the target environmental pressures (untreated wastewater discharges and agricultural runoff). This subset is reported

in Table 3.1.

Table 3.1: Water quality parameters – Río Sot.

Parameter	**Origin/biogeochemical interpretation**
1. In situ physico-chemical parameters	
pH (in situ)	Water acidity/alkalinity
Temperature	Water temperature
Electrical conductivity (EC)	Total ionic content / salinity
Dissolved oxygen saturation	Oxygen availability in the water column
2. Nutrients	
Ammonia	Organic waste, fertilisers, wastewater
Nitrites	Intermediate product of nitrification and incomplete oxidation of ammonia; indicates recent or unstable contamination
Nitrates	Final product of nitrification; accumulates in oxygenated waters and is strongly associated with soil leaching and agricultural fertilisation
Phosphates	Fertilisers, detergents
3. General physical and chemical parameters	
Chlorides	Wastewater discharges, agricultural runoff, evaporation
Total Chlorine	Disinfection by-products, urban wastewater inputs, treated water drainage
Chemical Oxygen Demand (COD)	Urban wastewater, agricultural and industrial inputs
Biological Oxygen Demand (BOD_5)	Organic pollution from wastewater discharges, agricultural and diffuse organic inputs
Color	Dissolved organic matter, runoff, pollution inputs
4. Metals	
Copper (Cu)	Agricultural fungicides, urban runoff
Iron (Fe)	Geogenic background, erosion, redox processes
Chromium VI (Cr VI)	Industrial contamination, anthropogenic pollution
5. Microbiological indicators	
Total coliforms	Diffuse organic pollution

Parameter	Origin/biogeochemical interpretation
Fecal coliforms	Recent fecal contamination
6. Pesticides	
Glyphosate	Herbicide

Figure 3.1 illustrates the temporal distribution of observations within the dataset. To provide a more representative characterization of the river's current conditions, only data collected during the last 20 years (2005–2025) were considered for the analysis. Table 3.2 summarises its main characteristics.

Table 3.2: Summary of water quality parameters data characteristics, units of measurement, temporal coverage, and number of observations.

Parameter	Units	N_tot	N_Warm	N_Cold	Years
EC at 20 °C (in situ)	μS/cm	69	17	37	2007-2025
pH (in situ)	–	69	17	37	2007-2025
DO Saturation (in situ)	%	69	17	37	2007-2025
T (in situ)	°C	69	17	37	2007-2025
Suspended Solids	mg/L	56	14	27	2007-2025
Ammonia	mg/L	55	14	27	2007-2025
BOD5	mg/L	55	14	27	2007-2025
Nitrate	mg/L	55	14	27	2007-2025
COD	mg/L	51	13	25	2007-2025
Copper	μg/L	46	11	26	2007-2021
Phosphate	mg/L	45	11	22	2007-2025
Chloride	mg/L	40	10	20	2005-2025
Nitrite	mg/L	34	9	16	2007-2025
Total Chlorine	mg/L	30	8	14	2007-2014
Fecal Coliforms	CFU/100 mL	30	8	15	2007-2014
Total Coliforms	CFU/100 mL	30	8	15	2007-2014
Iron	μg/L	21	4	14	2008-2021
Glyphosate	μg/L	19	4	12	2020-2025
Colour	mg/L	16	4	8	2010-2014
Chromium (Cr VI)	μg/L	12	2	8	2008-2012

After parameter selection, relevant regulatory thresholds were identified within

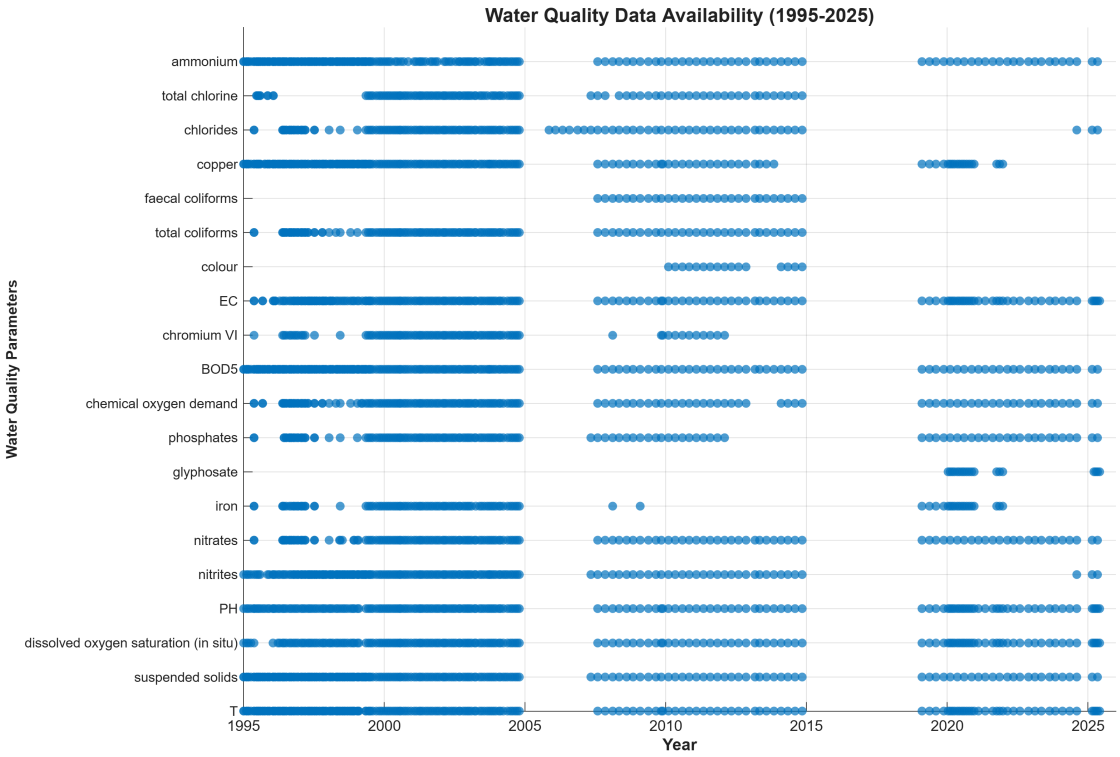

Figure 3.1: Temporal distribution of available water quality data for each parameter of interest in the dataset. Each point represents at least one available observation for a given year.

the Spanish and European legislative framework. Given the heterogeneous nature of the analysed variables, a hierarchical regulatory framework consistent with the Water Framework Directive (WFD; Directive 2000/60/EC) [50] was adopted. Reference standards were selected according to the functional classification of the analysed parameters.

Ecological status indicators (e.g., pH, dissolved oxygen, nutrients) were interpreted according to the Spanish implementation of the WFD through Royal Decree 817/2015 [51]. General physico-chemical parameters and indicators of organic pollution were assessed using the relevant Spanish water quality regulations, including Royal Decree 665/2023 [52], where applicable. Chemical contaminants, including selected pesticides, were assessed using European Environmental Quality Standards (EQS) under Directive 2008/105/EC [53], as amended by Directive 2013/39/EU [54].

Table 3.3 offers a synthesis of the regulatory limits and of the sources for each parameter.

Table 3.3: Regulatory water quality thresholds and corresponding sources.

Parameter	**Limits**	**Units**	**Source**	**Notes**
pH	6-9	-	RD 817/2015	Good-Moderate Threshold
Dissolved Oxygen Saturation	60-120	%	RD 817/2015	Good-Moderate Threshold
Chloride	200	mg/L	RD 665/2023	*NCA-MA
Total Chlorine	0.005	mg/L	RD 665/2023	*NCA-MA
BOD5	6	mg/L	RD 665/2023	*NCA-MA
COD	30	mg/L	RD 665/2023	*NCA-MA
Fecal coliforms	20000	CFU/100 mL	RD 665/2023	*NCA-MA
Total coliforms	50000	CFU/100 mL	RD 665/2023	*NCA-MA
Ammonia	0.6	mg/L	RD 817/2015	Good-Moderate Threshold
Nitrates	25	mg/L	RD 817/2015	Good-Moderate Threshold
Nitrites	0.03	mg/L	RD 665/2023	*NCA-MA
Colour	200	mg/L	RD 665/2023	*NCA-MA
Phosphates	0.4	mg/L	RD 817/2015	Good-Moderate Threshold
Copper	120	μg/L	RD 817/2015	*NCA-MA
Chromium VI	5	μg/L	RD 817/2015	*NCA-MA
Iron	2000	μg/L	RD 665/2023	*NCA-MA
Glyphosate	0.1	μg/L	EU EQS	*NCA
**NCA-MA (Norma de Calidad Ambiental - Media Anual) stands for AA-EQS (Annual Average Environmental Quality Standard)*				

Baseline Water Quality Assessment and Temporal Trend Analysis

To characterize baseline water quality conditions and investigate long-term changes in the Río Sot, an exploratory temporal analysis was performed using annual boxplots grouped by calendar year. This graphical approach enabled the assessment of compliance with regulatory thresholds, as well as the identification of temporal patterns, shifts in data distribution, and anomalous observations that could not be captured through summary statistics alone.

Parameters characterized by a high proportion of measurements below the analytical limit of detection (LOD) were interpreted with caution, as censored observations may reduce the sensitivity of trend analyses and affect the reliability of statistical inference.

To complement the exploratory analysis, long-term monotonic trends were evaluated using the Seasonal Kendall test. This non-parametric method is widely applied in environmental time series because it is robust to missing values, irregular sampling intervals, and non-normal data distributions. It also explicitly accounts for seasonal variability, which is particularly relevant in Mediterranean hydrological systems.

Accordingly, the hydrological year was divided into two seasonal periods reflecting the local climate regime: a Warm period (May–September) and a Cold period (October–April), as reported in Table 3.4. When multiple observations were available within the same seasonal block and year, values were aggregated using the arithmetic mean to ensure a single representative observation per period.

Trend significance was assessed at a 95% confidence level ($p < 0.05$), and Sen's slope was used to quantify the magnitude of change, both at the overall annual scale and separately for the two seasonal periods.

Seasonal Water Quality Analysis (Warm vs. Cold Periods)

To further explore the influence of seasonal variability on water quality, a comparative analysis between Warm and Cold periods was performed. This step is particularly relevant in the study area, where anthropogenic pressures such as agricultural runoff and wastewater inputs may vary significantly throughout the year.

For each parameter, boxplots were used to visualize differences between seasons, following the temporal scheme summarized in Table 3.4.

Table 3.4: Temporal subdivision of the data.

Season	Months
Hot season	5-9
Cold season	1–4, 10–12

To ensure statistical robustness, parameters containing fewer than 5 observations per period were excluded from the boxplots. Differences between Warm and Cold periods were then tested using the Mann–Whitney U test, a non-parametric method suitable for non-normal and heteroscedastic environmental datasets. This allowed for the identification of parameters exhibiting a statistically significant seasonal signal potentially linked to changes in hydrological conditions or human pressure patterns.

3.1.2 Field Data

To complement the historical trend analysis, field monitoring was conducted along the study reach. This framework had a dual purpose: first, to characterize the longitudinal variation of water quality along the Río Reatillo (or Río Sot), and second, to evaluate the post-event water quality status following the 2024 DANA extreme flood event.

Two field campaigns were conducted to capture distinct hydrological and seasonal behaviors: an autumn–winter campaign in November and December 2025 (between 19/11/2025 and 12/12/2025), and a spring campaign in April 2026. The spring campaign was completed within a single day (17 April 2026), whereas the autumn–winter campaign required several days due to concurrent vegetation mapping activities, which significantly extended fieldwork duration.

For logistical reasons all sampling activities were restricted to weekdays (mainly Wednesdays or Fridays). For the autumn-winter campaign, sampling was carried out on non-consecutive days. This constraint introduces a known source of uncertainty, as the main pressure is a point-source sewage discharge in a small municipality where pollution peaks are rapid, transient, and highly variable. In addition, the local population is significantly lower on weekdays than during weekends, meaning that the observed values likely represent a conservative lower bound of actual domestic pressures.

In both campaigns, data were collected across 12 monitoring stations distributed along the river section from about 4 km upstream from the village down to its confluence with the Turia River. The spatial distribution of these sampling points is illustrated in Figure 3.2. Among these stations, four specific locations are of particular interest for the analysis:

- **Station 3:** Located upstream of the village, represents the baseline water quality conditions before the river passes through the urbanized area.
- **Station 4:** Positioned immediately downstream of the untreated sewage discharge outlet, captures the maximum local impact of urban wastewater.
- **Station 10:** Coinciding with the historical monitoring station of the Júcar

River Basin Authority (CHJ), allows direct temporal comparison with official records.

- **Station 0:** Sampled within the Turia River immediately upstream of its confluence with the Río Reatillo, acts as an external hydrological control.

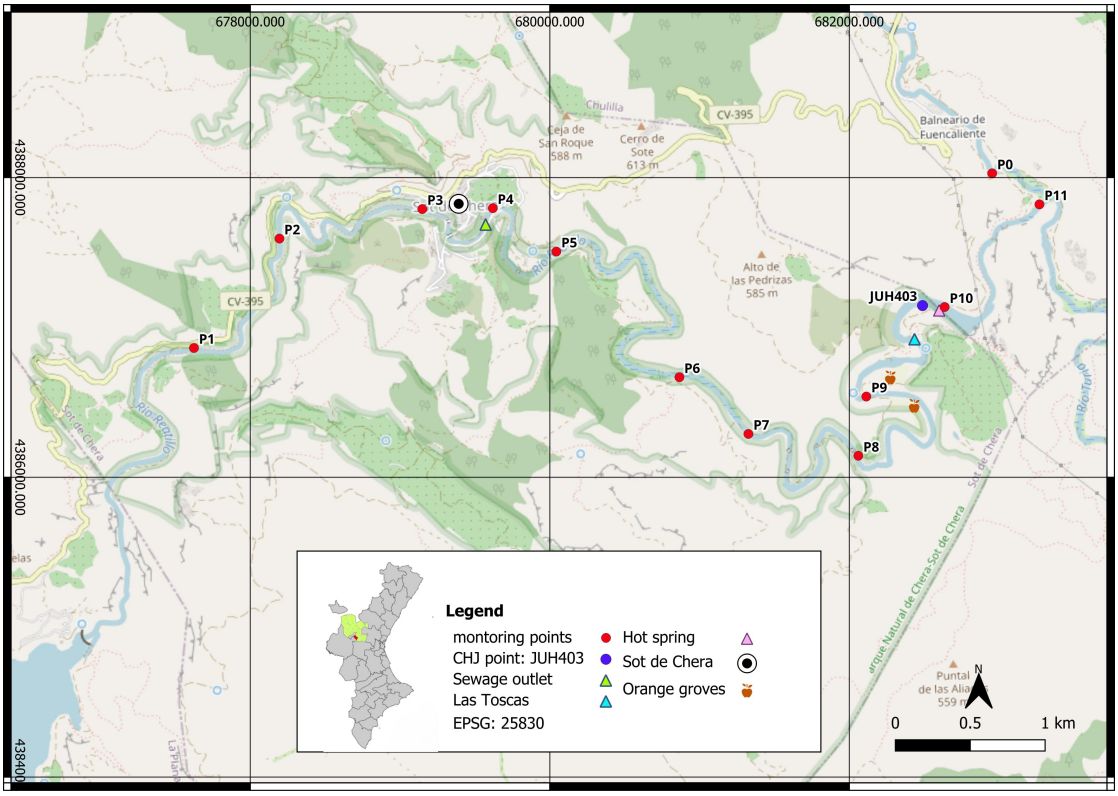

Figure 3.2: Spatial distribution of sampling points along the Sot River in Sot de Chera. Red points indicate the monitoring stations of the field campaigns, while the violet point represent the historical CHJ station (JUH403). Relevant landmarks (sewage outlet, Las Toscas, hot spring and orange groves) are highlighted to provide environmental context.

It must be noted that during the sampling period, extensive road reconstruction works were taking place upstream of Sot de Chera to repair the road connecting the village to Chera, which had been severely damaged by the DANA flood. These works caused significant physical disturbance directly within the riverbed influencing both local water quality and riparian vegetation conditions, particularly during the autumn-winter campaign when excavation works were at their peak. By Spring 2026, the construction site was significantly less active.

Physico-chemical parameters targeted for water quality assessment were determined directly in situ using portable, rapid-screening instrumentation categorized as follows:

Digital Multiparameter Testers

- A portable digital conductivity meter (TDS & EC meter) was used for the simultaneous measurement of electrical conductivity (EC, expressed in μS/cm), total dissolved solids (TDS, in ppm), and water temperature (T, in °C).
- An auxiliary immersion digital thermometer was employed as an independent control to validate the accuracy and thermal stability of the primary sensors.

colourimetric Kits and Test Strips

- **Ammonia Liquid Kit:** A liquid colorimetric assay designed for aquaculture monitoring was used for ammonia (NH_4^+/NH_3) screening. The protocol involved sampling a fixed 5 mL volume of river water into a graduated test tube, followed by the sequential addition of three liquid reagents. Following a fixed reaction time, the total ammonia concentration was determined visually by comparing the solution's color against a semi-quantitative chromatic scale ranging from 0 to 10 mg/L (ppm).
- **Multi-parameter Test Strips:** Dry chemical strip tests originally designed for rapid drinking water screening were used for the semi-quantitative assessment of the remaining parameters (including nitrates NO_3^-, nitrites NO_2^-, total hardness, and total alkalinity). The method relies on the color development of specialized reactive pads embedded in the strip, which are visually matched against a standardized reference scale.

Table 3.5 summarizes the monitored parameters, the respective monitoring instruments, and their technical measurement units, while Figure 3.3 represents the instruments.

While these in situ tools offer clear operational advantages, including portability, ease of use, and immediate results without the need for sample preservation or laboratory analysis, they also present methodological limitations. This is particularly the case for multi-parameter test strips, which rely on predefined categorical ranges that are relatively broad for some variables (especially nitrites and metals), thereby limiting measurement precision. In addition, their visual interpretation can be affected by environmental conditions such as direct sunlight and atmospheric visibility during field operations.

Following data collection, the spatial evolution of water quality from upstream to downstream was plotted. To account for uncertainty in visually interpreting the

Table 3.5: Summary of measured water quality parameters, field instrumentation, and corresponding resolutions.

Parameter	Units	Instrument/Kit	Resolution
EC	μS/cm	TDS&EC-meter	1 μS/cm
T	°C	TDS&EC meter and thermometer	0.1 °C
TDS	ppm	TDS&EC meter	1 ppm
Ammonia	mg/L	Liquid colourimetric test kit	Discrete scale (see Figure 3.5)
pH	-	Multi-par test strip kit	Discrete scale (see Figure 3.4)
Total alkalinity	mg/L	Multi-par test strip kit	Discrete scale (see Figure 3.4)
KH	mg/L	Multi-par test strip kit	Discrete scale (see Figure 3.4)
GH	mg/L	Multi-par test strip kit	Discrete scale (see Figure 3.4)
Cyanuric Acid	mg/L	Multi-par test strip kit	Discrete scale (see Figure 3.4)
Copper	mg/L	Multi-par test strip kit	Discrete scale (see Figure 3.4)
Mercury	mg/L	Multi-par test strip kit	Discrete scale (see Figure 3.4)
Total Chlorine	mg/L	Multi-par test strip kit	Discrete scale (see Figure 3.4)
Free Chlorine	mg/L	Multi-par test strip kit	Discrete scale (see Figure 3.4)
Bromine	mg/L	Multi-par test strip kit	Discrete scale (see Figure 3.4)
Nitrate	mg/L	Multi-par test strip kit	Discrete scale (see Figure 3.4)
Nitrite	mg/L	Multi-par test strip kit	Discrete scale (see Figure 3.4)
Iron	mg/L	Multi-par test strip kit	Discrete scale (see Figure 3.4)
Chromium/Cr(VI)	mg/L	Multi-par test strip kit	Discrete scale (see Figure 3.4)
Lead	mg/L	Multi-par test strip kit	Discrete scale (see Figure 3.4)
Fluoride	mg/L	Multi-par test strip kit	Discrete scale (see Figure 3.4)

Figure 3.3: Instruments used for field data collection.

colorimetric test strips, results were expressed as concentration ranges rather than discrete values. Conversely, for water temperature, the final value was computed as the arithmetic mean of the concurrent readings obtained from the the digital thermometer and the digital conductivity meter in order to minimize instrumental bias.

The results of the two monitoring campaigns were compared in order to investigate potential seasonal changes. Finally to contextualize these field results within the long-term behavior of the river, the field data were compared with the historical CHJ datasets. For seasonal consistency, the November–December data were compared with the historical "Cold Period" boxplots, while the April campaign results were evaluated against the "Warm Period" baseline.

(a)

(b)

Figure 3.4: Detail of the multi-parameter test strip bottle: (a) target water quality parameters and (b) corresponding discrete colorimetric reference scales and concentration ranges.

(a)

(b)

Figure 3.5: Ammonia liquid kit: (a) execution of the colorimetric ammonia test on-site; (b) detail of the liquid kit reference scale.

3.2 Riparian Vegetation

This study presents the results of a field survey conducted between November and December 2025 in the municipality of Sot de Chera, aimed at analysing the early stages of riparian vegetation recolonisation along the Río Sot, approximately one year after the extreme DANA event of October 2024.

3.2.1 Survey methodology and considered species

Given the preliminary nature of the investigation and its reliance exclusively on visual field observations, the analysis focused on a limited set of easily identifiable plant species selected according to their ecological relevance and frequency within the surveyed river reach. The mapping specifically targeted:

- Poplars, particularly *Populus alba* and *Populus nigra* / *P.* × *canadensis*;
- Emergent aquatic vegetation, with emphasis on *Phragmites australis* and associated marsh communities;
- *Tamarix* spp.;
- *Nerium oleander*;
- *Arundo donax*.

Table 3.6 presents a synthesis of the selected riparian species, including their ecological role, reproductive strategies, geomorphic preferences, and relevance for river restoration.

Species identification was primarily based on morphological traits observed directly in the field. In order to support preliminary recognition, mobile applications such as PlantNet and Google Lens were occasionally used as auxiliary tools during surveys. Field surveys were carried out on foot along the active channel and fluvial bars, recording species presence across the main morphological units. In some cases, observations were supported by binoculars due to limited accessibility and observation distance constraints. Given the spatial extent of the study area, restricted access to some fluvial bars, and the presence of juvenile individuals, a degree of uncertainty in species-level identification cannot be excluded, particularly for morphologically similar taxa and potential hybrids. Future surveys involving closer-range observations, targeted sampling, morphometric analyses, or genetic methods could improve taxonomic resolution and help validate the preliminary identifications presented in this study.

Figure 3.6: Use of binoculars during field survey activities for remote observation of riparian vegetation in the Río Sot study reach.

Table 3.6: Target riparian species mapped in the study area and their ecological, spatial and restoration relevance.

Species/group	**Ecological role**	**Reproductic strategy**	**Response to floods**	**Habitat**	**Notes for restoration**
Populus nigra / *P.* × *canadensis*	Pioneer tree; fast-growing riparian component; bank stabilization; habitat formation	Sexual reproduction and strong vegetative propagation (especially hybrids)	Rapid recolonization after disturbance; hybrids may spread more aggressively	Recently deposited alluvial bars with fine, moist sediments	Indicator of early riparian recovery; hybridization may affect genetic integrity

Continued on next page

Species/group	Ecological role	Reproductic strategy	Response to floods	Habitat	Notes for restoration
Populus alba	Riparian pioneer species; bank stabilization; habitat formation	Sexual and vegetative reproduction	More drought-tolerant; less competitive during early post-flood stages	Fine substrates; higher terraces within river corridor	Indicator of early riparian recovery
Nerium oleander	Riparian shrub; bank stabilization; micro-habitat provision	Sexual reproduction and vegetative resprouting	High resistance to flow; strong post-flood persistence	Gravelly-sandy bars and banks	Supports structural continuity of riparian corridor
Tamarix spp.	Shrub/tree; sediment trapping; pioneer in disturbed areas	Sexual and vegetative regeneration	Early recolonization; disturbance tolerant	Bars and elevated surfaces	Can form dense stands limiting native vegetation
Phragmites australis	Helophyte; sediment stabilization; habitat creation	Mainly vegetative reproduction (rhizomes)	Rapid colonization; sensitive to disturbance	Low-velocity depositional areas	May reduce plant diversity when dominant
Typha, *Juncus*, *Eleocharis* spp.	Emergent aquatic vegetation; sediment retention	Vegetative propagation (rhizomes)	Rapid recolonization of saturated substrates	Shallow water, secondary channels, wet margins	Important for wetland recovery

Continued on next page

Species/group	Ecological role	Reproductic strategy	Response to floods	Habitat	Notes for restoration
Arundo donax	Invasive riparian grass; highly competitive species	Vegetative reproduction (rhizomes and fragments)	Very rapid expansion after floods	Moist disturbed areas	Strong pressure on native vegetation

3.2.2 GIS processing and spatial analysis

Spatial analysis was conducted in a GIS environment using high-resolution (3 cm) orthophotography as the base layer [55]. This orthophotography was generated from an aerial drone (UAV) survey flown in July 2025, capturing the post-event (post-Dana) river morphology. All spatial data and digitised layers were projected in the official Spanish coordinate reference system: ETRS89 / UTM zone 30N (EPSG:25830).

Fluvial bars were manually digitised as polygon features by delineating their boundaries directly on the orthophoto. These polygons were subsequently subdivided into homogeneous sections based on visible geomorphological characteristics, which served as the spatial units for vegetation mapping and analysis.

All target species were mapped; however, a higher level of detail was dedicated to *Arundo donax*. Due to its well-documented invasive behaviour in Mediterranean river systems and its rapid post-DANA expansion, a dedicated spatial assessment was performed to identify the main colonisation nuclei in addition to the general distribution mapping.

A three-class visual scheme was adopted for most species, local species were depicted using a yellow–green scale, while the invasive Arundo donax was represented with a yellow–red scale:

- **Low / Absent (Yellow):** species sporadic or not detected within the surveyed reach;
- **Present (Light Green / Light Red):** vegetation present with moderate density, often forming discontinuous or linear stands along channel margins, generally composed of juvenile individuals;
- **Abundant (Dark Green / Dark Red):** dense and well-structured populations covering significant portions of the reach, often including mature

individuals and post-DANA survivors acting as key sources for further colonisation.

For selected species (e.g., poplars and *Tamarix*), classification was simplified to a binary presence/absence approach due to insufficient field resolution for a more detailed categorisation. The resulting maps provide a descriptive overview of the current vegetation structure and constitute a baseline for monitoring post-event dynamics and supporting future management or restoration strategies.

3.3 Hydrodynamic simulation and spatial exposure

Following the morphological alterations induced by the 2024 DANA event, a dual methodological approach was required to evaluate both the physical flow dynamics of the Río Sot and the subsequent regulatory implications for the surrounding territory: a 2D hydraulic model to characterize the kinematic and spatial behaviour of the river and its interaction with the new crossing structures; and a GIS-based spatial analysis conducted to quantify the intersection between the revised Hydraulic Public Domain (DPH) boundaries and the cadastral parcels in Sot de Chera. These analyses focused on a selected river reach of approximately 2.5 km flowing through the urban area of Sot de Chera, where the interaction between the water body and the anthropized environment is greatest.

3.3.1 2D Hydraulic modelling

A two-dimensional (2D) hydraulic modelling approach was implemented to simulate flood dynamics within the study reach of the Río Sot. The model was developed to reproduce post-DANA (2024) flow conditions and to analyse the hydraulic behaviour of the channel system under different discharge scenarios. In particular, the modelling framework allows for a detailed representation of flow patterns and their interaction with the river morphology and the new transversal structures within the urban section of Sot de Chera.

Digital Terrain Model (DTM) processing

The topographic basis for the hydraulic modelling consisted of a high-resolution Digital Terrain Model (DTM) (10 x 10 cm), derived from an aerial photogrammetric survey conducted after the 2024 DANA extreme event. To accurately reproduce the post-event river morphology, the original raster underwent a pre-processing phase within a Geographic Information System (GIS) environment. This operation was necessary to remove digital artefacts corresponding to old in-channel structures

that were destroyed or modified post-flood. Subsequently, the abutments and the piers of the newly planned transversal structures were digitally reconstructed at the boundaries of the Hydraulic Public Domain (DPH) to ensure a proper geometric transition between the natural terrain and the anthropogenic works.

Parametrization of hydraulic structures

The infrastructure within the study reach includes six main crossing structures, modelled from upstream to downstream based on field surveys and design specifications. Geometric information was collected through rapid in-situ surveys using a measuring tape.

- **Steel pedestrian bridge** (Structure 1): A shallow arch bridge with a clear span of 25 m. The springing line is supported by abutments extending 4 m on the left bank and 7 m on the right bank. The deck width is 4 m, with lateral earth embankments integrated into the approach zones.
- **Road bridge**(Structure 2): A reinforced concrete bridge with an 11 m span and a vertical clearance of 3 m. The right-bank abutment extends approximately 6 m. The bridge includes a longitudinal central pier with a rounded upstream cutwater of approximately 1 m in diameter.
- **Main ford**(Structure 3): A structure equipped with six basal tubular culverts. Based on the cross-sectional surveys, the culverts have an internal diameter of 1 m and are covered by an 80 cm thick layer of backfill and road surface.
- **Second steel pedestrian bridge** (Structure 4): A structure with a deck width of 3 m and a central span of 20 m. The bridge is supported by a 12 m left abutment and an 11 m right abutment.
- **Minor fords**(Structures 5 and 6): Two secondary crossings located at the downstream boundary of the modelled reach. the first with 5 culverts of 1 m of diameter and the second with 2 culverts.

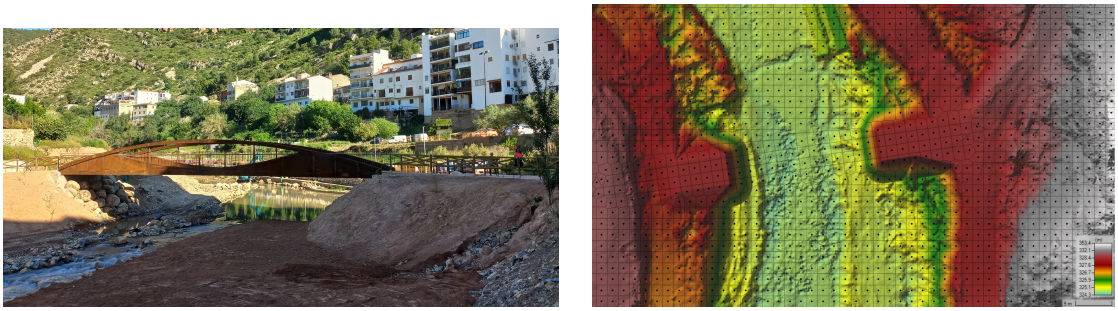

(a) Pedestrian bridge 1 **(b)** DTM modification

Figure 3.7: First steel pedestrian bridge. Left (a): photographic survey of the structure. Right (b): modification of the high-resolution DTM in HEC-RAS, showing the digital reconstruction of the lateral abutments integrated into the natural terrain. Pictures of April 2026.

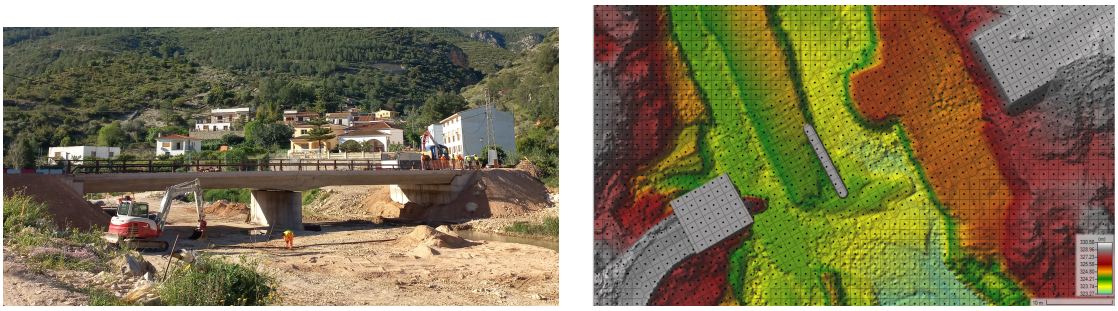

(a) Road bridge **(b)** DTM modification

Figure 3.8: Main road bridge. Left (a): structure under construction. Right (b): modification of the high-resolution DTM in HEC-RAS, showing the digital reconstruction of the lateral concrete abutments of the bridge integrated into the natural terrain and the central pier. Pictures of April 2026.

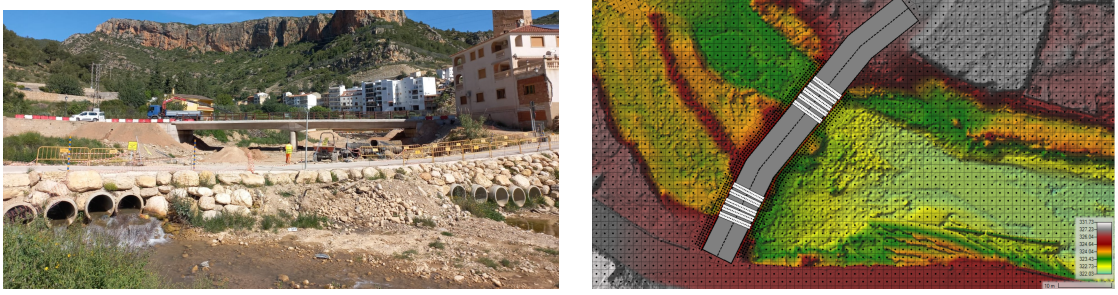

(a) Main Ford **(b)** 2D hydraulic structure setup

Figure 3.9: Main ford. Left (a): field view of the crossing. Right (b): implementation in the HEC-RAS 2D model. Unlike the bridge abutments directly embedded into the terrain raster, the ford is modelled as a hydraulic structure overlaying the DTM. The dashed white lines indicate the geometric configuration of the six basal culverts, while the high-density local mesh refinement ensures stability during overtopping and pressurised flow phases. Pictures of April 2026.

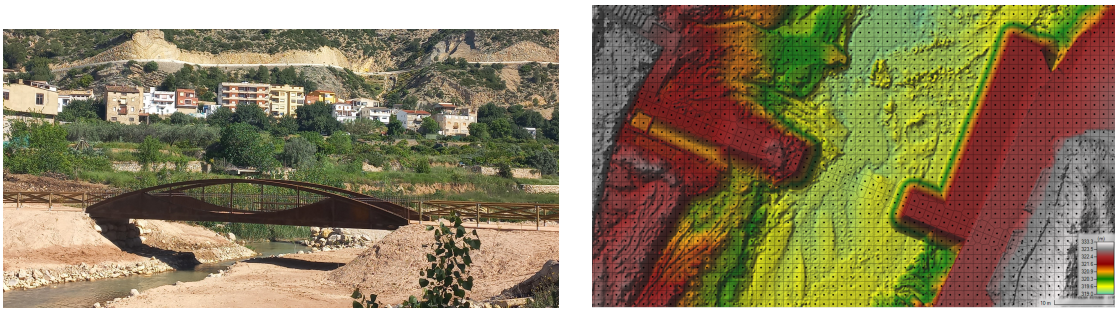

(a) Pedestrian bridge 2 **(b)** DTM modification

Figure 3.10: Second steel pedestrian bridge. Left (a): photographic survey. Right (b): corresponding geometric modification of the DTM to incorporate the lateral abutments of the pedestrian bridge within the computational domain. Pictures of April 2026.

2D Hydraulic model configuration

Flood routing was simulated using the HEC-RAS software, implementing a two-dimensional (2D) model under unsteady flow conditions. The computational domain was discretised using a structured mesh with a base cell size of 1.5 x 1.5 m. To optimise computational efficiency without compromising numerical stability and accuracy, refinement regions and breaklines were introduced along the most pronounced topographic discontinuities and the aforementioned transversal structures.

The numerical solution of the flow field was performed using the 2D Shallow Water Equations (SWE) solved via the Eulerian-Lagrangian Method (SWE-ELM). This equation set was specifically selected over the simpler Diffusion Wave approximation because it fully accounts for momentum conservation. This capability is strictly required to accurately simulate highly dynamic flow conditions, such as rapid accelerations, backwater effects, and complex flow interactions induced by the crossing structures.

A uniform Manning's roughness coefficient (n) of 0.05 s/m$^{1/3}$ was assigned to the computational domain. The downstream boundary condition was set using the normal depth method, applying an estimated friction slope of 0.005 m/m, while the upstream boundary condition was defined by the inflow hydrograph.

Furthermore, to ensure numerical stability while optimising computational times, an adaptive time step based on the Courant-Friedrichs-Lewy (CFL) condition was implemented. Setting a target maximum Courant number of 1.0, the temporal resolution was allowed to vary dynamically between 0.06 and 16.00 seconds, starting from a base interval of 1 second. This approach guaranteed stable flow routing over the 3-hour simulation time window. Output mapping and hydrograph intervals were set to 30 minutes.

A geometric configuration incorporating the new crossing structures was developed to simulate their hydraulic behaviour under flood conditions. The model was tested under three different hydrological scenarios:

- **1 m^3/s**: Representing ordinary low-flow conditions.
- **60 m^3/s**: Corresponding to the Maximum Ordinary Flood (Máxima Crecida Ordinaria - MCO). According to the Spanish Water Law, the MCO delineates the natural riverbed and defines the extent of the Hydraulic Public Domain (DPH) [56]. It is typically derived as the statistical mean of the annual maximum instantaneous discharges under natural flow conditions, computed over a long-term hydrological record, generally exceeding 10 consecutive years.
- **358 m^3/s**: A high-magnitude flood hydrograph considered broadly representative of the 2024 DANA event based on the available information. This

scenario was used as a stress-test condition to assess flood dynamics under extreme flow conditions.

For the 1 m^3/s and 60 m^3/s scenarios, the hydraulic model was run using the complete geometric configuration, including the explicit representation of the main crossing structures. In this configuration, the ford crossings were modelled as hydraulic structures with culverts, while the bridge abutments, piers, and lateral embankments were incorporated into the terrain geometry according to the available field measurements and design information.

For the 358 m^3/s scenario, the implementation of the complete hydraulic configuration led to numerical instability and did not provide a stable solution. This behaviour was associated with the highly dynamic hydraulic conditions expected during such an extreme event, including rapid transitions between free-surface flow, pressurised flow, overtopping, and extensive floodplain activation. Therefore, the extreme flood scenario was simulated using a simplified hydraulic configuration.

In the simplified configuration, the post-DANA Digital Terrain Model was retained as the main topographic control, including the terrain modifications associated with the lateral abutments and structural embankments. The ford crossings were still represented as hydraulic structures with culverts, allowing the partitioning between culvert flow and overtopping flow to be assessed. Conversely, the bridge decks were not explicitly included in the hydraulic computation. As a result, the 358 m^3/s simulation was used to evaluate maximum water levels, inundation patterns, flow velocities, and ford performance under extreme conditions, while the bridge results were interpreted in terms of maximum water surface elevation.

3.3.2 Spatial analysis of agricultural parcels within regulated river areas

This study is based on the integration of cadastral and hydraulic-regulation spatial datasets within a Geographic Information System (GIS) environment. The objective was to identify agricultural parcels affected by hydraulic regulation zones following the post-DANA revision of the Hydraulic Public Domain and quantify the extent of the associated restrictions.

Hydraulic regulation zones

The hydraulic regulation framework applied in this study is defined by the Spanish Water Law [57], which establishes the Hydraulic Public Domain and its associated protection zones. The spatial framework of the analysis was provided by the updated hydraulic regulation dataset corresponding to the Third Cycle of the

SNCZI, managed by the Confederación Hidrográfica del Júcar (CHJ) [58]. This dataset integrates the three regulatory zones associated with the river management:

- Hydraulic Public Domain (DPH), corresponding to the river channel and adjacent riparian areas, it belongs to the State and is spatially delimited by the extent of the Maximum Ordinary Flood (*Máxima Crecida Ordinaria - MCO*).
- Easement Zone (SERV), defined as a 5 m-wide buffer surrounding the DPH. This zone is established to guarantee access for inspection, maintenance, and conservation activities. Permanent constructions are strictly forbidden, and agricultural practices are heavily restricted (e.g., tree planting is not allowed).
- Police Zone (POL), defined as a 100 m-wide buffer surrounding the DPH. Within this zone, land-use activities and construction works are subject to specific administrative controls and authorizations.

Figure 3.11 illustrates the spatial distribution of the three regulatory zones within the municipality of Sot de Chera. To evaluate changes in the delineation of the hydraulic public domain, a historical DPH layer representing the First Cycle of the SNCZI was included in the analysis [59]. This dataset represents the previous official delimitation before the recent post-DANA update.

Cadastral parcel data

Cadastral parcel boundaries were obtained through the Spanish INSPIRE Cadastral Downloader [60], which provides open-access cadastral information compliant with the INSPIRE Directive. The downloaded dataset includes rural cadastral parcels located within the municipality of Sot de Chera and constitutes the basic spatial unit used in the analysis.

Each parcel is associated with a set of attributes, including its geographic coordinates, parcel area, and the National Cadastral Reference (Referencia Catastral), which uniquely identifies each cadastral unit within the Spanish cadastral system. These attributes were used to spatially locate the parcels, quantify the extent of affected land, and link the results of the spatial analysis to individual cadastral records.

GIS processing and Parcel exposure analysis

The spatial analysis was performed in a Geographic Information System (GIS) environment. Cadastral parcels and hydraulic regulation layers were projected in the same coordinate reference system (ETRS89 / UTM Zone 30N, EPSG:25830) to ensure geometric consistency during spatial analyses.

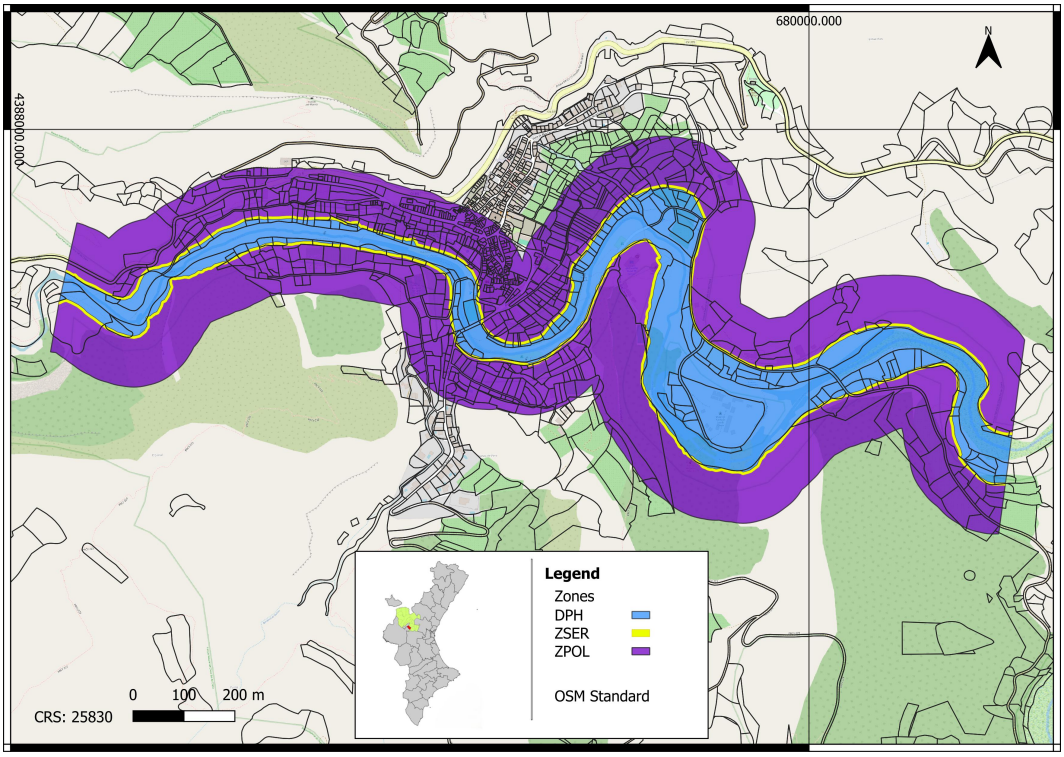

Figure 3.11: Spatial distribution of the three regulatory zones within the municipality of Sot de Chera. The Hydraulic Public Domain (DPH) is shown in blue, the Easement Zone (SERV) in yellow, and the Police Zone (POL) in purple.

Spatial overlay operations were used to compare the historical and current DPH delineations and to identify the portions of cadastral parcels included within the DPH, SERV, and POL regulatory zones. First, the historical and current DPH layers were compared to quantify the spatial changes resulting from the post-DANA revision of the hydraulic public domain. The surface difference between the two delineations was calculated to evaluate the extent of the updated DPH. Subsequently the cadastral parcels were intersected with each regulatory zone to identify the portions of each parcel falling within the corresponding regulated area. The area of intersection was then calculated for each parcel and for each regulatory zone separately.

For each cadastral parcel, the following indicators were computed:

- area included within the historical (pre-DANA) DPH;
- area included within the current (post-DANA) DPH;
- area included within the SERV zone;

- area included within the POL zone;
- percentage of parcel area included within each regulatory zone relative to the total parcel area;
- variation in parcel area included within the DPH between the pre-DANA and post-DANA delineations, expressed both in square metres and as a percentage of the total parcel area.

To compare the historical and current DPH frameworks, parcel-level exposure was calculated for both delineations. Parcels intersecting the DPH were grouped into five exposure classes according to the percentage of parcel area included within the hydraulic public domain:

- $< 25\%$;
- $25-50\%$;
- $50-75\%$;
- $75-99\%$;
- 100%.

For each exposure class, the number of affected parcels and the total intersected area were calculated for both the historical and current DPH datasets, allowing a direct comparison of parcel exposure before and after the DPH revision. In addition, for each regulatory zone (DPH, SERV, and POL), the total number of affected parcels, the total intersected area, and the average percentage of parcel area affected were calculated.

Finally, a cumulative exposure indicator was computed to quantify the overall extent of hydraulic regulation. This indicator was derived from the geometric union of the DPH and POL zones. Since the Police Zone fully encompasses the Easement Zone, the latter was not considered separately in order to avoid double counting. The results were summarized through a series of thematic maps and associated attribute tables.

Chapter 4

Results

4.1 Water Quality Results

4.1.1 Annual historical analysis

The following section presents the results of the long-term historical analysis of water quality in the Río Sot, based on the annual dataset provided by the CHJ monitoring station JUH403.

Overall a general state of compliance of the stream with legal thresholds for almost all monitored chemical-physical, biological, and anthropogenic parameters is assessed. Basic indicators such as pH (consistently ranging within a slightly alkaline interval between 7.5 and 8.2), nutrients (nitrates and phosphates), and heavy metals (hexavalent chromium, copper, and iron) remain consistently and significantly below regulatory limits throughout the entire study period. Microbiological load (total and fecal coliforms) is also generally under control, although an isolated peak was observed in 2009 (see Figure 4.1).

The main historical anomalies concern nitrites, which exhibit an unusual peak in 2013, and total chlorine, whose median values exceed the regulatory threshold. However, a more detailed examination of the data about total chlorine revealed that these values correspond to the instrument's limit of detection (LOD), which is higher than the relevant regulatory standard. Consequently, this apparent exceedance is not due to real environmental contamination, but to an analytical artefact (see Figure 4.2).

Regarding agricultural pressures, glyphosate shows an almost constant behaviour, remaining below the detection limit, although it is interrupted in 2020 by a single anomalous value significantly above the regulatory threshold.

For the temporal trend analysis, the approach combined annual boxplot visualisation with the non-parametric Seasonal Kendall test, in order to isolate the structural trends of the water body from seasonal variability and background noise.

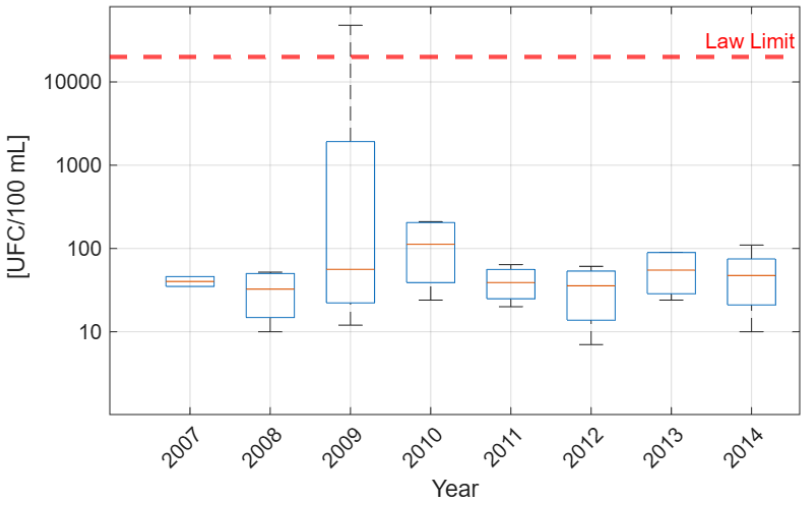

(a) Annual boxplots of Faecal Coliforms (Log scale).

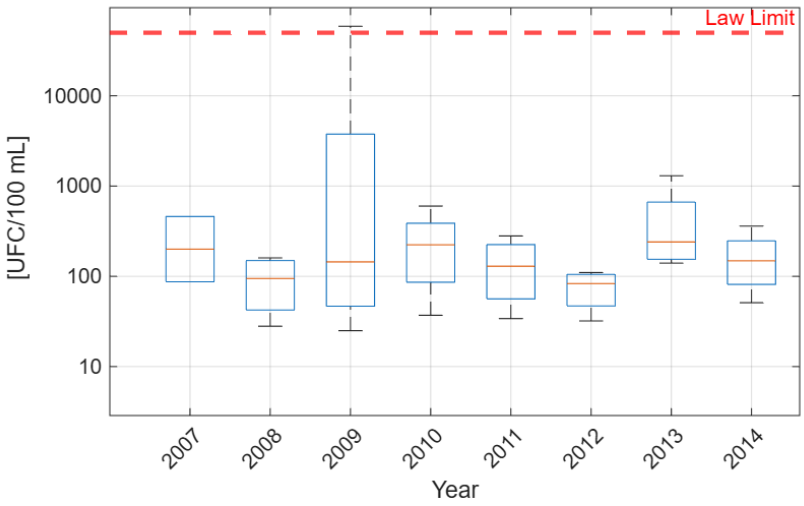

(b) Annual boxplots of Total Coliforms (Log scale).

Figure 4.1: Microbiological parameter concentrations at the Río Sot monitoring station (JUH403). The annual boxplots cover the last 20 years of historical data, highlighting the isolated microbial peak observed in 2009.

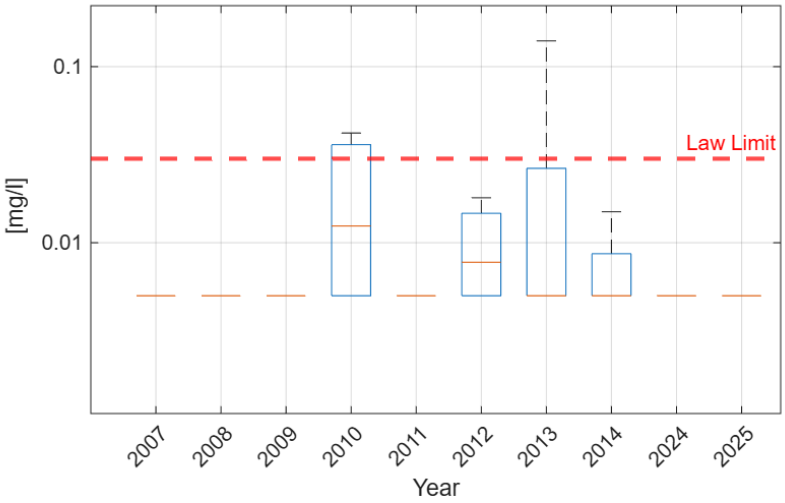

(a) Annual boxplots of Nitrites (Log scale).

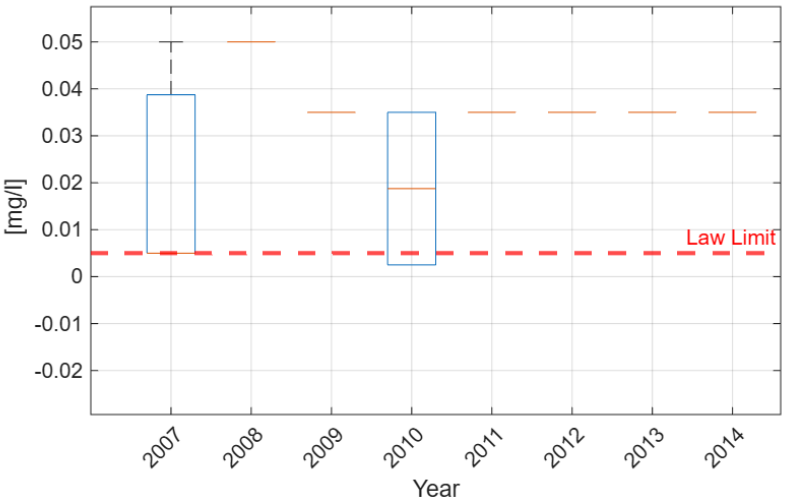

(b) Annual boxplots of Total Chlorine.

Figure 4.2: Annual historical boxplots of water quality parameters showing critical thresholds or apparent regulatory exceedances. The total chlorine values reflect the analytical limit of detection (LOD) rather than actual environmental contamination. The boxplots cover the last 20 years of data.

The results of the seasonal Mann-Kendall trend analysis indicate that the majority of chemical and nutrient parameters (including nitrates, phosphates, and ammonium) do not exhibit statistically significant temporal trends ($p > 0.05$). In contrast, statistically significant positive trends ($p < 0.05$) were detected for two key variables: water temperature (+0.071 °C/year) and chemical oxygen demand (+0.056 mg/L/year).

In fact, as shown in the corresponding boxplots, the interannual evolution shows a gradual increase in water temperature and organic matter over the last two decades. These trends suggest a combined effect of climate variability and seasonal human pressure on the Río Sot before the 2024 flood event.

The Seasonal Mann-Kendall analysis reveals that these trends vary between seasons. Water temperature increases slightly more in the cold season (+0.083 °C/year) than in the warm season (+0.062 °C/year), suggesting stronger winter warming. In contrast, chemical oxygen demand increases more in the warm season (+0.083 mg/L/year) than in the cold season (+0.05 mg/L/year), indicating higher organic matter levels during summer, likely due to lower dilution and higher human pressure.

Finally, a relevant finding concerns biochemical oxygen demand (BOD_5). This parameter does not display a statistically significant overall trend because most values before 2023 are below the detection limit. However, the boxplots show a clear change in 2023–2024, with higher values of biodegradable organic matter. Figure 4.3 shows the boxplot of these parameters and Table 4.1 the results of the relative Seasonal Kendall tests.

Parameter	***p*-value**	**Global Slope**	**Slope C**	**Slope W**
Temperature	0.036	0.071	0.083	0.062
COD	0.002	0.056	0.050	0.083
BOD_5	0.080	0.000	0.000	0.000

Table 4.1: Seasonal Mann-Kendall trend analysis results for Temperature, COD, and BOD_5. Global Slope, Slope C, and Slope W denote the global and seasonal (cold and warm) Sen's slope estimates, respectively. Highlighted green cells indicate statistically significant trends ($p < 0.05$).

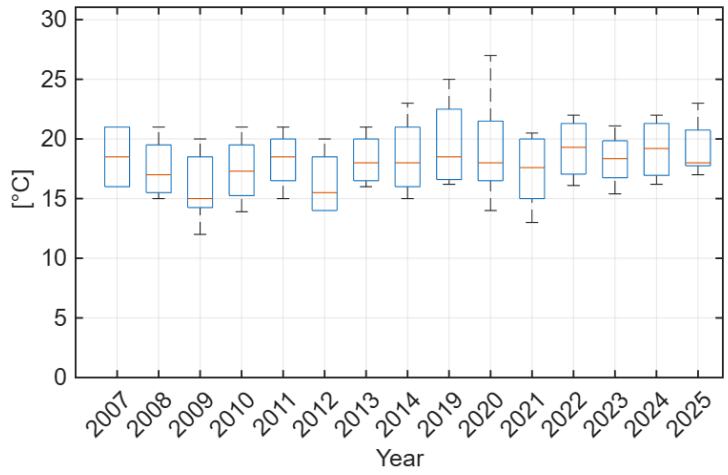

(a) Annual boxplots of Water Temperature.

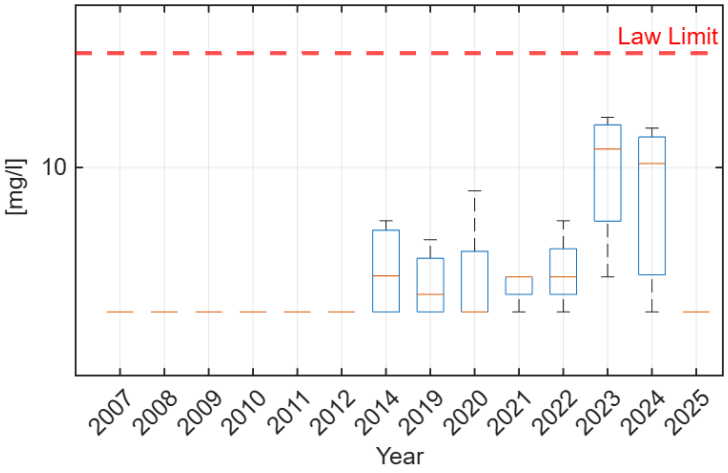

(b) Annual boxplots of COD (Log scale).

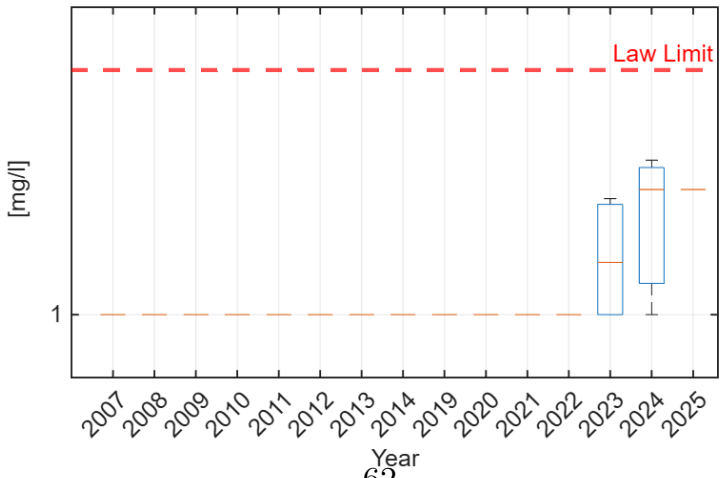

(c) Annual boxplots of BOD_5, Log scale.

Figure 4.3: Interannual evolution and historical trends of Water Temperature, COD, and BOD_5 over the last 20 years. The plots show the gradual long-term shifts in thermal and organic matter baselines in the last period.

Seasonal historical analysis

Hydrochemical baseline conditions The river exhibits generally stable hydrochemical conditions throughout the year. Electrical conductivity and chloride concentrations show no significant seasonal variation, indicating a dominant control by water–rock interactions at catchment scale. In contrast, pH displays a small but statistically significant seasonal difference (Mann–Whitney test $p = 0.034$), with slightly lower median values in the warm period. Water temperature shows the expected strong seasonal signal (Mann–Whitney test $p = 2.22 \times 10^{-8}$), confirming the sensitivity of the dataset to climatic forcing.

Nutrient concentrations

No statistically significant seasonal differences are observed for nutrient parameters, indicating stable background conditions across the year. Nitrate concentrations remain relatively constant, although higher dispersion is observed during the warm season. Ammonium levels are consistently low in both periods, while nitrites show greater variability, with occasional exceedances of regulatory thresholds occurring only in the warm season. Phosphate concentrations remain uniformly low and well below regulatory limits in both seasons, with only isolated minor peaks.

Organic pollution indicators

Indicators of organic pollution do not show significant seasonal differences. Biochemical oxygen demand (BOD_5) and chemical oxygen demand (COD) remain generally low, with slightly higher variability during the warm period. Dissolved oxygen saturation remains within typical ranges, although isolated low values are observed in summer, without affecting overall seasonal patterns. Total chlorine shows comparable distributions between seasons, with apparent exceedances attributable to analytical detection limits rather than environmental conditions.

Microbiological parameters

Total coliforms show a statistically significant increase during the warm period (Mann–Whitney test $p = 0.001$), while faecal coliforms do not exhibit a significant seasonal trend. However, isolated extreme values are observed in summer, indicating episodic contamination events not reflected in median conditions.

Metals and trace elements

Metal concentrations remain generally low and stable across seasons. Hexavalent chromium is consistently below the limit of quantification, while iron shows minor variability without seasonal differences. Copper does not exhibit a statistically

significant trend, although higher dispersion and occasional elevated values are observed during the warm period. Glyphosate concentrations remain consistently below detection limits, with a single isolated exceedance recorded during the warm season. Total suspended solids show no seasonal differences but occasional high-magnitude outliers in both periods.

Synthesis of main results Overall, the statistical analysis indicates a predominantly stable hydrochemical regime, with significant seasonal differences limited to pH and water temperature. Most chemical variables, including nutrients, major ions, organic pollution indicators, and metals, do not show robust seasonal variability, supporting the presence of a relatively stable baseline water quality.

In contrast, microbiological parameters show a clearer seasonal response: total coliforms exhibit a statistically significant increase during the warm period, while faecal coliforms do not show significant seasonal differences but present occasional extreme values, particularly in summer.

Beyond statistical significance, a few consistent patterns emerge across parameters. Major ions (electrical conductivity and chlorides) remain stable throughout the year, confirming a strong geochemical control at catchment scale. Nutrient concentrations are generally low, with occasional summer-driven increases in variability, particularly for nitrites. Organic matter indicators show stable central tendencies, although with higher dispersion during the warm period. Metal concentrations are uniformly low and show no evidence of seasonal structuring.

From a methodological perspective, results should be interpreted considering the nature of the monitoring design. Particularly, it must be highlighted that historical microbiological datasets (Total and Faecal Coliforms) are limited to the 2007–2015 period, resulting in a lack of recent long-term baselines for fecal contamination. Furthermore, the wastewater discharge is a highly variable point source, potentially generating short-duration contamination peaks that may not be captured by periodic sampling. In addition, the monitoring station (CHJ JUH403) is located several kilometers ($\sim$7 km) downstream of the discharge point. This spatial separation, together with dilution processes and riparian vegetation (more developed prior to the 2024 flood event), likely attenuates localised pollution signals, leading to a smoothing of short-term impacts in the recorded dataset.

Table 4.2 summarizes the parameters with statistically significant Mann–Whitney test results and their corresponding p-values, while their seasonal boxplots are depicted in Figure 4.4. All other seasonal charts are available in Appendix B.

4.1.2 Field Monitoring data

This section presents the results of two field monitoring campaigns conducted along the Reatillo River at Sot de Chera during autumn 2025 (November–December) and

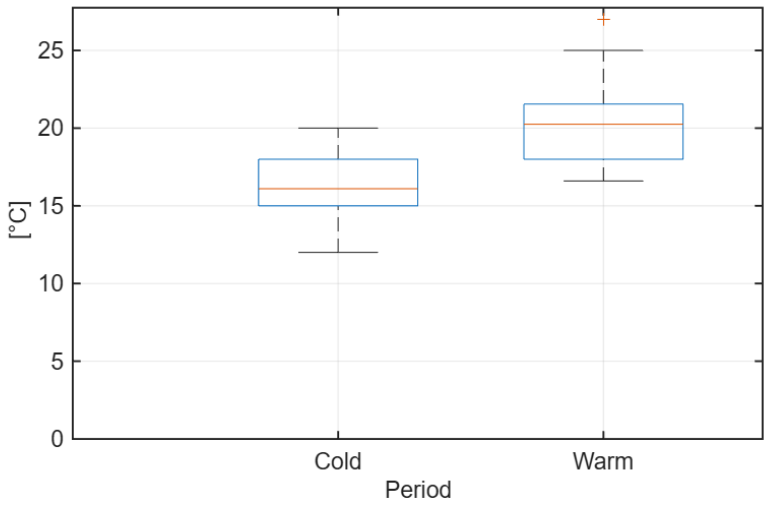

(a) Water Temperature (°C)

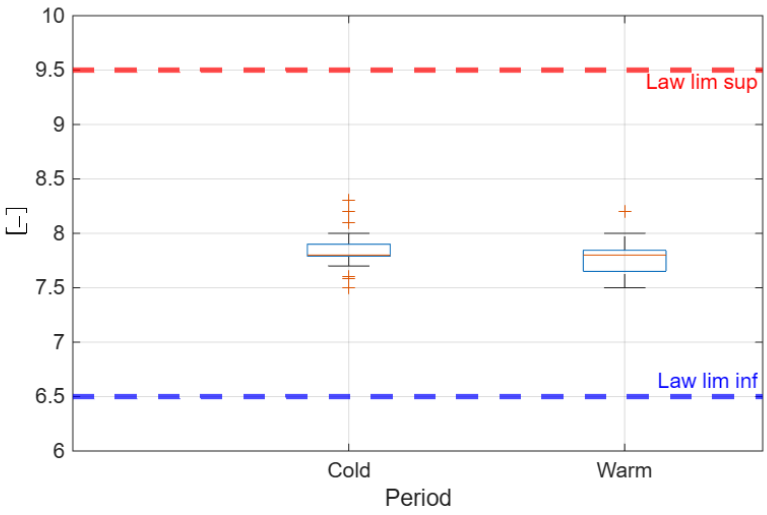

(b) pH units

Figure 4.4: Seasonal boxplots of hydrochemical and microbiological parameters exhibiting statistically significant differences ($p < 0.05$) between the warm and cold periods at the JUH403 station (continues on next page).

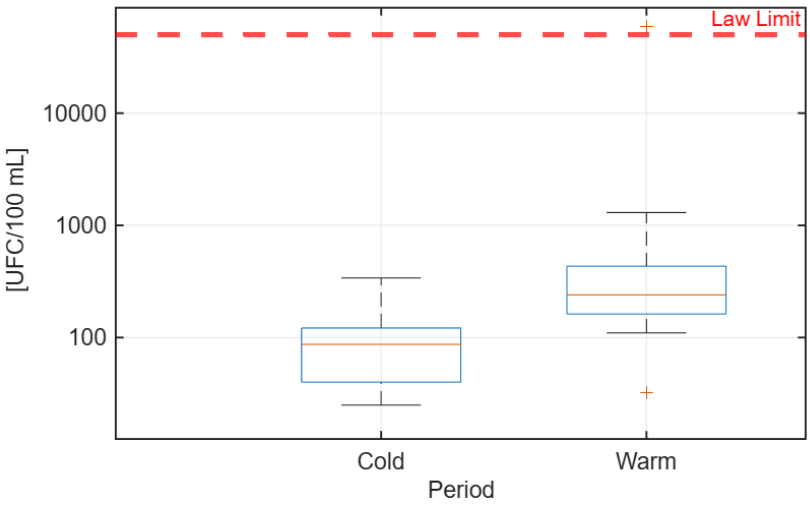

(c) Total Coliforms (Log scale, CFU/100 mL)

Figure 4.4: Seasonal boxplots of hydrochemical and microbiological parameters exhibiting statistically significant differences ($p < 0.05$) between the warm and cold periods at the JUH403 station, according to the Mann–Whitney U test (concluded).

Table 4.2: Summary of CHJ JUH403 monitoring parameters showing statistically significant seasonal differences according to the Mann–Whitney U test. W = warm season; C = cold season.

Parameter	**Unit**	**Median (W)**	**Median (C)**	***p*-value**	**W > C**
Water Temperature	°C	20.25	16.10	2.22×10^{-8}	Yes
Total Coliforms	CFU/100 mL	240	87	0.001	Yes
pH	–	7.80	7.80	0.034	No

spring 2026 (April 2026).

Water quality parameters were analysed along a longitudinal upstream–downstream gradient in order to identify spatial variations associated with both natural processes and anthropogenic pressures. For this purpose, the river was divided into distinct hydrochemical sectors (upstream, village, downstream recovery sector, and lower reaches).

The longitudinal monitoring campaigns revealed a consistent spatial organization of water quality along the Río Sot, with localised perturbations associated with anthropogenic inputs and natural hydrogeological features. Despite some seasonal differences in concentration levels, the overall spatial patterns observed during autumn 2025 and spring 2026 were remarkably similar. Baseline electrical conductivity remained remarkably stable along the river profile within each campaign, averaging around 400 $\mu S\,cm^{-1}$ during the autumn survey and increasing slightly to approximately 450–500 $\mu S\,cm^{-1}$ in spring, indicating a modest seasonal shift in hydrochemical conditions

The upstream reach before the village (P1–P3) exhibited the first signs of anthropogenic influence. Nutrient concentrations were already elevated relative to downstream background conditions, particularly nitrates (up to 10–25 mg/L) and nitrites, while occasional detections of iron, copper, and hexavalent chromium suggest localised inputs potentially associated with sediment mobilization works and diffuse agricultural activities. Simultaneously, decreases in pH and alkalinity between P1 and P2 indicate temporary alterations of the carbonate equilibrium.

The most pronounced anthropogenic signal was recorded at P4, immediately downstream of the urban wastewater outlet of Sot de Chera. Both campaigns showed increases in nitrogen species and halogens at this location, identifying the discharge as the main point source affecting river chemistry. The effect was particularly evident during spring, when ammonium reached 0.2 mg/L, nitrites increased to 1–5 mg/L, and nitrates reached approximately 10–25 mg/L, representing the highest nutrient concentrations observed along the monitored reach. pH also increased markedly, reaching values between 8.4 and 8.8.

Downstream of the village (P5–P8), water quality progressively recovered. The tributary inflow at P6 generated a clear dilution signal characterized by reductions in electrical conductivity, alkalinity, and nutrient concentrations, with EC reaching the minimum value recorded during the monitoring campaigns. From P7 onwards, most parameters gradually returned toward upstream background values, indicating a substantial natural attenuation capacity of the river system.

A second hydrochemical anomaly was observed at P10, where the contribution of the Las Toscas thermal spring modified the carbonate system, producing increases in pH, alkalinity, and carbonate hardness. During autumn, KH reached approximately 250 mg/L, the highest value measured along the river, while nitrate

concentrations increased to 10–25 mg/L, likely reflecting the influence of surrounding agricultural land. Downstream at P11, most parameters partially returned toward pre-disturbance conditions, suggesting rapid hydrochemical re-equilibration.

Overall, the spatial distribution of water quality parameters highlights alternating phases of anthropogenic disturbance and natural recovery along the river corridor. The urban wastewater outlet at P4 represents the main localised source of contamination, whereas tributary inflows and natural hydrological processes promote downstream dilution and recovery. Seasonal differences between autumn and spring were generally limited, indicating that the dominant controls on river chemistry are primarily spatial rather than seasonal.

It should be noted that the wastewater discharge at P4 is likely highly variable due to the small population of Sot de Chera. As a result, short-term pollution peaks may not be fully captured by punctual sampling. The presence of a brownish-olive diatom biofilm near the outlet suggests episodic organic enrichment potentially stronger than measured during the campaigns, particularly during weekends or periods of increased tourist activity.

The occurrence of hexavalent chromium and copper should be interpreted with caution due to the relatively broad detection intervals associated with the colorimetric analytical method. Although their sporadic presence may indicate localised contamination sources, further investigations using higher-resolution analytical techniques would be required to confirm their environmental significance. In contrast, lead, mercury, and cyanuric acid were never detected during the monitoring campaigns.

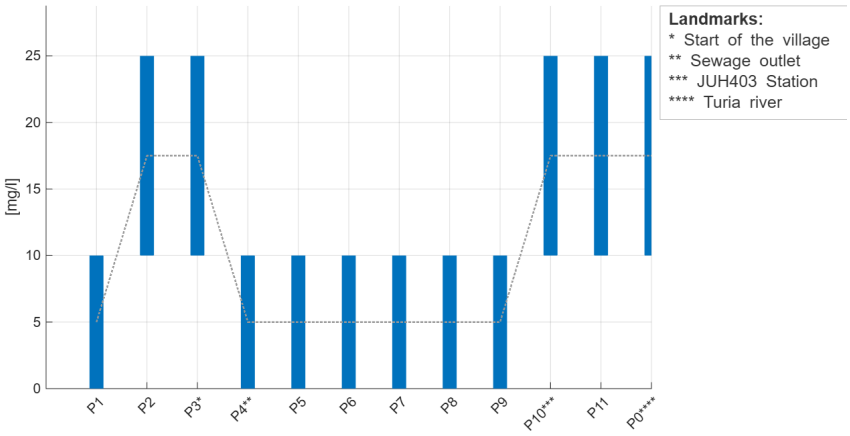

(a) Nitrates - Autumn 2025

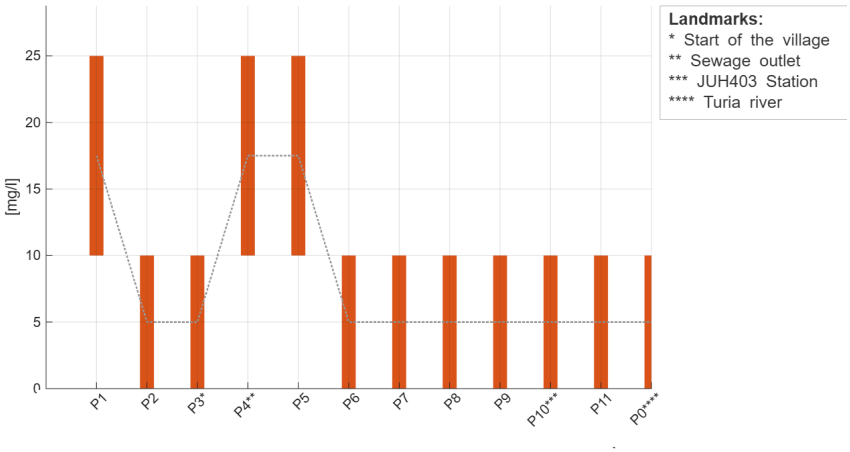

(b) Nitrates - Spring 2026

Figure 4.5: Longitudinal trends of Nitrates along the river sector in Autumn (blue) and Spring (orange).

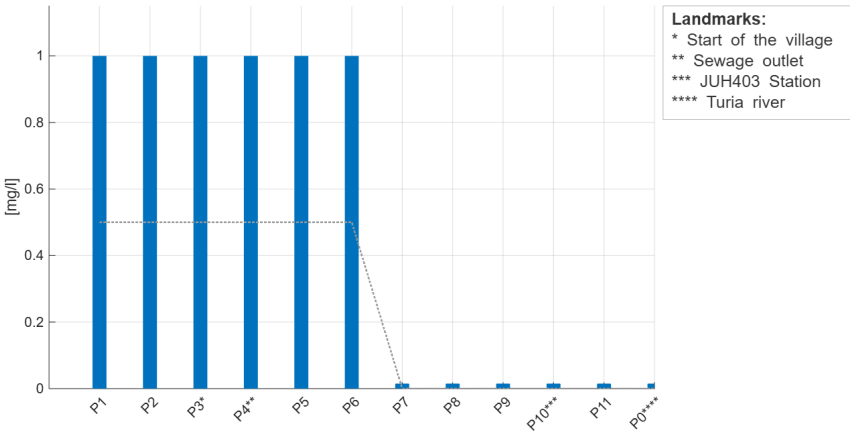

(a) Nitrites - Autumn 2025

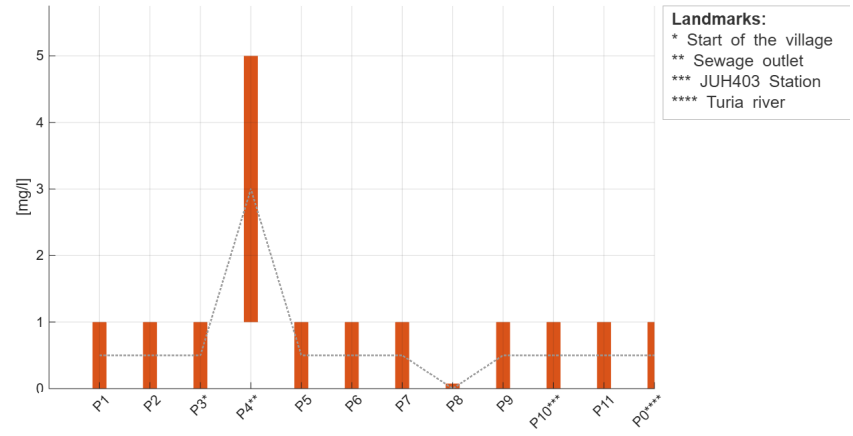

(b) Nitrites - Spring 2026

Figure 4.6: Longitudinal trends of Nitrites along the river sector in Autumn (blue) and Spring (orange).

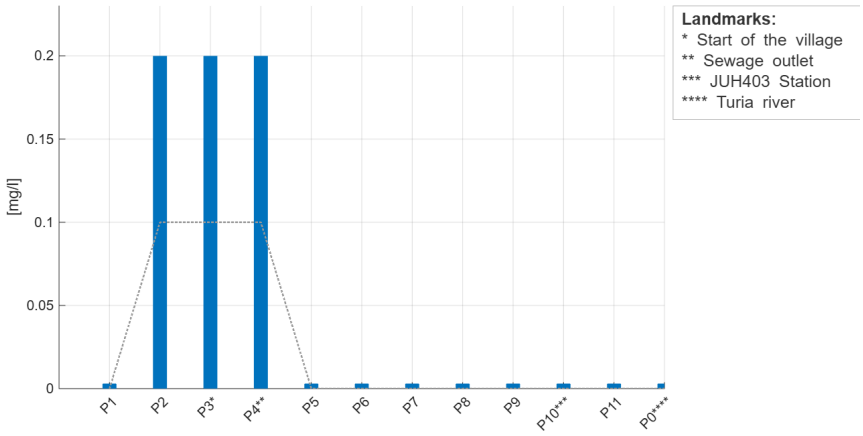

(a) Ammonia - Autumn 2025

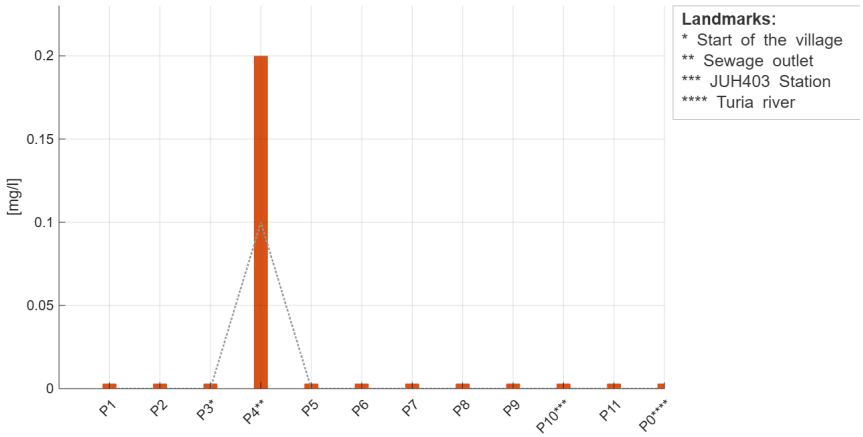

(b) Ammonia - Spring 2026

Figure 4.7: Longitudinal trends of Ammonia along the river sector in Autumn (blue) and Spring (orange).

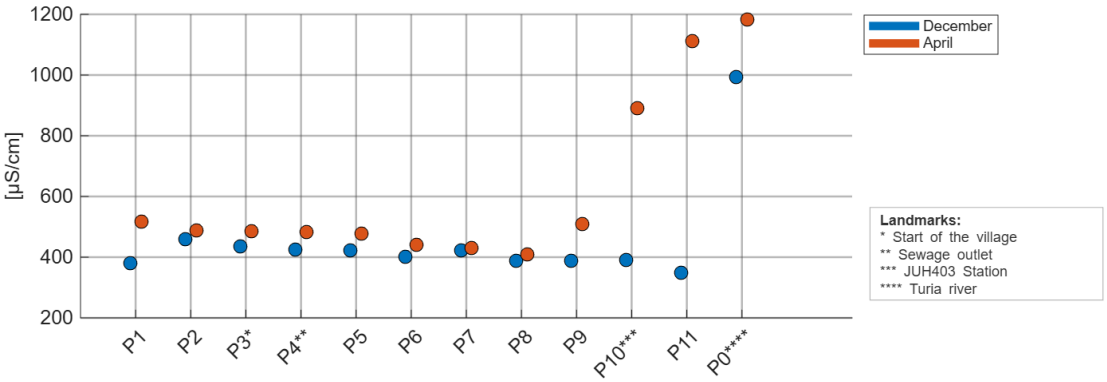

(a) Electrical Conductivity (Autumn vs Spring)

Figure 4.8: Longitudinal trends of Electrical Conductivity (EC) along the river sector in Autumn (blue) and Spring (orange).

4.1.3 Comparison between field monitoring data and historical data

Overall, the hydrochemical conditions observed at Point P10 remain largely consistent with the historical variability of the basin. Water temperature was approximately 15.3°C during the autumn campaign and 17.4°C during the spring campaign, both close to the historical seasonal medians. Electrical conductivity remained around 900 μS/cm in both campaigns, falling within the typical historical range observed at the JUH403 station.

Most nutrient concentrations were also compatible with historical conditions. Ammonium remained close to zero during both monitoring campaigns. Nitrate concentrations, however, showed a moderate increase during autumn, reaching approximately 10–25 mg/l at P10, compared with a historical median of about 4.5 mg/l for the cold season. Despite this increase, measured values still fall within the broader historical variability observed at the station. During spring, nitrate concentrations returned to values close to the historical median. Nitrite concentrations remained generally low, although spring measurements were slightly higher than the near-zero median of the historical dataset.

The increase of nutrients concentrations (nitrates and nitrites) coincides with the hydrochemically distinct P10 reach, which is influenced both by downstream agricultural areas and by the inflow of Las Toscas and of a thermal spring.

The main difference between field observations and historical records concerns total chlorine. During the autumn campaign, concentrations at P10 reached approximately 3 mg/l, whereas historical measurements at the JUH403 station are consistently close to zero in both seasons and show virtually no long-term variability. In contrast, spring measurements at P10 returned to values comparable with the historical record.

Overall, the comparison suggests that the hydrochemical characteristics of the Río Sot downstream of Sot de Chera remain broadly comparable to pre-flood conditions. Although some localised anomalies were observed, particularly for nitrates and total chlorine during the autumn campaign, field measurements generally fall within the historical range of variability recorded at the JUH403 station.

However, these results should be interpreted considering several methodological limitations: the monitoring campaigns were conducted during periods of relatively low population pressure in Sot de Chera, whereas wastewater inputs are likely characterized by irregular and short-lived peaks that may not be captured through punctual sampling. Furthermore, the JUH403 station is located downstream of the urban area and integrates the effects of dilution, natural attenuation processes, and riparian ecosystem functioning over several kilometres of river channel.

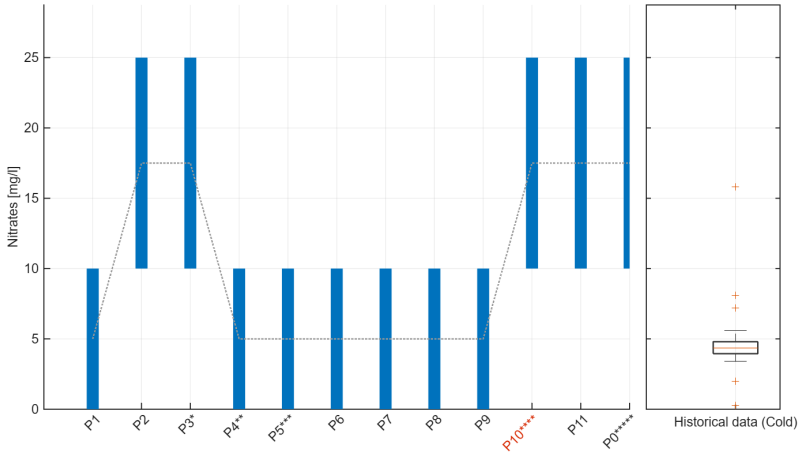

(a) Nitrates - Autumn 2025

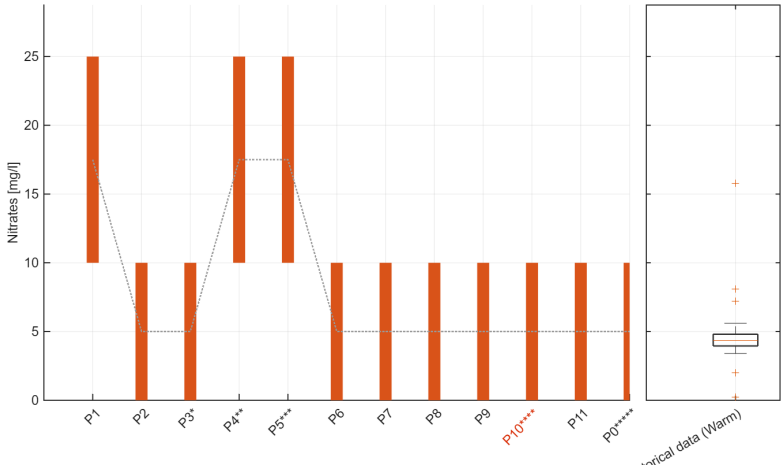

(b) Nitrates - Spring 2026

Figure 4.9: Longitudinal trends of nitrate concentrations during autumn (blue) and spring (orange) compared with the respective seasonal boxplots at the JUH403 monitoring station (located near P10). Sampling points denote: P3 (start of the village), P4 (sewage outlet), P5 (end of the village), P10 (JUH403 station), and P0 (Turia river confluence).

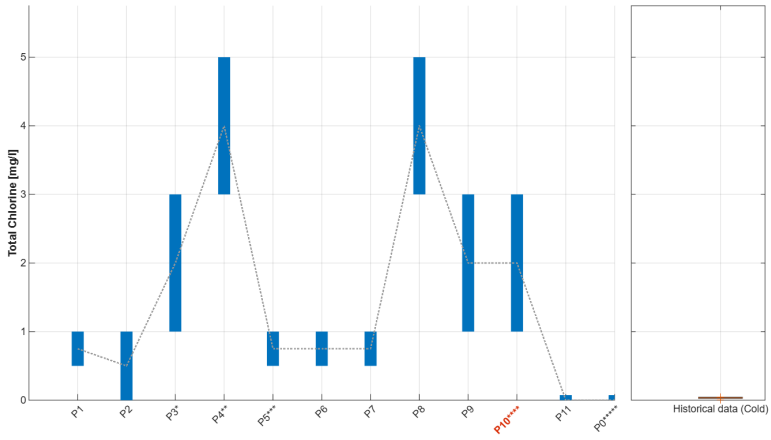

(a) Total Chlorine - Autumn 2025

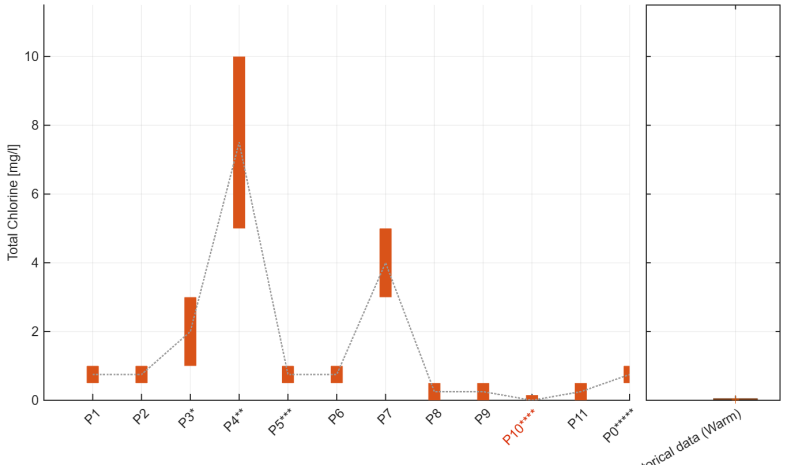

(b) Total Chlorine - Spring 2026

Figure 4.10: Longitudinal trends of Total Chlorine concentrations during autumn (blue) and spring (orange) compared with the respective seasonal boxplots at the JUH403 monitoring station (located near P10). Sampling points denote: P3 (start of the village), P4 (sewage outlet), P5 (end of the village), P10 (JUH403 station), and P0 (Turia river confluence).

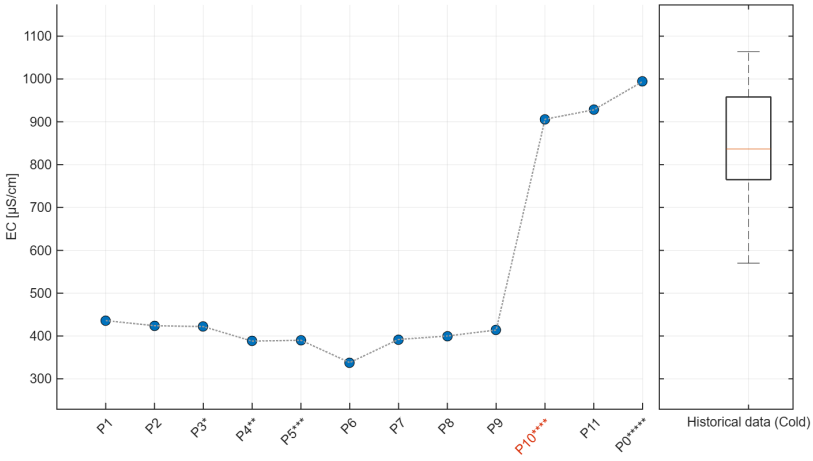

(a) Autumn 2025

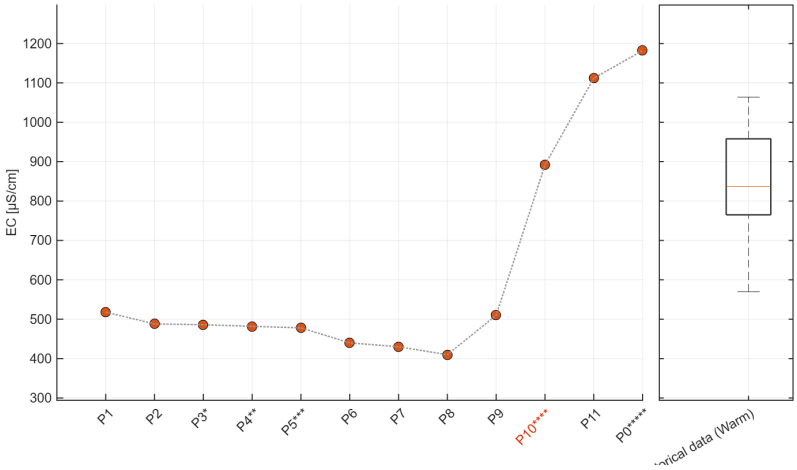

(b) Spring 2026

Figure 4.11: Longitudinal trends of Electrical Conductivity during autumn (blue) and spring (orange) compared with the respective seasonal boxplots at the JUH403 monitoring station (located near P10). Sampling points denote: P3 (start of the village), P4 (sewage outlet), P5 (end of the village), P10 (JUH403 station), and P0 (Turia river confluence).

4.2 Riparian Vegetation

One year after the October 2024 DANA event, riparian vegetation within the municipal area of Sot de Chera shows clear signs of early-stage recovery, although spatial patterns remain highly heterogeneous across the study reach.

Overall, vegetation dynamics appear to be influenced by local geomorphology, substrate availability, hydrological conditions, and the distribution of surviving adult individuals acting as propagule sources. In addition, anthropogenic disturbances in selected reaches appear to significantly influence recolonisation trajectories.

4.2.1 Arboreal vegetation: Populus spp.

Poplar species exhibit a fragmented spatial distribution along the Río Sot. Recolonisation is mainly associated with recently deposited alluvial bars composed of fine and moist sediments, although establishment success varies significantly along the river corridor. Most individuals correspond to early-stage recruits (seedlings and juveniles), indicating recent establishment on newly available substrates. Upstream of the urban area, poplar continuity is interrupted by road restoration works along the Chera–Sot de Chera connection: earthmoving activities have modified local substrate conditions and reduced natural recruitment. In this sector, the main poplar nucleus is associated with surviving mature *Populus nigra* individuals located approximately 3 km upstream of the village. From the village downstream, active regeneration is observed across all studied poplar groups, with young individuals occupying recently formed alluvial deposits and in proximity to surviving adult trees. In the village, recruitment is also supported by replanting interventions. Downstream sectors, particularly near Las Toscas, show a marked reduction in poplar presence. This pattern is associated with confined channel morphology, steep and rocky slopes, and coarse substrates, which limit suitable conditions for establishment. In these reaches, the high abundance of *Arundo donax* further constrains recruitment occupying potential colonisation niches. Within the study area, *Populus alba* shows a more discontinuous and restricted distribution compared to the *P. nigra* / *P.* × *canadensis* complex, which represents the dominant poplar component. Most *P. alba* individuals are concentrated in the reach immediately downstream of the village, with a few additional scattered occurrences further downstream before Las Toscas.

Figure 4.13 illustrates the distribution of the two poplar groups along the Río Sot, while separate distribution maps for each taxon are presented in Appendix E.

(a)

(b)

(c)

Figure 4.12: Examples of Poplars dynamics along the Río Sot: (a) seedlings of *Populus alba*; (b) seedlings of *P. nigra* / *P.* × *canadensis* group; (c) survival pattern of a mature *Populus nigra* stand post-flood.

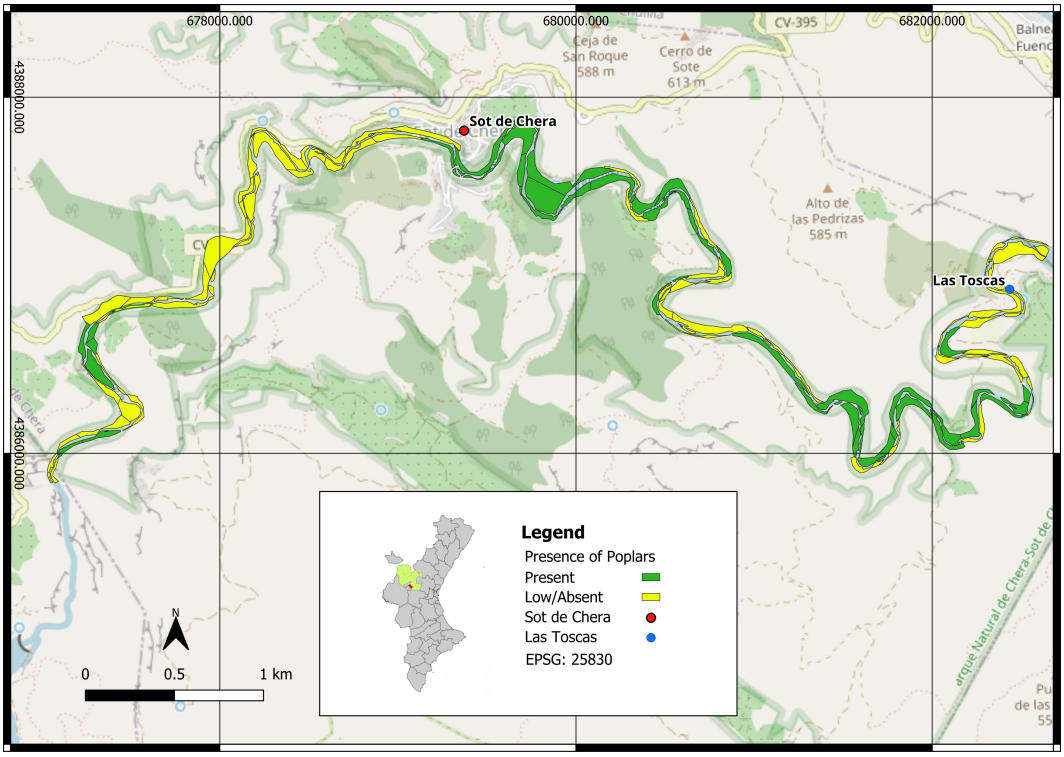

Figure 4.13: Spatial distribution of Poplars along the Rio Sot, November-December 2025.

4.2.2 Shrub layer: Nerium oleander and Tamarix spp.

Shrub species display higher post-disturbance resilience compared to arboreal vegetation. *Nerium oleander* shows a relatively continuous distribution along the river corridor, occurring across a wide range of geomorphic settings, from low alluvial zones to higher and more rocky, coarse-substrate areas. Both surviving mature individuals and new recruits are observed across most reaches. While much of the arboreal layer was removed by the flood, numerous mature oleander individuals survived, likely due to the flexibility of their stems, which allowed them to bend under flood flows rather than being uprooted (see Figure 4.14c).

This structural resistance contributed to the persistence of the species across disturbed sections of the channel.

Conversely, *Tamarix* spp. remains scarce and spatially fragmented, with almost only young individuals detected. The distribution maps of *Tamarix* spp. and *Nerium oleander* can be found in Appendix E.

(a)

(b)

(c)

Figure 4.14: Examples of shrub dynamics along the Río Sot: (a) young *Tamarix* individual; (b) young *Nerium oleander* individual; (c) mature *Nerium oleander* shrub surviving the flood, bent by flow forces.

Emergent aquatic vegetation, dominated by *Phragmites australis* and associated helophytic taxa (e.g. *Typha*, *Juncus*, *Eleocharis*), shows active recolonisation of low-energy environments. These communities are mainly concentrated in reaches characterised by reduced flow velocity, channel widening, and the presence of secondary channels within recently deposited alluvial sediments. Higher abundance is observed in the downstream portion of the study area, from the urban reach onwards, particularly in less accessible sections. In the upstream areas affected by

post-flood restoration works and associated anthropogenic disturbance, *Phragmites australis* is generally scarce, with the exception of a patch located a few kilometres upstream of the village. Figure 4.15 shows the spatial distribution of this group of species.

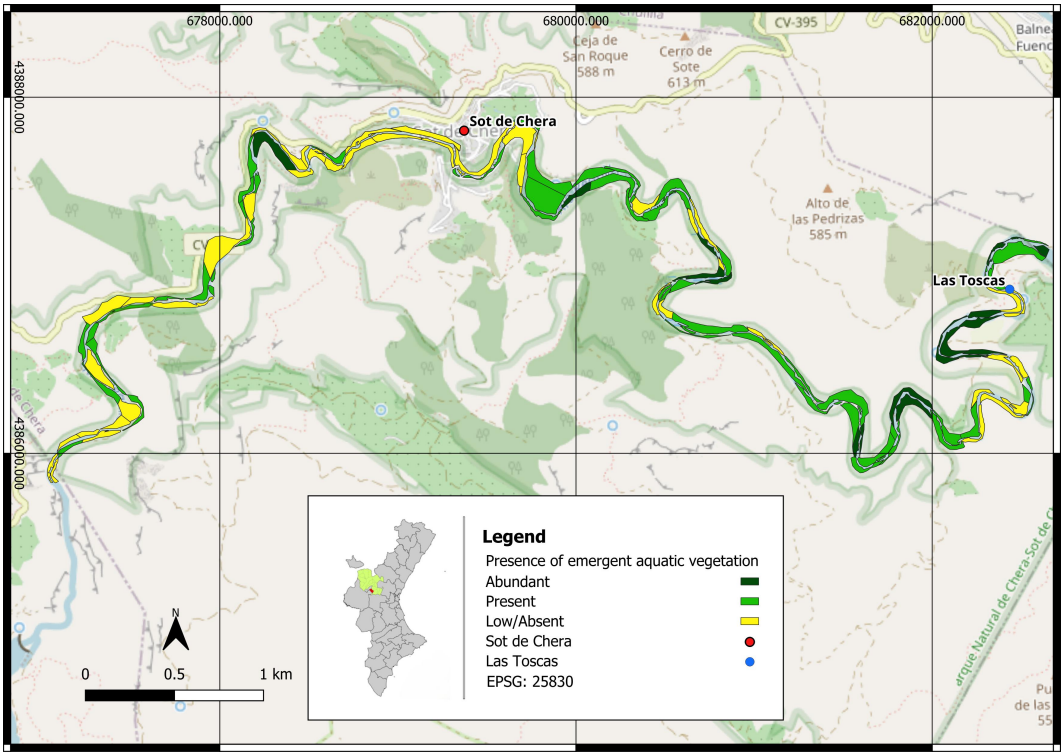

Figure 4.15: Spatial distribution of emergent aquatic vegetation along the Rio Sot, November-December 2025.

(a)

(b)

(c)

Figure 4.16: Examples of emergent aquatic vegetation along the Río Sot: (a) detail of helophytic taxa (e.g. *Typha* or *Juncus*); (b) specific clump of *Phragmites australis*; (c) overview of a large *Phragmites australis* patch colonising recently deposited alluvial sediments on the valley floor.

4.2.3 Arundo donax distribution

Spatial analysis highlights a progressive increase in *Arundo donax* presence downstream in both density and spatial continuity. Near Las Toscas, extensive monospecific stands occupy lower alluvial bars and lateral channel slopes. In this reach, the

steep and highly incised rocky morphology, together with the presence of water along channel margins and rock faces, appears to favour establishment in moist but well-drained microsites where other riparian species are less competitive. Further downstream, towards the confluence with the Turia River, *A. donax* reaches its highest cover, forming extensive patches on lateral bars. This area is not included in the mapping extent, which is limited to the municipal boundary of Sot de Chera. In mid-reach sections, *A. donax* frequently co-occurs with *Phragmites australis*, with evidence of competitive spatial segregation. This pattern is consistent with the ecological preferences reported in the literature, where *A. donax* is described as favouring moist or periodically saturated soils but generally not tolerating prolonged inundation [61]. Consequently, it establishes in zones where the substrate remains wet but not permanently flooded. In mixed stands, *P. australis* typically occupies areas closer to or within the water, while *A. donax* is found in slightly elevated, non-inundated zones immediately behind (see Figure 4.17). Figures 4.19a and 4.19b illustrate the distribution of *Arundo donax* within the study area.

Figure 4.17: Example of co-occurrence and spatial segregation of *Phragmites australis* and *Arundo donax* on a fluvial bar.

(a)

(b)

Figure 4.18: Examples of *Arundo donax* distribution along the Río Sot: (a) *Arundo donax* patch established along the river corridor; (b) downstream reach extensively colonized by *Arundo donax*.

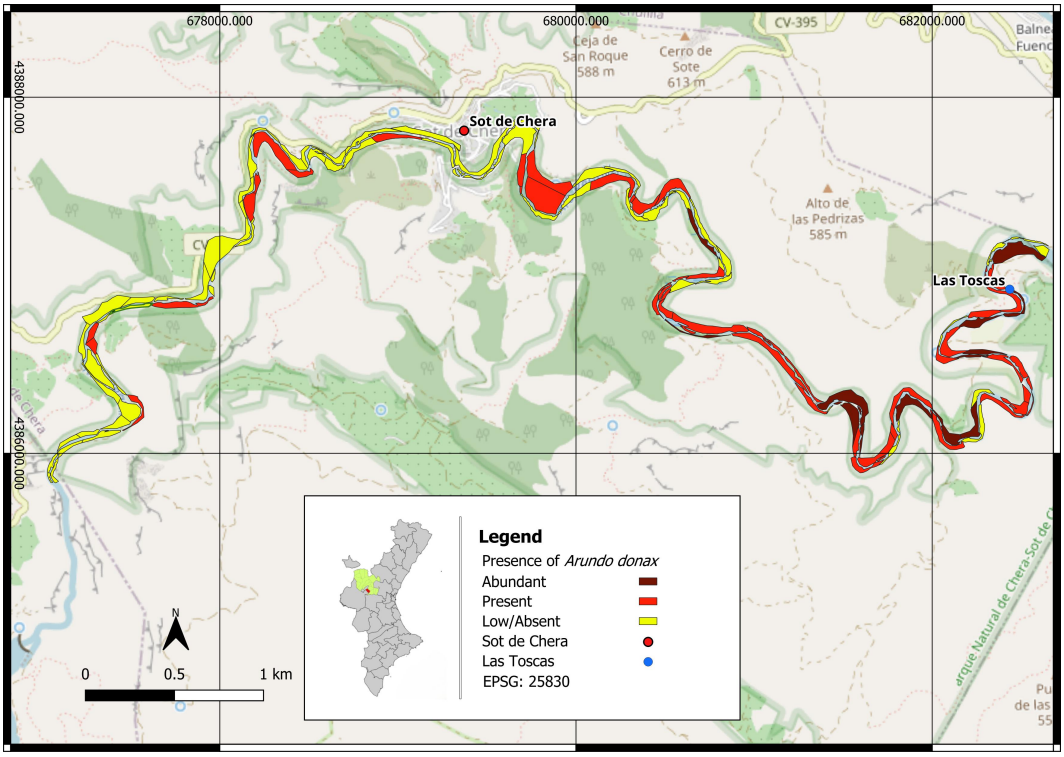

(a) Spatial distribution.

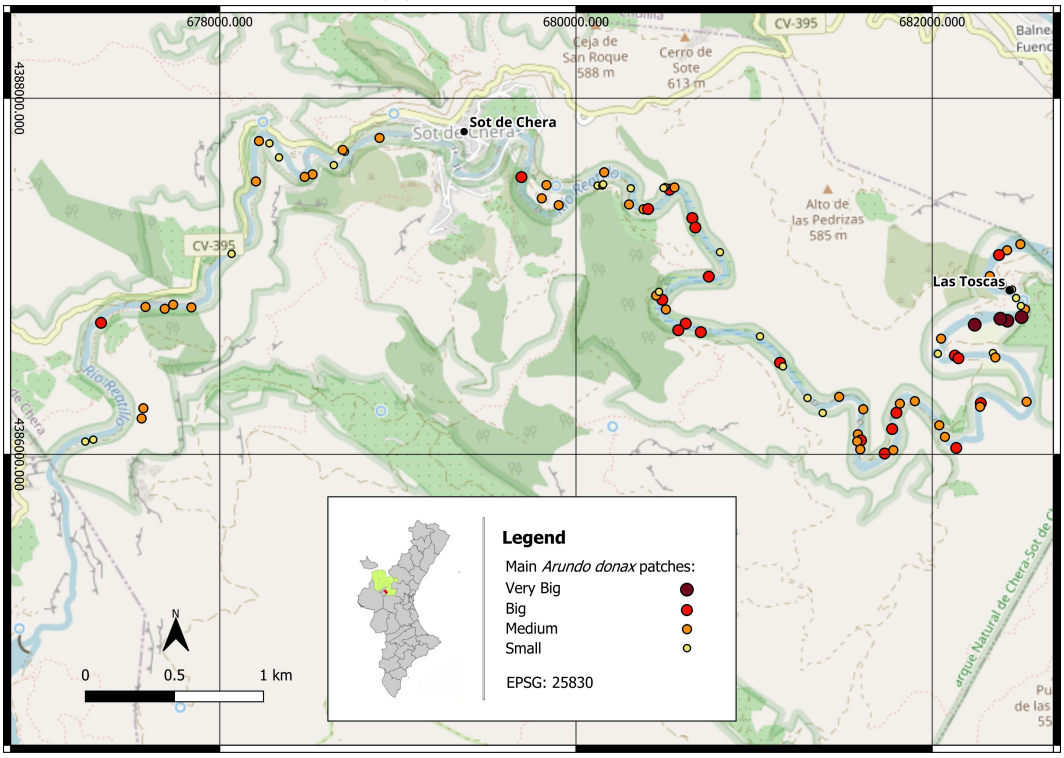

(b) Distribution of the main patches.

Figure 4.19: Mapping of *Arundo donax* along the Rio Sot, November-December 2025.

4.2.4 Summary of spatial patterns

Across the study reach, riparian vegetation shows a clear functional and spatial organisation driven by geomorphic setting and post-flood disturbance. Arboreal vegetation is largely restricted to suitable depositional environments and shows strong sensitivity to substrate conditions, and anthropogenic impacts. Shrub species, particularly *Nerium oleander*, display higher resilience and a broader ecological amplitude, occupying a wide range of geomorphic settings across the entire corridor. Emergent aquatic vegetation is mainly concentrated in low-energy reaches, showing reduced continuity in upstream disturbed sections and increasing abundance downstream of the urban area.

Finally, *Arundo donax* shows strong expansion capacity, with a downstream increase in both density and spatial continuity. A consistent pattern for all the analysed species is its reduced presence in upstream sectors affected by post-DANA road reconstruction and channel restoration works (Figure 4.20).

(a)

(b)

Figure 4.20: Pictures of channel and road restoration works (Chera–Sot de Chera connection) following the October 2024 DANA event.

4.3 Hydrodynamic simulation and spatial exposure

4.3.1 2D Hydraulic modelling

This section presents the results of the 2D hydrodynamic simulations for three discharge scenarios: base flow (1 m^3/s), ordinary high flow (60 m^3/s), and the extreme flood event (358 m^3/s). The analysis focuses on water depth, flow velocity, the hydraulic performance of the transverse structures, and the spatial extent of inundation, with particular attention to its relationship with the Hydraulic Public Domain (DPH) under the MCO scenario.

Base Flow Scenario (1 m^3/s)

Under the base flow scenario (1 m^3/s), the discharge remains entirely confined within the low-flow channel. The simulated wetted area closely matches the riverbed extent observed during the field surveys and in the 2025 post-event orthophoto (see Figure 4.21. Under these conditions, all transverse structures provide sufficient hydraulic capacity without inducing upstream backwater effects.

The discharge hydrographs extracted at the control sections confirm that the three fords operate efficiently. In all cases, the entire flow is conveyed through the culverts, while no discharge passes over the road surface. Consequently, the culverts remain under free-surface flow conditions, and no pressurisation or overtopping occurs.

Ordinary High Flow Scenario (60 m^3/s)

The ordinary high flow scenario (60 m^3/s), corresponding to the Máxima Crecida Ordinaria (MCO), exhibits a more complex hydraulic response. Maximum water depth reaches 3.08 m within the study reach. Comparison between the simulated inundation extent and the official post-DANA Hydraulic Public Domain (DPH) reveals a high degree of spatial agreement, although minor discrepancies are observed in some sectors. These differences are expected, as the legal DPH boundary is not defined exclusively by the modelled MCO extent but also incorporates geomorphological criteria.

Flow velocities increase considerably under this discharge. The maximum simulated velocity reaches 6.8 m/s, while the domain-average velocity is 1.37 m/s. The highest velocities are concentrated within narrow channel sections and at the six modelled crossing structures, where local flow constrictions occur (see Figure 4.22).

The hydraulic performance of the crossing structures was evaluated using the

(a) Maximum water depth (m)

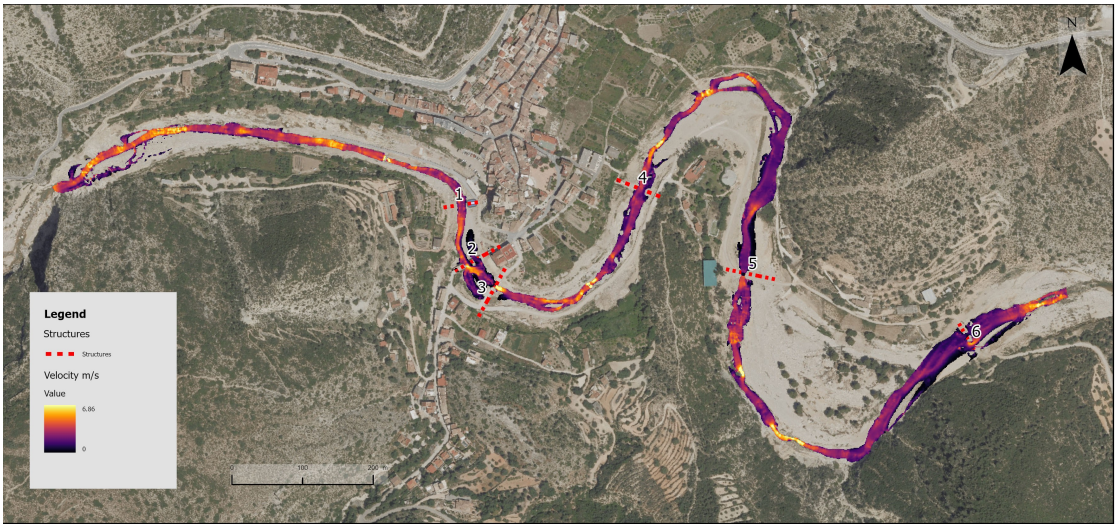

(b) Flow velocity (m/s)

Figure 4.21: Hydrodynamic simulation results for the base flow scenario (1 m^3/s). The spatial distribution of water depth (a) and flow velocity (b) is mapped. The transverse infrastructures are numbered as follows: (1) Pedestrian footbridge, (2) Road bridge, (3) Ford, (4) Second pedestrian footbridge, (5) Ford, and (6) Ford.

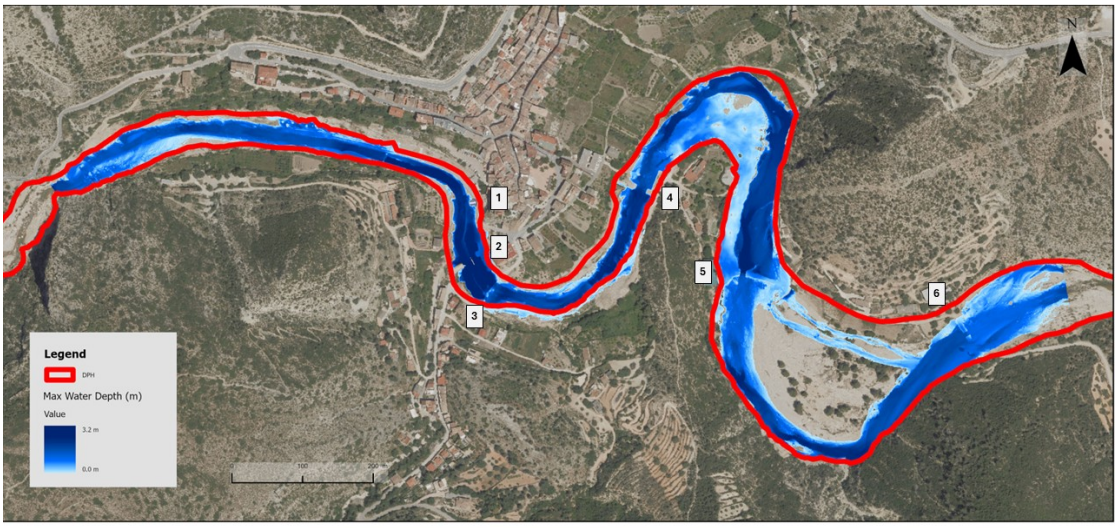

(a) Maximum water depth (m)

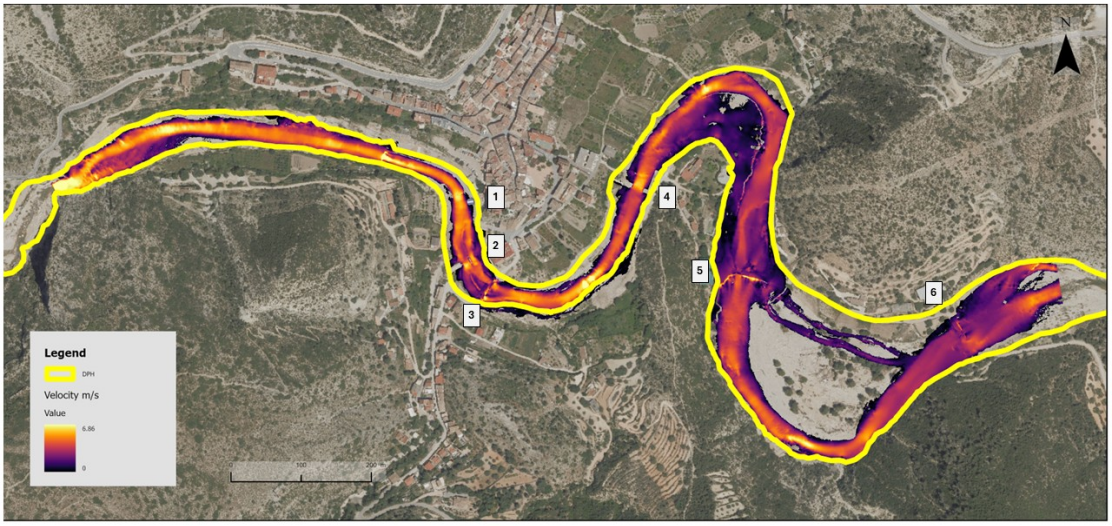

(b) Flow velocity (m/s)

Figure 4.22: Hydrodynamic simulation results for the ordinary high flow scenario (60 m^3/s). The spatial distribution of water depth (a) and flow velocity (b) is shown together with the official Hydraulic Public Domain (DPH). The transverse structures are numbered as follows: (1) Pedestrian footbridge, (2) Road bridge, (3) Ford, (4) Second pedestrian footbridge, (5) Ford, and (6) Ford.

hydrographs extracted at the control sections. While both pedestrian bridges and the road bridge maintain sufficient freeboard without deck overtopping, all three fords experience overtopping, indicating insufficient hydraulic capacity under the MCO discharge (see Figure 4.23 and Figure 4.24).

The upstream ford (Structure 3) receives a total discharge of 59.93 m^3/s, of which 25.34 m^3/s is conveyed through the culverts and 34.59 m^3/s passes over the road surface. This results in an overtopping depth of 0.7 m and an upstream–downstream water level difference of 1.71 m.

A similar hydraulic behaviour is observed at the intermediate ford (Structure 5). Approximately 17 m^3/s reaches the structure, with only 7 m^3/s conveyed through the culverts and the remaining 10.00 m^3/s overtopping the crossing. The resulting overtopping depth is 0.53 m, while the upstream–downstream water level difference reaches 0.70 m.

At the downstream ford (Structure 6), the total incoming discharge is 25.61 m^3/s. Only 0.84 m^3/s is conveyed through the culverts, whereas almost the entire flow (24.77 m^3/s) passes over the road surface. The overtopping depth was 0.42 m and the upstream–downstream water level difference was 0.11 m.

Overall, the MCO simulation identifies the three fords as the most hydraulically vulnerable structures within the study reach. In contrast, both pedestrian bridges and the road bridge retain adequate conveyance capacity and remain free from overtopping under the simulated discharge.

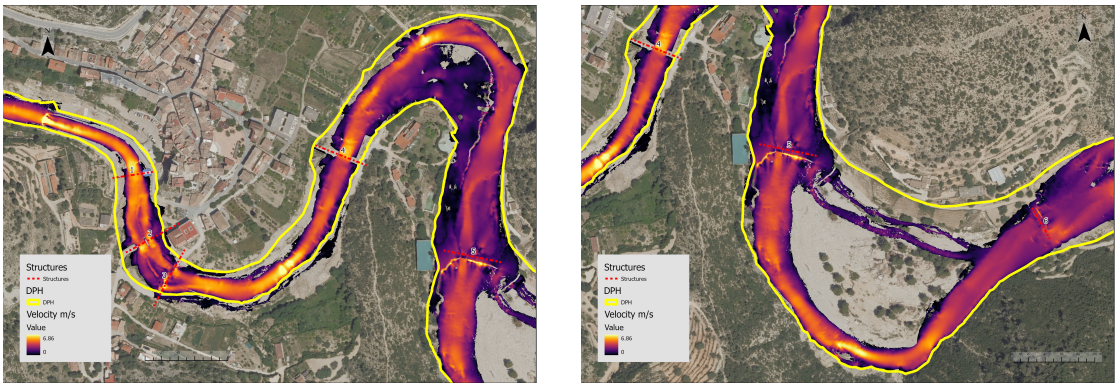

(a) Velocity field upstream part **(b)** Velocity field downstream part

Figure 4.23: Detailed views of the flow velocity field during the 60 m^3/s scenario. The maps highlight the localised hydrodynamic behavior and flow contractions at the crossing structures. Significant flow accelerations and weir flow conditions are clearly observable over the fords (structures 3, 5, and 6), indicating their hydraulic insufficiency under ordinary high flow conditions.

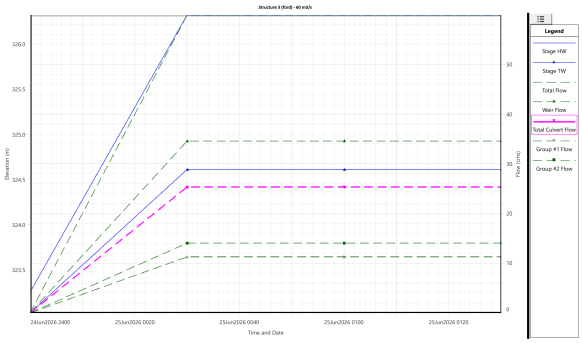

(a) Structure 3 (Main ford)

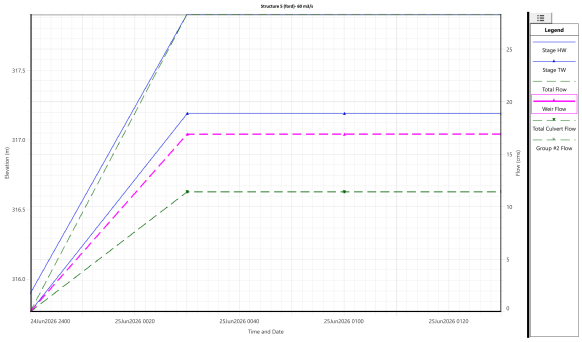

(b) Structure 5 (Minor ford)

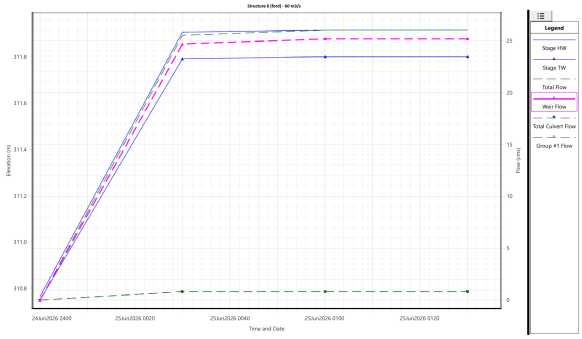

(c) Structure 6 (Minor ford)

Figure 4.24: Stage and flow hydrographs for the three ford structures during the 60 m^3/s ordinary high flow scenario. The blue solid lines indicate the water surface elevations computed upstream (Stage HW) and downstream (Stage TW) of each crossing. The green dashed lines illustrate the discharge partitioning: overall incident discharge (Total Flow), portion conveyed through the basal pipes (Total Culvert Flow), and discharge overtopping the infrastructure deck (Weir Flow). The marked divergence between the Total Flow and the Culvert Flow clearly demonstrates the hydraulic insufficiency of all three fords, leading to significant overtopping and upstream backwater effects.

Extreme Flood Scenario (358 m^3/s)

The extreme flood scenario, corresponding to a discharge of 358 m^3/s, was used to analyse the maximum hydraulic response of the study reach under severe flow conditions considered comparable to those associated with the 2024 DANA event. As described in Section 3, this simulation was carried out using the simplified hydraulic configuration. The results presented in this section therefore focus on maximum water levels at the bridge sections and on flow partitioning at the ford crossings.

The spatial distribution of maximum water depth and velocity shows that the inundated area extends over the active channel and the adjacent low-lying areas within the DPH boundary. The highest water depths are mainly concentrated along the main channel and in the wider meander bends, where the maximum simulated depth reaches 5.49 m. Lower depths are observed along the lateral margins of the inundated area and in the shallow floodplain zones activated during the event.

The velocity map shows high flow velocities along the main preferential flow paths, with maximum values up to 7.70 m/s. The highest velocities are generally located in confined channel sections, along the outer bends, and along the main preferential flow paths. In contrast, lower velocities are observed in the wider inundated areas and along the lateral margins of the flood extent. In contrast, lower velocities are observed in the wider inundated areas and along the lateral margins of the flood extent (see Figure 4.25).

At the three ford structures, the discharge hydrographs show that the culvert capacity is largely exceeded during the peak phase of the event, with most of the flow conveyed over the road surface as weir flow. At the first ford, corresponding to Structure 3, the total discharge reaches 324.80 m^3/s. Only 29.95 m^3/s is conveyed through the culverts, while 294.85 m^3/s passes over the road surface as weir flow. The maximum headwater-tailwater difference is 1.59 m, while the maximum overtopping depth above the structure is 2.52 m.

At the second ford, corresponding to Structure 5, the total discharge reaches 102.73 m^3/s. The culvert contribution is limited to 12.13 m^3/s, while most of the discharge, equal to 90.59 m^3/s, is conveyed over the crossing as weir flow. The maximum headwater-tailwater difference is 0.83 m, and the maximum overtopping depth above the structure is 1.69 m.

At the third ford, corresponding to Structure 6, the total discharge reaches 157.25 m^3/s. As observed for the other ford crossings, the discharge conveyed through the culverts represents only a minor fraction of the total flow, with 1.18 m^3/s passing through the culvert and 156.08 m^3/s conveyed over the road surface as weir flow. The maximum headwater-tailwater difference is 0.35 m, with a maximum overtopping depth above the structure of 1.87 m.

The maximum water surface profiles extracted at the bridge sections show

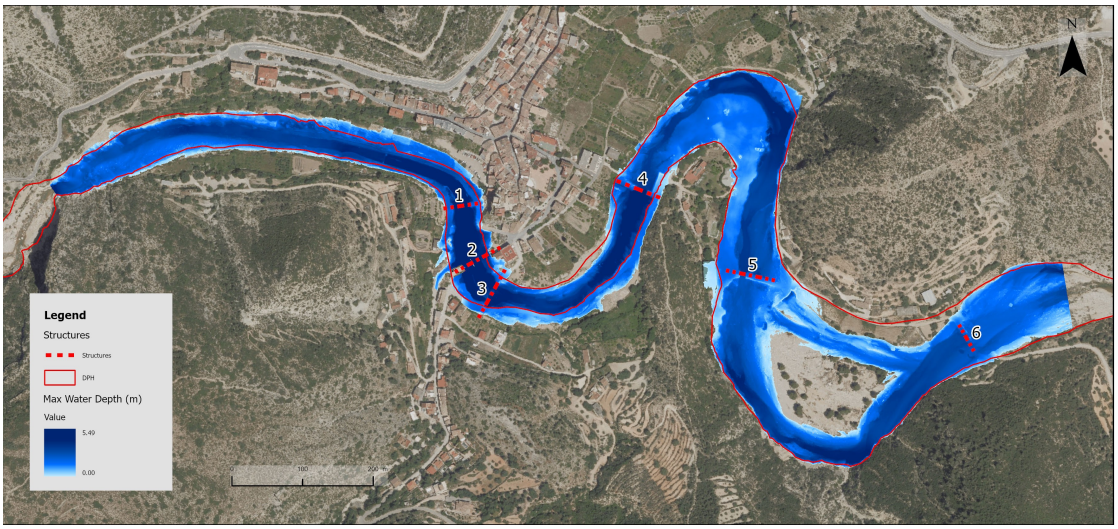

(a) Maximum water depth (m)

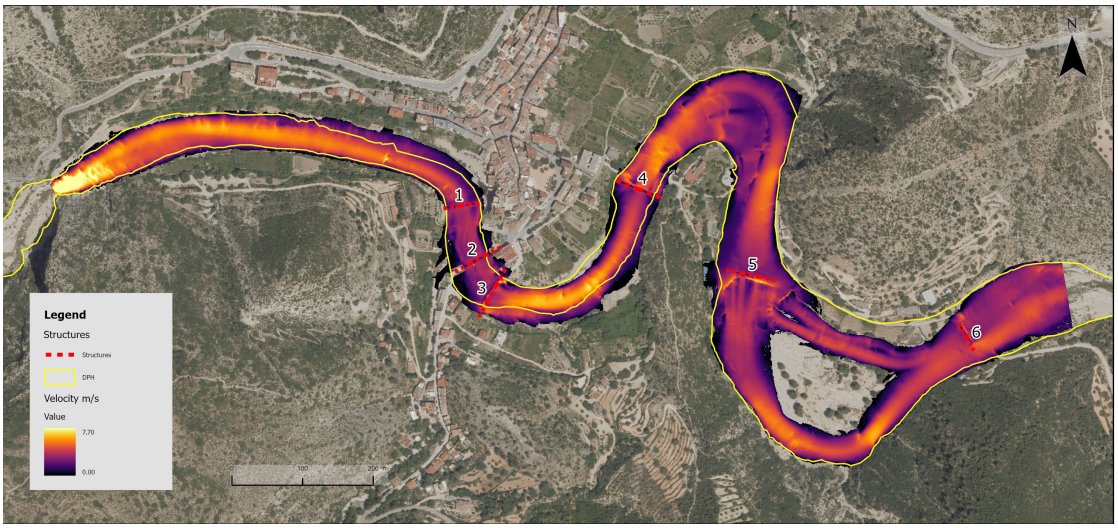

(b) Flow velocity (m/s)

Figure 4.25: Hydrodynamic simulation results for the extreme flood scenario (358 m^3/s). The spatial distribution of water depth (a) and flow velocity (b) is shown together with the official Hydraulic Public Domain (DPH). The transverse structures are numbered as follows: (1) Pedestrian footbridge, (2) Road bridge, (3) Ford, (4) Second pedestrian footbridge, (5) Ford, and (6) Ford.

different hydraulic conditions for the two pedestrian footbridges and the road bridge. At the first pedestrian footbridge, the maximum water surface elevation exceeds the structure elevation by 2.40 m. A similar condition is observed at the second pedestrian footbridge, where the maximum water surface elevation exceeds the structure elevation by 2.16 m. In contrast, at the road bridge section, the maximum water surface remains below the bridge deck elevation, and no overtopping is observed.

Overall, the 358 m^3/s scenario shows that all ford crossings are overtopped during the peak phase of the event. At these structures, culvert flow represents only a minor component of the total discharge, while weir flow over the road surface is the dominant conveyance mechanism. The two pedestrian footbridges are also exceeded by the computed maximum water levels, whereas the road bridge remains above the simulated water surface (see Figure 4.26 and Figure 4.27).

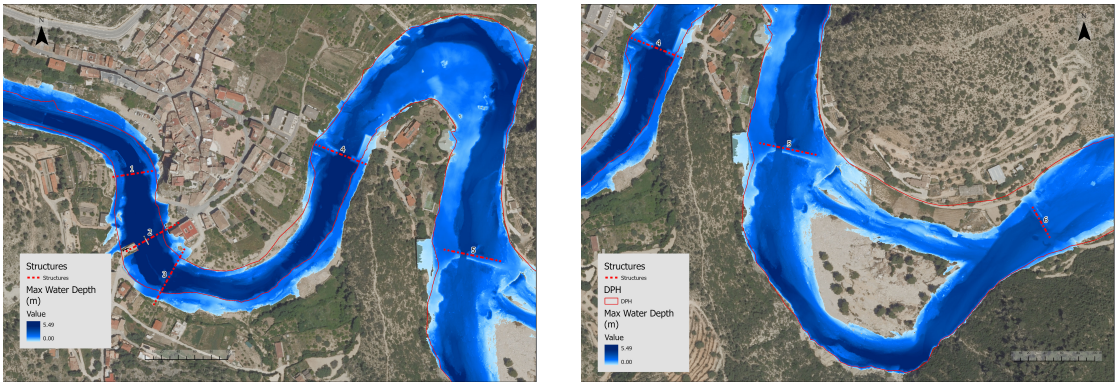

(a) Maximum water depth upstream part

(b) Maximum water depth downstream part

Figure 4.26: Detailed views of the maximum water depth during the 358 m^3/s extreme flood scenario. The maps show the spatial distribution of inundation depths around the crossing structures and within the DPH boundary. Higher water depths are observed along the main channel and in the wider inundated areas, while the ford crossings are located within zones of extensive flow overtopping.

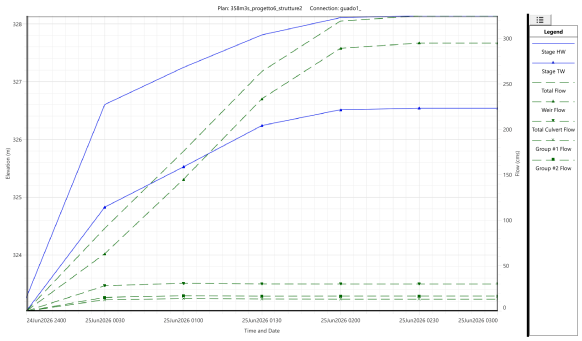

(a) Structure 3 (Main ford)

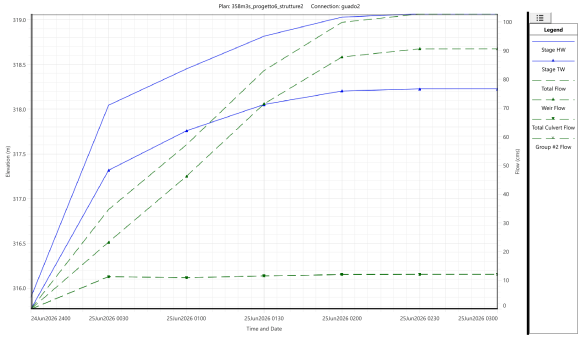

(b) Structure 5 (Minor ford)

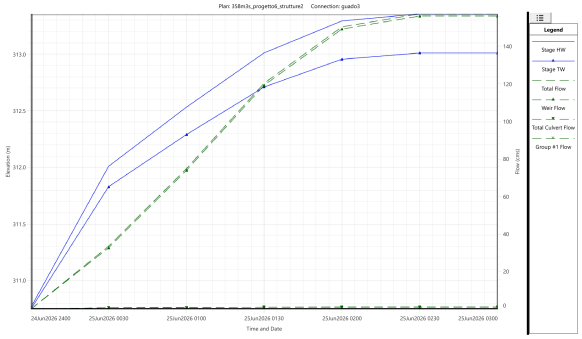

(c) Structure 6 (Minor ford)

Figure 4.27: Stage and flow hydrographs for the three ford structures during the 358 m^3/s extreme flood scenario. The blue solid lines indicate the water surface elevations computed upstream (Stage HW) and downstream (Stage TW) of each crossing. The green dashed lines show the discharge partitioning between the total flow, the portion conveyed through the basal culverts, and the discharge passing over the road surface as weir flow. In all three fords, the large difference between Total Flow and Total Culvert Flow shows that culvert conveyance is only a minor component of the total discharge, while weir flow over the crossing dominates during the peak phase of the event.

4.3.2 Spatial analysis of agricultural parcels within regulated river areas

Comparison Between Historical and Current DPH Delineation

The October 2024 DANA induced significant geomorphological changes along the Río Sot, leading to a revision of the Hydraulic Public Domain (DPH) boundaries by the Confederación Hidrográfica del Júcar (CHJ).

The comparison between the historical and the revised DPH boundary reveals a substantial expansion of the hydraulic public domain within the municipality of Sot de Chera. The current framework incorporates an additional 5.34 hectares compared to the previous regulatory status. Figure 4.28 illustrates the spatial distribution of the differences between the former and updated DPH boundaries along the Río Sot.

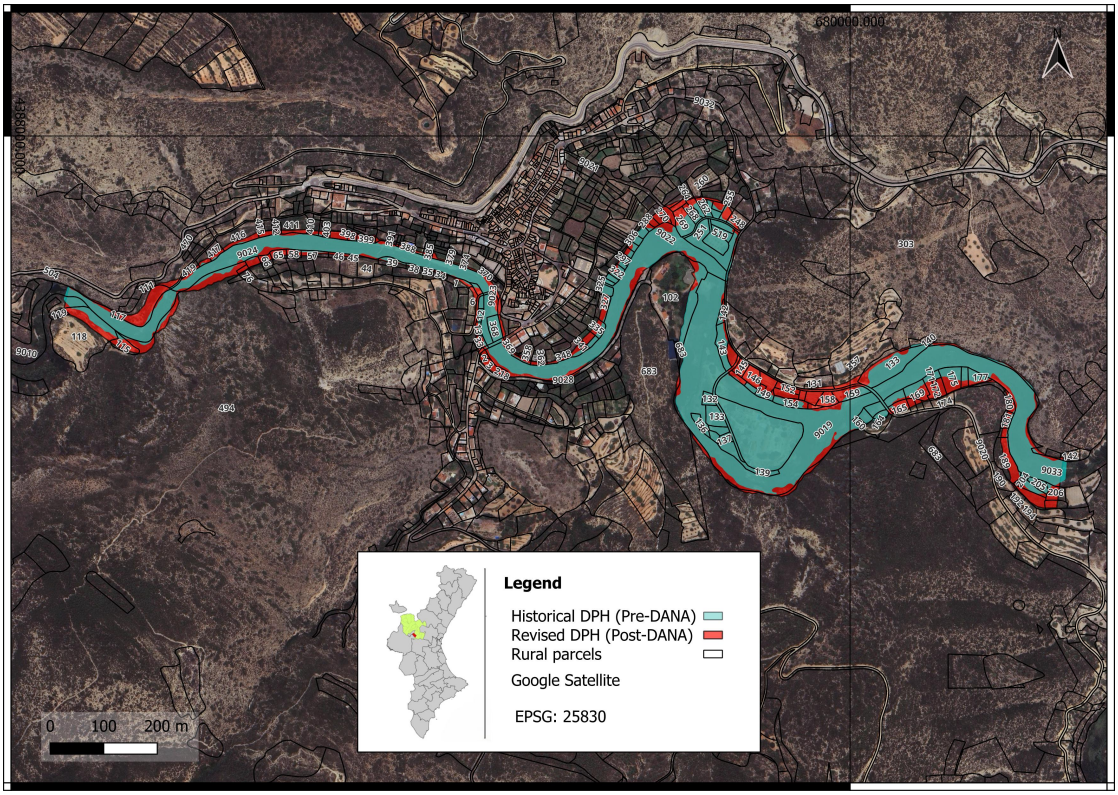

Figure 4.28: Comparison between pre-DANA and current post-DANA Hydraulic Public Domain boundaries.

Impact of Individual Hydraulic Regulation Zones (DPH, SERV, POL)

To assess the spatial impact of the different hydraulic regulation zones on the cadastral framework of Sot de Chera, the intersection analysis was performed separately for each of the three legally defined areas currently in force. Table 4.3 summarizes the main metrics obtained from the spatial analysis.

Table 4.3: Synthesized cadastral metrics for the current individual hydraulic regulation zones in Sot de Chera.

Regulatory Zone	N. of Affected Parcels	Tot Intersected Area (ha)	Avg Intersection (%)
DPH (Current)	215	19.63	57.61
SERV	187	2.46	19.97
POL	830	52.14	84.19

Hydraulic Public Domain (DPH) Under the updated post-DANA delineation, 215 cadastral parcels intersect the DPH, accounting for a total affected surface of 19.63 ha. Under the pre-DANA framework, 145 parcels intersected the DPH; the updated delineation therefore includes a net increase of 70 parcels (+48.3%). When examining the individual intensity brackets (see Table 4.4), the most significant change occurred in the 100% exposure class, where the number of fully affected parcels increased from 12 to 53. Figure 4.29 depicts the percentage of area of each parcel included within the current post-DANA DPH delineation at Sot de Chera.

Table 4.4: Comparative distribution of DPH (Hydraulic Public Domain) exposure classes between the historical (Pre-DANA) and current (Post-DANA) regulatory frameworks in Sot de Chera. Legend: n represents the number of affected parcels; ha indicates the total intersected surface area within the DPH boundaries; Δn denotes the net variation in the number of parcels between old and new DPH; Δha the net variation in the intersected surface area.

Exposure Class	Pre-DANA DPH		Post-DANA DPH		Net Variation	
(%)	(n)	(ha)	(n)	(ha)	(Δn)	(Δha)
< 25	73	3.08	64	3.89	-9	+0.81
$25 - 50$	16	0.31	35	0.95	+19	+0.64
$50 - 75$	17	0.91	19	0.66	+2	-0.25
$75 - 99$	27	8.02	44	9.80	+17	+1.78
100	12	1.97	53	4.33	+41	+2.36
Total	**145**	**14.29**	**215**	**19.63**	**+70**	**+5.34**

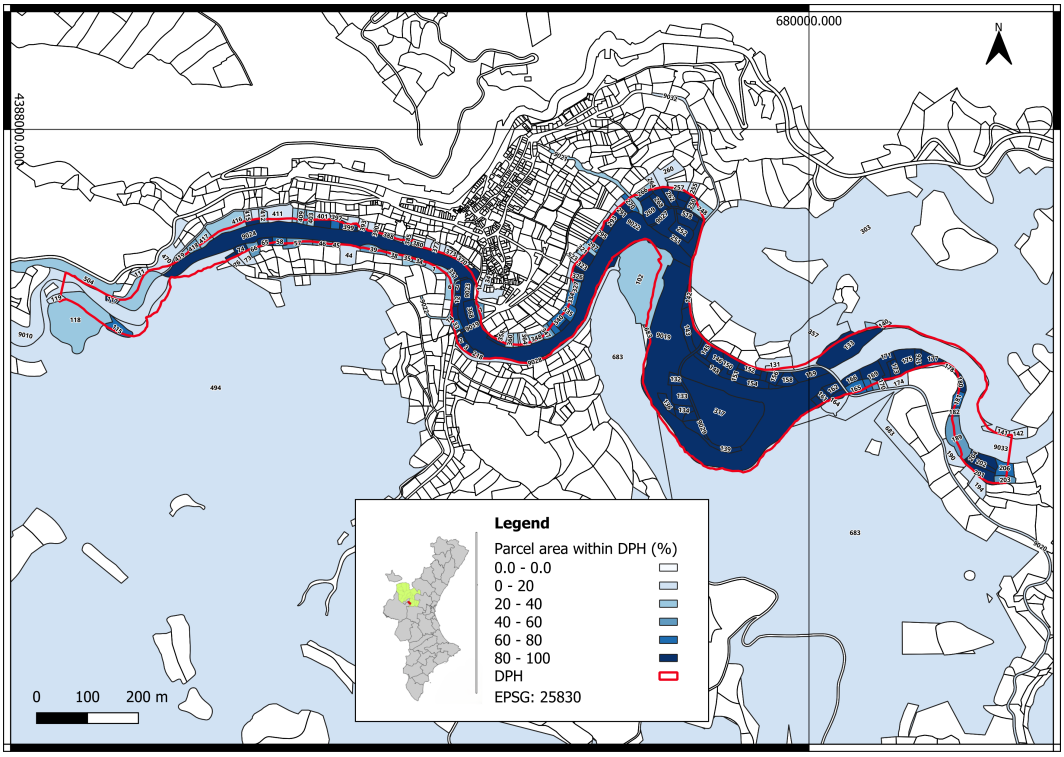

Figure 4.29: Cadastral parcel exposure analysis showing individual percentage of area included within the current post-DANA DPH delineation.

Easement Zone (SERV) The Easement Zone (*Zona de Servidumbre*) consists of a 5-metre-wide buffer measured from the outer boundary of the DPH. The spatial analysis indicates that this zone intersects 187 cadastral parcels and covers a total surface of 2.46 ha. Figure 4.30 depicts the percentage of area of each parcel included within the current post-DANA Easement Zone at Sot de Chera.

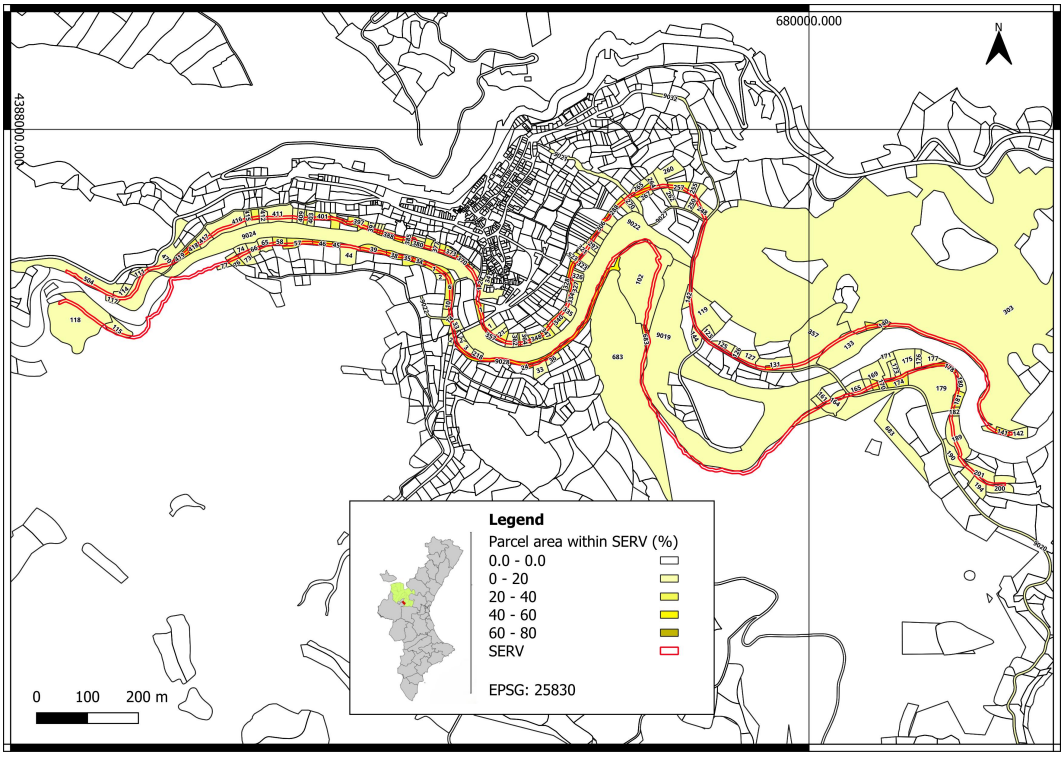

Figure 4.30: Cadastral parcel exposure analysis showing individual percentage of area included within the current post-DANA Easement Zone.

Police Zone (POL) The Police Zone (*Zona de Policía*) extends 100 metres outward from the DPH. The analysis identifies 830 intersected parcels, corresponding to a cumulative affected surface of 52.14 ha. The average parcel intersection percentage reaches 84.19%, indicating that parcels intersected by the Police Zone are generally affected over most of their total area. Figure 4.31 depicts the percentage of area of each parcel included within the current post-DANA Police Zone at Sot de Chera.

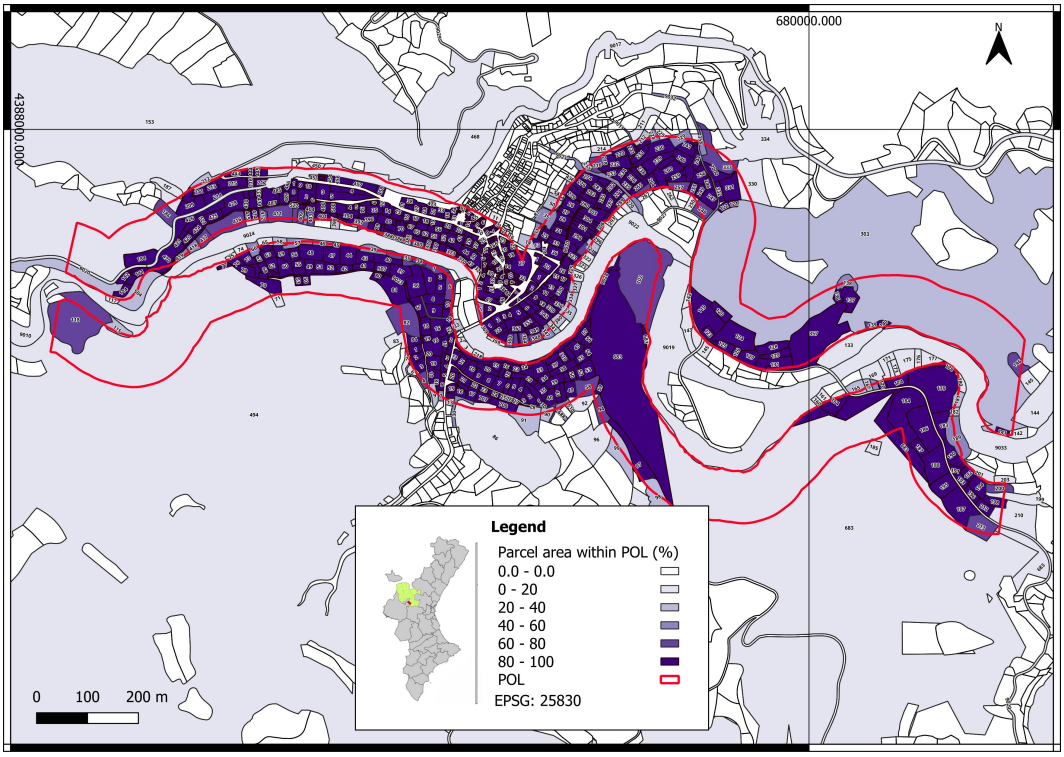

Figure 4.31: Cadastral parcel exposure analysis showing individual percentage of area included within the current post-DANA Police Zone.

Cumulative Exposure of Agricultural Land

To quantify the overall spatial extent of hydraulic regulation within the rural cadastral framework, the cumulative regulated area was calculated as the geometric union of the Hydraulic Public Domain (DPH) and the Police Zone (POL).

The resulting cumulative regulation zone intersects 884 unique cadastral parcels, corresponding to a total affected surface of 71.76 ha. Figure 4.32 depicts the percentage of area of each parcel included within the current post-DANA regulatory zones (Police Zone + DPH) at Sot de Chera.

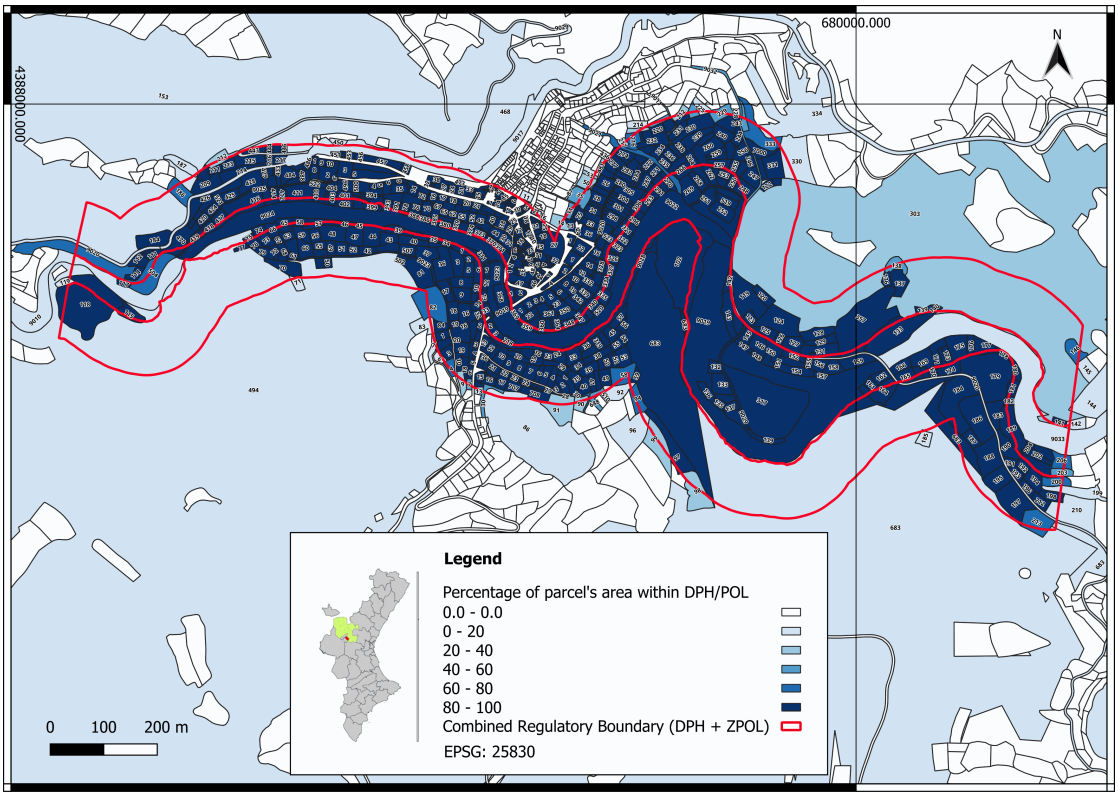

Figure 4.32: Cadastral parcel exposure analysis showing individual percentage of area included within the total regulatory framework (DPH + Police zone) at Sot de Chera.

Chapter 5

Discussion

5.1 Water quality dynamics and anthropogenic pressures

The integration of historical datasets from the CHJ (station JUH403) with seasonal longitudinal field monitoring provides a comprehensive understanding of the hydrochemical dynamics of the Río Sot and its vulnerability to anthropogenic pressures. Overall, the historical analysis depicts a resilient fluvial system characterized by baseline compliance with Spanish and European water quality standards for most physico-chemical parameters, nutrients, and heavy metals. Major ions (*EC* and chlorides) exhibit persistent stability across years and seasons, confirming that the fundamental hydrochemical regime is regulated by large scale water-rock interactions and geochemical controls at the catchment scale.

However, despite the overall hydrochemical stability, Seasonal Kendall and Mann–Whitney tests reveal statistically significant temporal and seasonal shifts. The steady increase in water temperature (+0.071°C/year), which is particularly pronounced during the cold season (+0.083°C/year), is consistent with broader warming trends reported across Mediterranean river systems. This thermal degradation is coupled with a positive trend in Chemical Oxygen Demand (*COD*, +0.056 mg/L/year), which accelerates during the warm season (+0.083 mg/L/year). This seasonal signal is further supported by microbiological indicators. The Mann–Whitney test reveals a statistically significant seasonal increase in total coliforms during the warm period ($p = 0.001$), with median values rising from 87 to 240 CFU/100 mL. This suggests an increased contribution of organic inputs both from diffuse and point source during summer, likely associated with reduced dilution capacity and increased seasonal human pressure within the catchment. Concurrent with these seasonal dynamics, an interannual shift in organic pollution indicators emerges during the final years of the historical series. While BOD_5 does

not exhibit a statistically significant trend due to a high proportion of observations below the analytical detection limit (1 mg/L), the annual distributions suggest a shift in central tendency and variability during the 2023–2024 period. During these two years, both COD and BOD_5 show an increase in median values and dispersion, suggesting a recent increase in biodegradable organic inputs.

The field monitoring campaigns conducted in late 2025 and early 2026 provided a picture of the main water quality gradients along the river, allowing the identification of localised pollution sources and post-flood disturbances along the longitudinal profile.

In the upstream sector (P1–P3), post-flood reconstruction works coincide with increases in mineralization, nutrient concentrations, and the presence of heavy metals not detected in historical records or in downstream stations. In the urban reach, the discharge of untreated domestic wastewater at Station P4 results in elevated ammonium concentrations (0.2 mg/L), nitrites, and halogen species. Partial attenuation of these signals is observed downstream (P5–P8), likely enhanced by tributary inflows. However, the magnitude of this pressure is likely underestimated due to the temporal limitations of field sampling, which was restricted to weekdays. In a small municipality like Sot de Chera, wastewater inputs are expected to vary significantly over short time scales, particularly during weekends and holiday periods associated with seasonal tourism. The A brownish-olive diatom layer observed near the wastewater outlet suggests recurrent organic enrichment events, which were not fully captured by punctual chemical sampling. Further downstream, the system transitions toward an agricultural landscape influenced by groundwater inputs. Elevated nitrate concentrations during the autumn campaign ($10 - -25$ mg/L at P10) suggest diffuse nutrient inputs associated with surrounding agricultural land use (extensive citrus cultivation), likely enhanced by rainfall-driven mobilization. Concurrently, the groundwater input from the warm thermal spring of Las Toscas introduces a localised geochemical anomaly, producing an increase in carbonate hardness (KH up to 250 mg/L) and strongly alkaline conditions ($pH \approx 8.4$).

Despite these localised anomalies, the downstream sector of the Río Sot largely retains the characteristics observed in the historical record. Most parameters measured at P10, including water temperature, electrical conductivity, and ammonium concentrations, remained inside the range of historical variability documented at the JUH403 station. Nitrate concentrations increased during the autumn campaign but remained within the historical range and returned to near-baseline values during spring. Similarly, the elevated chlorine concentrations detected in autumn were not observed during the subsequent campaign, suggesting a transient rather than persistent disturbance. These observations suggest that, while agricultural activities and localized groundwater inputs may influence water quality at P10, the downstream hydrochemical regime remains comparable to pre-flood conditions and does not provide evidence of strong alteration.

These interpretations, however, must be evaluated within the methodological constraints of the monitoring framework: historical records exhibit temporal discontinuities and limited parameter continuity for specific trace elements, while field measurements rely on semi-quantitative test strip methods with low analytical resolution, particularly for trace metals and nitrites. Furthermore, their visual interpretation is susceptible to ambient environmental conditions. In addition, the non-consecutive sampling of the autumn campaign introduces potential biases, especially in a highly dynamic catchment systems characterized by rapid hydrological and anthropogenic variability like the one object of this study. While these limitations prevent the absolute quantification of mass loads, the data remain highly valuable as a semi quantitative screening tool for identifying macro spatial patterns and guiding future analytical monitoring.

Overall, the Río Sot shows a generally stable hydrochemical baseline, despite the influence of post-flood recovery works and persistent urban and agricultural pressures. While these stressors can induce short-term degradation at the reach scale, their downstream attenuation suggests that dilution and natural recovery processes contribute significantly to the resilience of the system. At the same time, the widespread loss of riparian vegetation caused by the flood may have temporarily reduced the buffering capacity of the river corridor. As a result, the system may currently be more sensitive to localized pollutant inputs, particularly during periods of increased anthropogenic activity that were not captured by the present monitoring campaigns.

5.2 Riparian vegetation recovery and invasive species dynamics

The mapping conducted in autumn 2025 documents the early stages of ecological succession following the October 2024 DANA event. The intense hydraulic forces associated with the flash flood caused extensive loss of riparian canopy cover and substantial geomorphological changes along the channel. The monitoring highlights an ongoing and spatially variable recovery process, with both native pioneer species and invasive taxa colonizing areas made available by the disturbance.

The distribution of native pioneer trees, specifically the *Populus nigra* / *P.* × *canadensis* complex and *Populus alba*, exhibits a fragmented pattern primarily controlled by local geomorphological conditions and disturbance legacies. The majority of observed individuals are juveniles, established on alluvial bars characterized by fine, moist substrates. In the upstream and mid-reach sectors, regeneration appears to be supported by post-flood survival processes. Although many mature individuals were uprooted during peak discharge, some survived in situ and now function as structural biological legacies, contributing to vegetative resprouting and

seed dispersal. Overall, poplars are more abundant in the upstream and mid-reach sections, while their presence is more limited downstream.

The shrub layer displays higher structural continuity and post-disturbance resilience compared to arboreal vegetation. *Nerium oleander* maintains a relatively widespread distribution colonizing especially gravelly-sandy bars. Its stem flexibility and mechanical resistance enhanced survival during high-flow conditions and facilitated the establishment of recruitment nuclei. In contrast, *Tamarix spp.* remains scarce and is largely restricted to isolated juvenile cohorts.

In low-energy depositional environments, secondary channels, and saturated substrates, emergent macrophytes, particularly Phragmites australis, together with helophytic taxa such as Typha, Juncus, and Eleocharis spp., show rapid colonisation. The longitudinal continuity of these communities is influenced by two main factors: the expansion of invasive species and localized anthropogenic channel modifications.

The invasive giant reed, *Arundo donax*, represents one of the most relevant ecological pressures observed along the corridor of the Río Sot. Field observations reveal a clear longitudinal gradient, with sparse and fragmented stands in the upstream sectors and progressively larger and more continuous populations towards the confluence with the Turia River. In these downstream sectors, *A. donax* frequently occupies extensive portions of alluvial bars and appears to compete with native pioneer vegetation for newly available substrates.

This distribution is consistent with the ecological characteristics of the species, which combines rapid vegetative growth, efficient clonal propagation, and high tolerance to seasonal drought, enabling the rapid colonization of recent alluvial environments. While *Phragmites australis* is predominantly associated with wetter margins adjacent to the active channel, *A. donax* is more abundant on slightly elevated and better-drained surfaces, where reduced inundation frequency may confer a competitive advantage.

The post-flood landscape created by the October 2024 DANA appears particularly favourable to the expansion of *A. donax*. The same geomorphological processes that promote the regeneration of native pioneer communities may also enhance the establishment and spread of invasive species [34]. Extreme flood events, infact, can facilitate the downstream transport of vegetative propagules, like rhizome fragments and stem sections, while generating extensive areas of bare sediment suitable for colonization. This concern has gained increasing attention across the Valencian region after the 2024 DANA, as several affected river systems hare reporting rapid recolonization of disturbed reaches by *A. donax*, highlighting the importance of early management interventions during the post-flood recovery phase [62].

The relevance of this process extends beyond vegetation dynamics alone. Dense stands of *A. donax* can reduce riparian habitat heterogeneity, limit the recruitment of native species, and alter channel hydraulic conditions and roughness through

increased biomass accumulation [34]. These effects have led Spanish and Valencian environmental authorities to identify this species as a priority target for riparian management and dedicated technical guidelines have been developed to support its control in fluvial corridors [63].

Given that many of the populations mapped along the Río Sot remain relatively young and spatially fragmented, the current recovery phase offers a valuable opportunity for early intervention. Targeted management actions should prioritize sectors where native species such as *Nerium oleander* and *Populus nigra* are actively recruiting and invasive populations remain localized. In particular, the elimination of small upstream colonies may provide disproportionate long-term benefits by reducing the production and downstream transport of vegetative propagules during future high-flow events. Integrating selective *Arundo* control into river restoration and maintenance activities could therefore support both the ecological recovery and the hydrogeomorphological resilience of the Río Sot corridor.

(a)

(b)

(c)

Figure 5.1: Invasion mechanics, opportunistic establishment, and targeted management of *Arundo donax* in post-flood riparian environments: (a) Rhizome fragment of *Arundo donax*, capable of being transported by flow and of vegetative regeneration after deposition; (b) early-stage juvenile shoots emerging on a recently cleared fluvial bar in Pedralba, downstream of Sot de Chera along the Turia river, capitalizing on newly available bare substrates; and (c) field implementation of a long-term eradication strategy based on soil shading, where a heavy-duty black plastic membrane is deployed for a continuous period after mechanical cutting before executing active native replanting.

5.3 Hydraulic risk and river corridor management

The hydraulic simulations and spatial analyses provide complementary evidence that the October 2024 DANA did not simply represent an exceptional hydrological event but also exposed structural weaknesses in the current management of the Río Sot corridor. The updated delineation of the Hydraulic Public Domain (DPH) reflects the geomorphological adjustment produced by the flood, while the hydraulic modelling demonstrates that several existing crossing structures already experience critical conditions under discharges considerably lower than the extreme event.

The simulation of the ordinary high-flow scenario (60 m^3/s), corresponding to the Máxima Crecida Ordinaria (MCO), shows that all three ford crossings are hydraulically inadequate. Although the culverts remain capable of conveying part of the discharge, a large proportion of the flow passes over the road surface, producing overtopping and local backwater effects. These results suggest that the current design of the fords does not match the hydraulic regime of the river and may increase flood hazard by locally obstructing the flow and encouraging sediment deposition upstream of the structures. In contrast, the pedestrian bridges and the main road bridge retain sufficient conveyance capacity under the simulated MCO discharge, indicating that bridge structures with adequate freeboard are substantially more resilient than low-level crossings.

Under the extreme flood scenario (358 m^3/s), the hydraulic response is characterized by extensive inundation of the active channel and adjacent low-lying areas within the DPH boundary. The simulated maximum water depth reaches 5.49 m, while maximum velocities reach 7.70 m/s along the main preferential flow paths.

The results obtained at the crossing structures show that, even during an event dominated by floodplain activation, local hydraulic controls remain relevant. All three ford crossings are overtopped, with maximum overtopping depths ranging from 1.69 to 2.52 m. At these structures, culvert flow represents only a minor fraction of the total discharge, while weir flow over the road surface becomes the dominant conveyance mechanism. This behaviour confirms that the fords are not able to provide effective hydraulic conveyance during high-magnitude events and may instead act as local discontinuities in the flow field.

The bridge sections show a more differentiated response. The two pedestrian footbridges are exceeded by the computed maximum water levels, with overtopping depths of 2.40 m and 2.16 m, respectively. In contrast, the main road bridge remains above the simulated water surface and does not experience overtopping in the 358 m^3/s scenario. This difference suggests that not all crossing structures contribute equally to hydraulic risk. Low-level crossings and pedestrian footbridges are more exposed to overtopping, while the road bridge appears to retain sufficient

elevation under the simulated extreme condition. However, the presence of high water levels and high velocities near the structures still indicates that local hydraulic conditions may be critical during extreme floods.

These results highlight that, during extreme Mediterranean flash floods, flood hazard cannot be mitigated solely through local engineering interventions but requires maintaining sufficient space for the river to expand naturally, together with the adaptation or removal of the most vulnerable low-level crossings.

The comparison between the historical and post-DANA DPH further supports this interpretation. The expansion of the regulated river corridor by more than 5 hectares and the increase from 145 to 215 affected cadastral parcels demonstrate that the active river space has changed substantially following the flood. Particularly significant is the fourfold increase in parcels entirely included within the DPH, indicating that areas previously considered outside the active river corridor are now legally recognised as part of the flu vial system. Rather than representing merely an administrative update, this revision reflects the dynamic nature of Mediterranean rivers, whose morphology may undergo rapid adjustments during extreme flood events.

The cadastral analysis also reveals the extent to which agricultural land is exposed to hydraulic regulation. While only a relatively limited proportion of parcels lies within the DPH itself, almost 900 parcels fall within the cumulative regulatory framework defined by the DPH and the Police Zone. This does not imply that all these parcels are subject to direct flood inundation, but rather that agricultural activities increasingly coexist with regulatory constraints intended to preserve flood conveyance and reduce future hydraulic risk. In several parcels field observations indicate that the 2024 flood removed a substantial portion of the fertile topsoil, leaving coarse alluvial deposits that currently limit agricultural productivity. These areas therefore illustrate the emergence of new land-use conflicts, where privately owned agricultural land has become functionally degraded while simultaneously falling under stricter hydraulic regulation. Managing these situations will require balancing river restoration objectives, flood risk reduction, and the socio-economic needs of local landowners.

5.4 The role of technical-scientific data in participatory processes

The results presented in the previous sections highlight several management challenges for the Río Sot, ranging from localised water quality pressures and invasive species expansion to flood risk and land-use conflicts. Addressing these challenges requires not only technical knowledge but also mechanisms that integrate local perspectives and stakeholder interests into decision-making processes.

River systems are complex socio-ecological systems shaped by the continuous interaction of hydrological, geomorphological, biological, and anthropogenic processes. Effective management strategy therefore requires an understanding of this inherent complexity. The data generated in this study contribute to this objective by providing a structured evidence base that supports the identification of key priorities and the design of targeted interventions. Equally important is the way this information is communicated. Making technical results accessible can support a more transparent dialogue among the actors involved in river management.

Participatory spaces also play a key role in addressing tensions arising from competing interests and management objectives. The coexistence of ecological restoration goals, flood risk mitigation, agricultural activities, and recreational uses inevitably generates trade-offs that require collective discussion. Rather than eliminating conflicts, participatory processes can help make these trade-offs explicit and support more transparent and socially grounded decision-making.

Preliminary results of the field monitoring were actively shared during the second Asamblea del Río in December 2024. The meeting provided an opportunity to present observations on post-flood morphological changes, newly formed landscape features and their potential recreational value, as well as the current state of riparian vegetation. It also allowed participants to discuss the differences between native and invasive species, emphasizing the ecological importance of local flora and the threats posed by invasive taxa.

While scientific data supports decision-making by providing necessary boundaries and objective guidelines, it is crucial to recognize that technical information alone is not a definitive solution. During the Asambleas del Río, discussions often extended beyond hydrological or ecological aspects to include local memories, cultural values, and concerns about future development. These dimensions strongly influence how problems are perceived and which interventions are considered desirable or acceptable. At the same time, the Asamblea demonstrated that information does not simply flow from researchers to the community. Rather, the exchange operates in both directions. Local knowledge, direct experience, and everyday interactions with the river provide valuable information that can complement technical analyses and help identify elements that may not emerge from scientific monitoring alone. For these reasons, technical expertise and participatory processes should be viewed as complementary rather than separate components of river management.

(a) **(b)**

Figure 5.2: Active participatory processes during the *Asambleas del Río* in Sot de Chera, promoted by the RIVIVE project framework. (a) A collaborative spatial mapping session in which local residents and stakeholders discuss key issues and restoration proposals using participatory geographic methods. (b) Guided community dialogue, facilitated by participatory process experts (La Dula), aimed at co-designing local river management strategies.

(a)

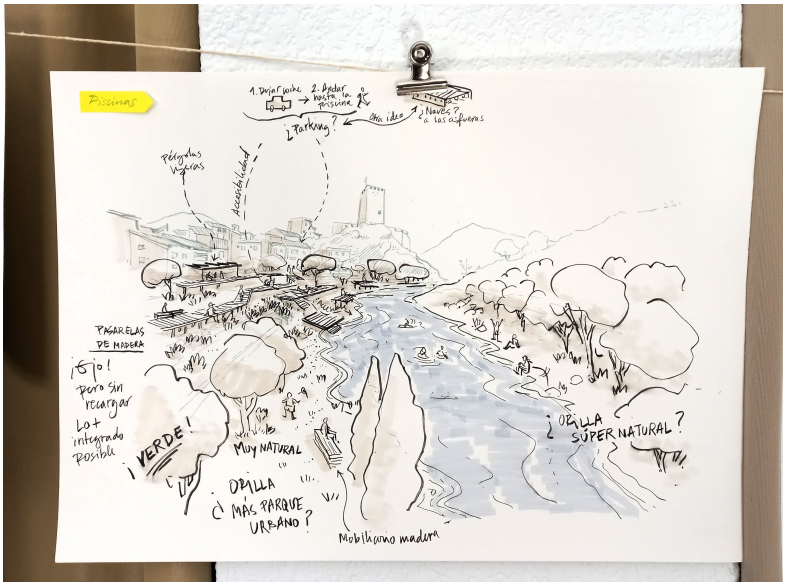

(b)

Figure 5.3: Active participatory processes during the *Asambleas del Río* in Sot de Chera, promoted by the RIVIVE project framework. (a) Session presenting the preliminary results of the November and December 2025 field monitoring campaigns to the assembly. (b) A conceptual sketch generated during the assemblies synthesizing community proposals for the rehabilitation of the river bathing area (*la zona de baño*).

Chapter 6

Conclusion

6.1 Concluding remarks

The October 2024 DANA profoundly reshaped the Río Sot, highlighting the need for restoration strategies capable of integrating ecological, hydrological, and social dimensions. Within this context, this thesis provides a multidisciplinary assessment of the post-flood river corridor by combining water quality analyses, riparian vegetation mapping, hydraulic modelling, and spatial analysis of land-use interactions.

The water quality assessment indicates that, despite the exceptional disturbance caused by the flood, the river generally maintains good physicochemical conditions. Nevertheless, localised anthropogenic pressures remain evident, particularly within the urban reach, where wastewater inputs contribute to increased concentrations of ammonium and nitrites, while diffuse agricultural activities continue to influence background nitrate levels. These findings underline the importance of maintaining long-term monitoring programmes capable of distinguishing natural variability from persistent human pressures.

The analysis of riparian vegetation demonstrates that ecological recovery is already underway but remains spatially heterogeneous. Native riparian species are progressively recolonizing newly formed surfaces; at the same time, the persistence and local expansion of *Arundo donax* highlight the need for targeted management actions during the early stages of restoration, when interventions are likely to be most effective in contrasting its expansion and supporting the establishment of native vegetation.

The hydrodynamic simulations characterized the flow fields, water depths, and hydraulic response of the newly established river crossings under different discharge scenarios. The results show that the ford crossings already experience critical conditions under the 60 m^3/s MCO scenario, while the 358 m^3/s extreme flood

scenario produces extensive inundation of the active river corridor and high-energy flow conditions. Under this extreme scenario, all ford crossings are overtopped, the two pedestrian footbridges are exceeded by the computed maximum water levels, whereas the main road bridge remains above the simulated water surface. These findings indicate that hydraulic risk is controlled both by the availability of sufficient river corridor space and by the vulnerability of low-level crossing structures. At the same time, the hydraulic results indicate that some of the crossing structures implemented to rapidly restore local accessibility after the flood, especially low-level fords, may require further assessment as part of medium- to long-term river corridor planning. Their possible adaptation or replacement with more hydraulically resilient solutions should be evaluated to ensure connectivity under a wider range of flow conditions. When integrated with the spatial analysis of cadastral parcels, the modelling results demonstrate how the updated delineation of the Hydraulic Public Domain and its associated protection zones significantly increases the exposure of agricultural land to regulatory constraints. Together, these analyses establish a robust quantitative framework for supporting infrastructure planning, floodplain management, and future environmental restoration actions.

Beyond the individual findings, this work suggests the potential value of integrating different sources of environmental information into a common analytical framework. The combination of field observations, historical datasets, GIS analyses, and hydraulic modelling provides a more comprehensive understanding of the processes currently shaping the Río Sot and may contribute to a useful scientific basis for future restoration planning.

Finally, the experience of Sot de Chera highlights that river restoration should not be regarded solely as a technical or engineering challenge. In complex socio-ecological systems such as the Río Sot, effective restoration requires the involvement of local communities alongside scientific and technical knowledge. By providing accessible technical information to support the River Assemblies promoted within the RIVIVE project, this research contributes to a more informed dialogue among researchers, public authorities, and local stakeholders. In doing so, it supports restoration strategies that aim not only to recover ecological functions but also to strengthen the long-term coexistence between river dynamics and the communities that depend on them.

6.2 Limitations and future perspectives

While this study establishes a base for the post-flood recovery phase, several limitations should be acknowledged. Water quality monitoring was based on two seasonal field campaigns and on rapid in situ screening methods, which provided a framework for identifying longitudinal patterns and localised pressures but did

not allow the characterization of short-term fluctuations associated with episodic wastewater discharges or peak tourist activity. Likewise, the analytical methods based on concentration ranges limited the precision of several parameters, particularly nitrites and nitrates. Future monitoring programmes could therefore integrate periodic laboratory analyses with continuous measurements of key indicators. In particular, the installation of a conductivity sensor immediately downstream of the urban area would provide a simple and cost-effective solution for detecting wastewater inputs in real time and capturing transient pollution events that are difficult to observe through conventional sampling campaigns.

The riparian vegetation survey provides a snapshot of the early stages of ecological recovery following the 2024 flood. Since riparian vegetation is inherently dynamic, repeated surveys over the coming years will be essential to quantify recruitment, mortality, competitive interactions, and the long-term evolution of both native communities and *Arundo donax*. Extending the monitoring programme would also make it possible to evaluate the effectiveness of future restoration and invasive species management actions. Future improvements could further include the use of more precise spatial mapping techniques to enhance the accuracy and spatial resolution of vegetation surveys.

Regarding the hydraulic and spatial analyses, the developed modelling framework represents a simplified reconstruction of a highly complex and rapidly evolving post-disaster environment. Since the study was initiated shortly after the flood, definitive post-event orthophotos were not yet available, and several terrain modifications and bridge geometries had to be reconstructed from rapid field surveys and engineering approximations. In addition, the 358 m^3/s scenario required a simplified hydraulic configuration because the complete representation of bridge decks and structural elements did not provide a stable numerical solution. The model retained the post-DANA terrain modifications and ford culverts, but excluded bridge decks from the computation. Therefore, the results should be interpreted as a floodplain-scale assessment of inundation patterns and ford performance, rather than as a detailed structural verification of the bridges.

More broadly, this research documents a river corridor during a transitional phase of its recovery. Since the completion of the field activities, several of the analysed infrastructures have already been modified: the main ford investigated in the hydraulic model has been removed, bank stabilization works using wooden cribwalls (muri Krainer) and native vegetation have been initiated, and the traditional bathing area has been restored using natural materials such as local rock, gravel, and timber (see Figure 6.1). These interventions illustrate how rapidly the Río Sot continues to evolve after the DANA event and highlight the importance of considering this study as a baseline for future monitoring rather than a definitive representation of the system. Continuous updating of hydraulic, ecological, and spatial datasets will therefore remain essential for supporting adaptive river restoration.

(a) Restoration of *la zona de baño*.

(b) Bank stabilization with vegetated krainer cribwalls.

Figure 6.1: Recent post-flood recovery interventions and nature-based bioengineering works implemented within the urban reach of Sot de Chera.

Appendix A

Annual historical water quality data

This appendix presents the annual boxplots for the water quality parameters analyzed in the historical dataset of the Río Sot over the last 20 years.

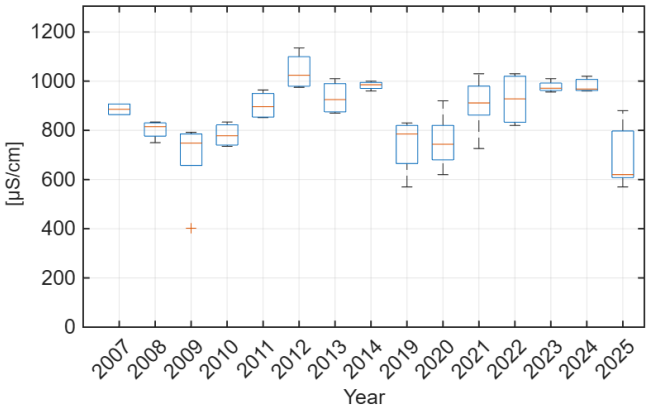

(a) Electrical Conductivity (EC)

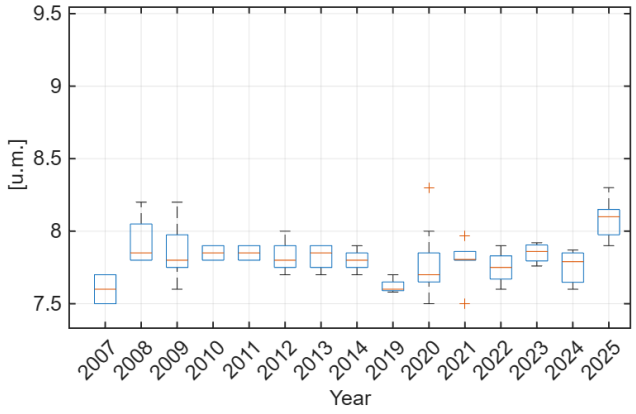

(b) pH

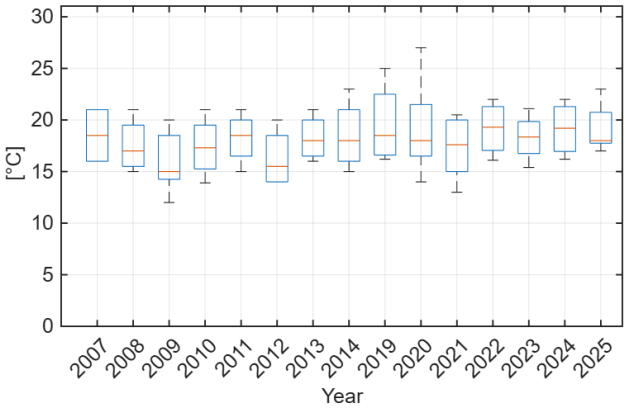

(c) Water Temperature (T)

Figure A.1: Annual distributions of core physical and chemical baseline parameters.

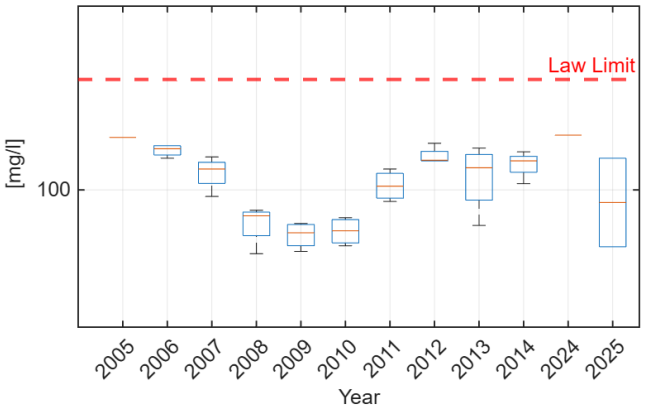

(a) Chloride (Log scale)

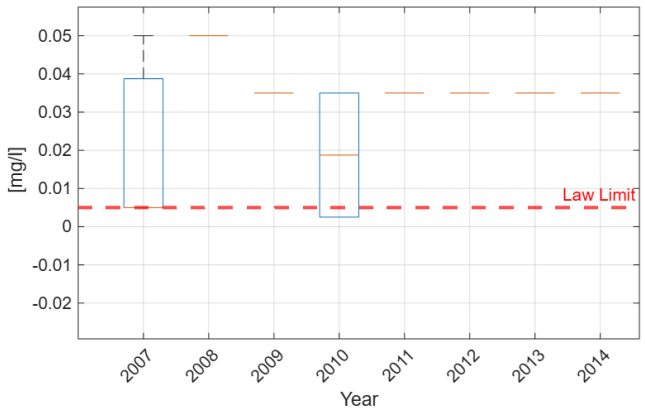

(b) Total Chlorine

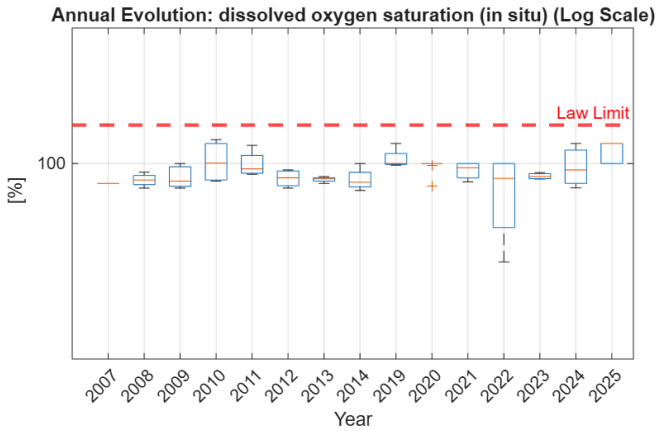

(c) Dissolved Oxygen Saturation (DO Saturation)

Figure A.2: Annual trends for chlorine compounds and dissolved oxygen saturation.

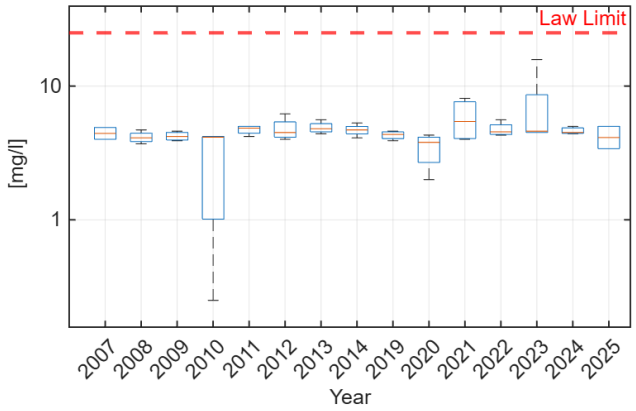

(a) Nitrate (Log scale)

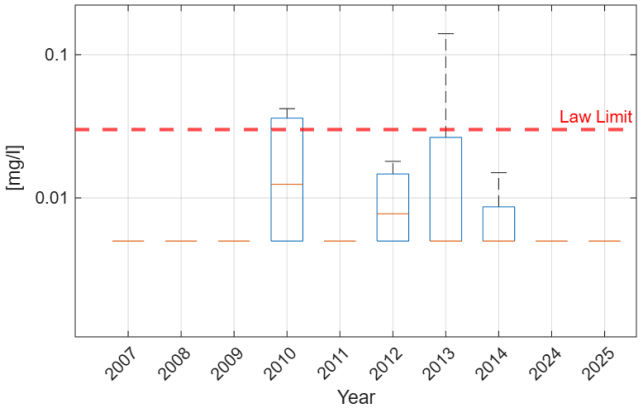

(b) Nitrite (Log scale)

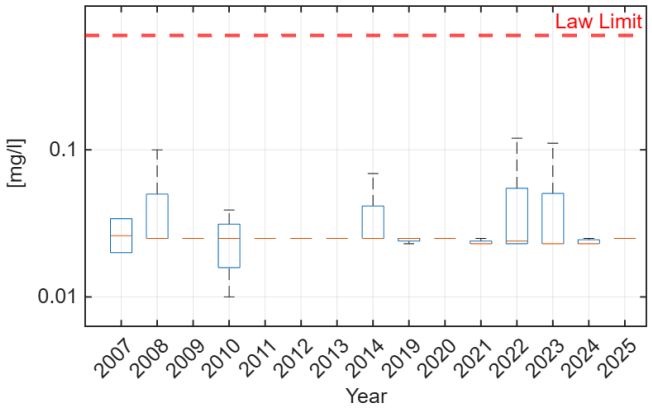

(c) Ammonium (Log scale)

Figure A.3: Annual concentrations of nitrogen-based nutrient parameters.

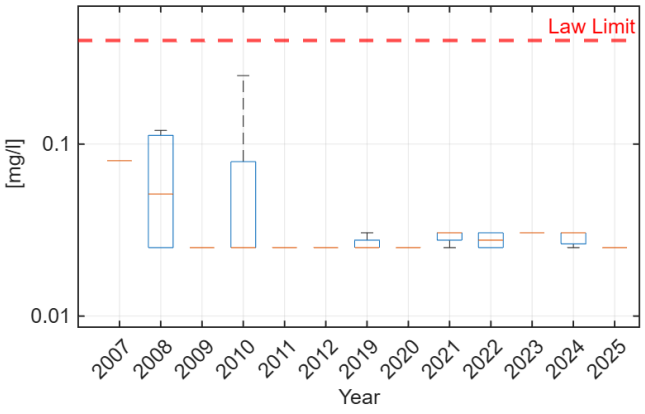

(a) Phosphate (Log scale)

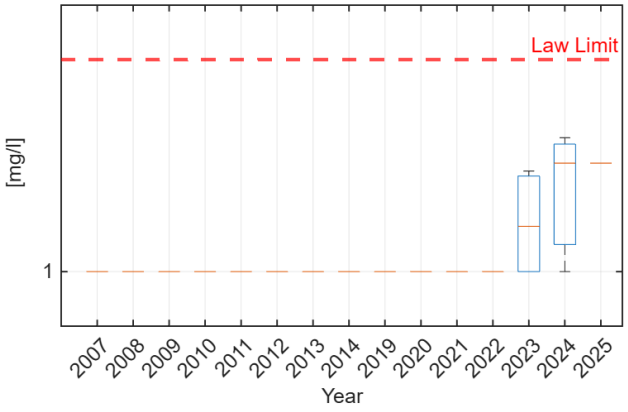

(b) BOD_5 (Log scale)

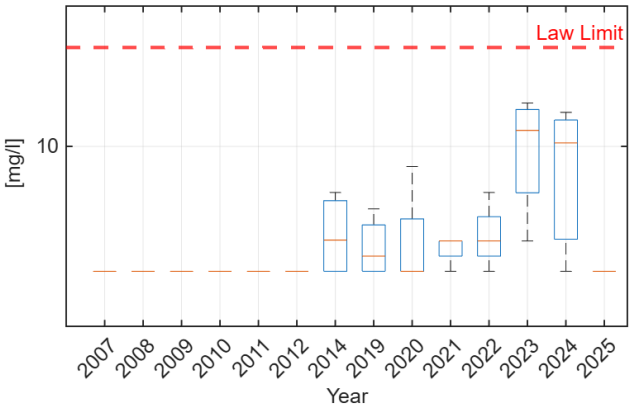

(c) COD (Log scale)

Figure A.4: Annual concentrations of phosphates and macro-indicators of organic pollution.

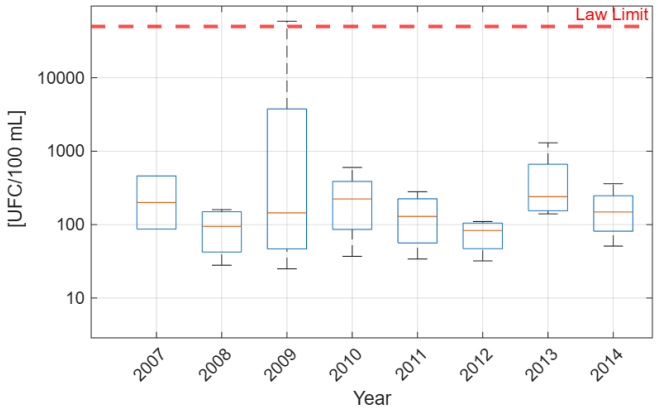

(a) Total Coliforms (Log scale)

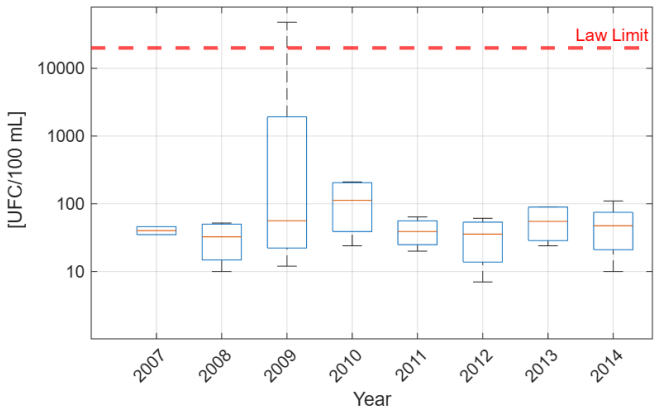

(b) Fecal Coliforms (Log scale)

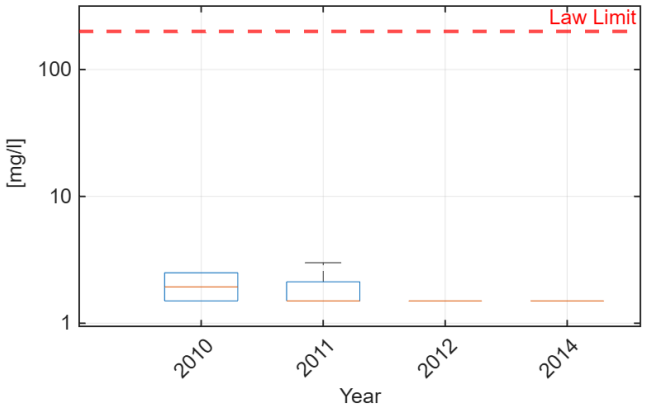

(c) Colour (Log scale)

Figure A.5: Annual trends for microbiological indicators and water colouration.

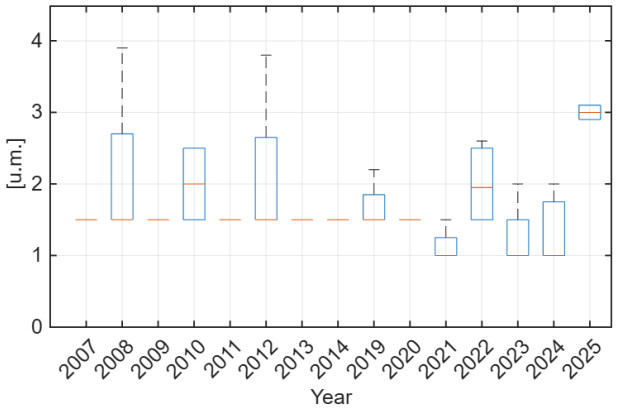

(a) Total Suspended Solids

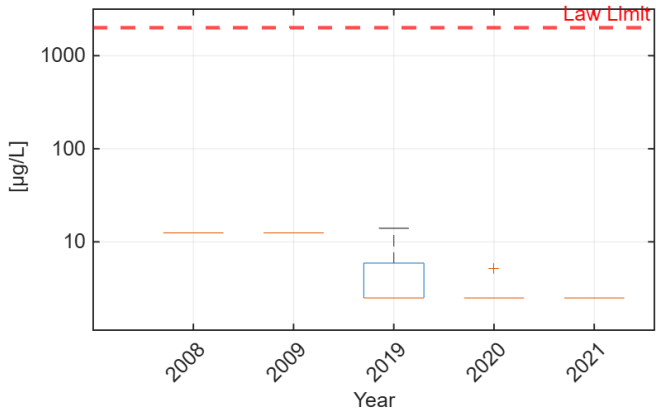

(b) Iron (Log scale)

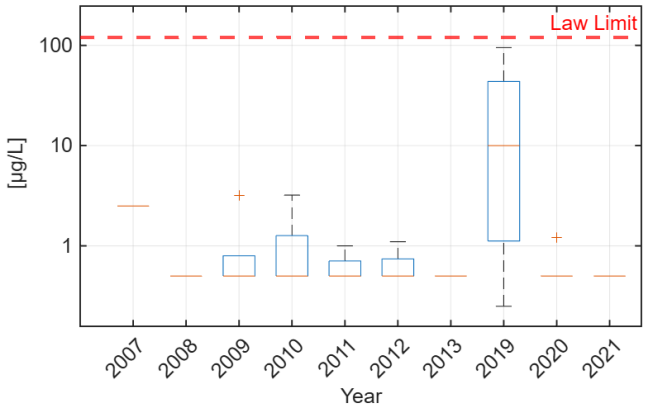

(c) Copper (Log scale)

Figure A.6: Annual concentrations of total suspended solids, iron, and copper.

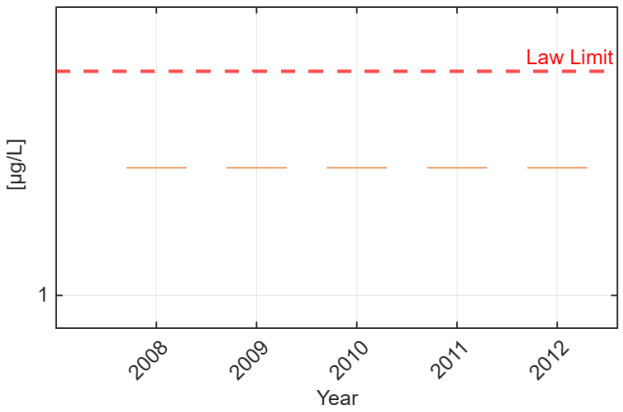

(a) Chromium VI (Log scale)

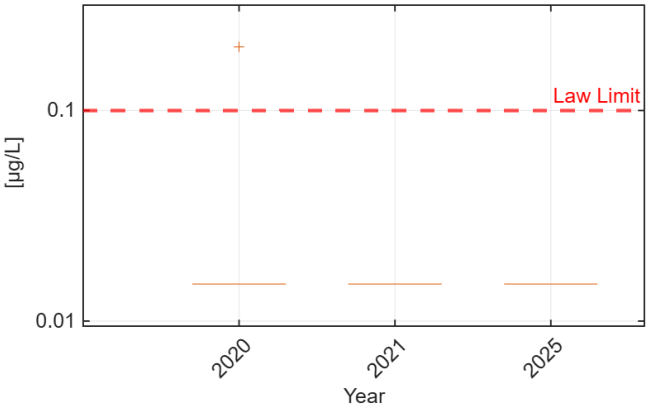

(b) Glyphosate (Log scale)

Figure A.7: Annual concentrations of specific trace pollutants and agrochemicals.

Appendix B

Seasonal Water Quality Plots

This appendix presents the seasonal boxplots for all the water quality parameters analyzed in the historical dataset.

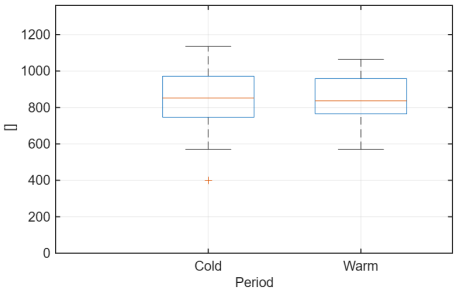

(a) Electrical Conductivity (EC)

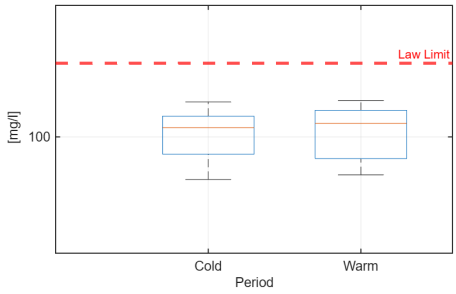

(b) Chloride (Log scale)

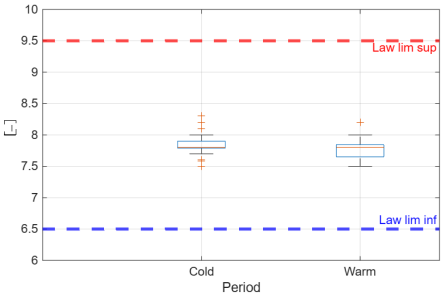

(c) pH

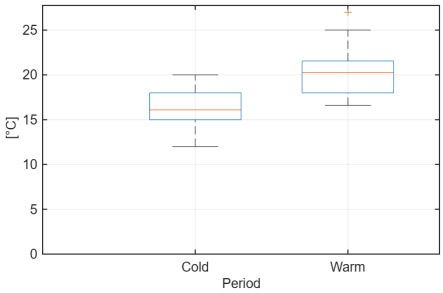

(d) Water Temperature (T)

Figure B.1: Seasonal distributions of physical and chemical baseline parameters.

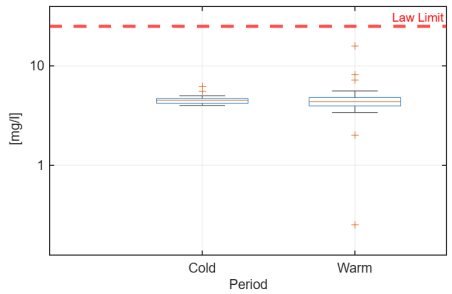

(a) Nitrate (Log scale)

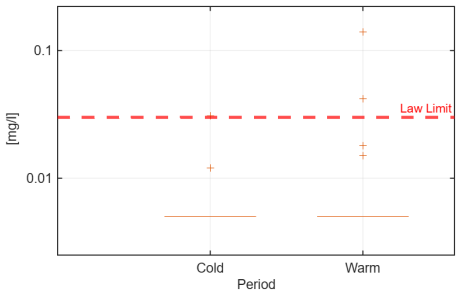

(b) Nitrite (Log scale)

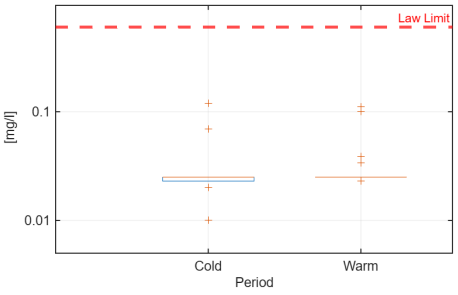

(c) Ammonium (Log scale)

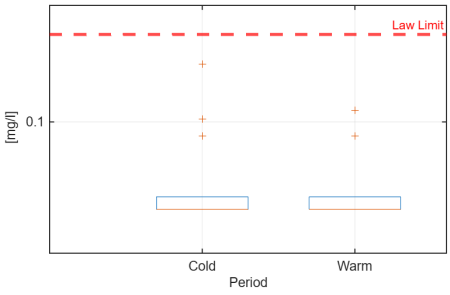

(d) Phosphate (Log scale)

Figure B.2: Seasonal concentrations of nutrient parameters.

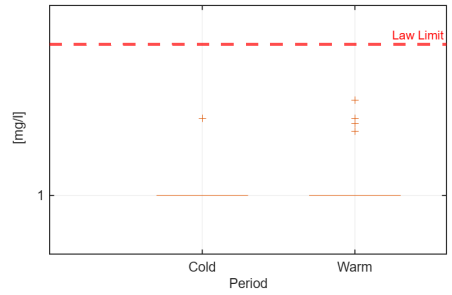

(a) BOD_5 (Log scale)

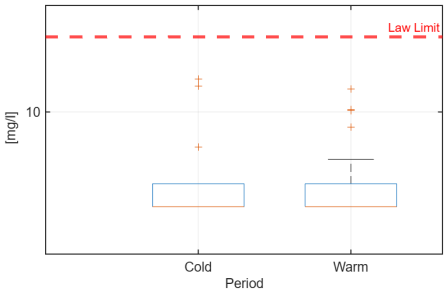

(b) COD (Log scale)

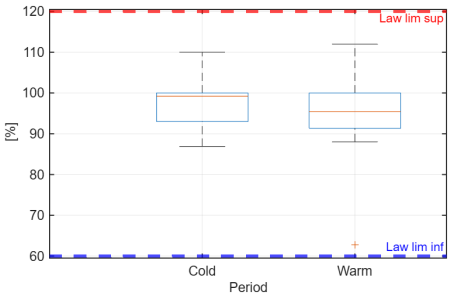

(c) Dissolved Oxygen Saturation (DO Saturation)

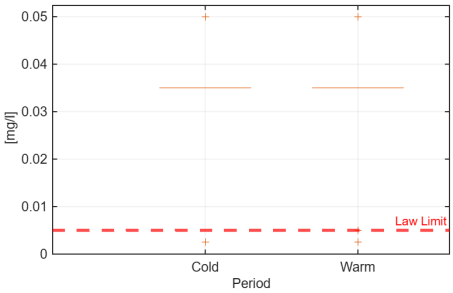

(d) Total Chlorine

Figure B.3: Seasonal concentrations of organic pollution indicators.

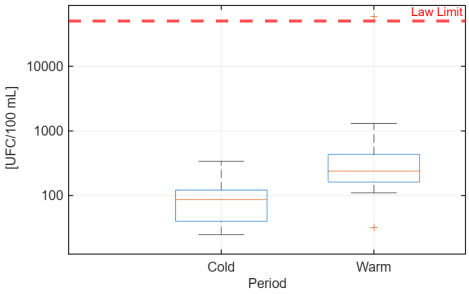

(a) Total Coliforms (Log scale)

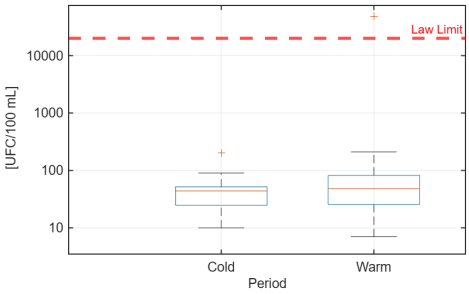

(b) Fecal Coliforms (Log scale)

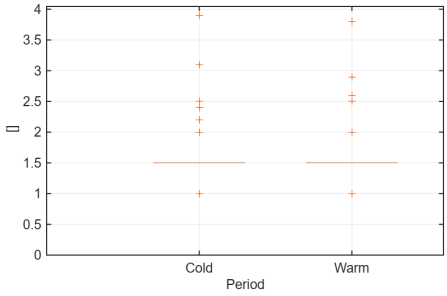

(c) Total Suspended Solids (Suspended)

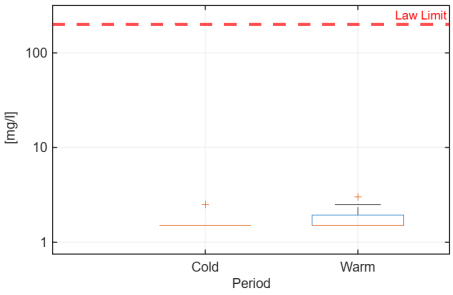

(d) Colour (Log scale)

Figure B.4: Seasonal trends for microbiological parameters, suspended solids, and colour.

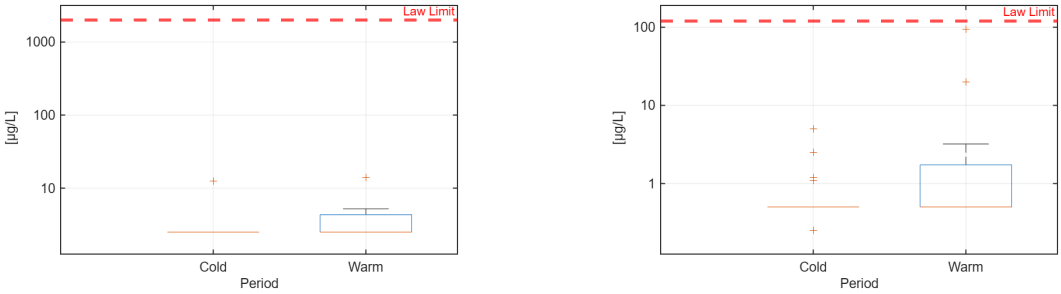

(a) Iron (Log scale)

(b) Copper (Log scale)

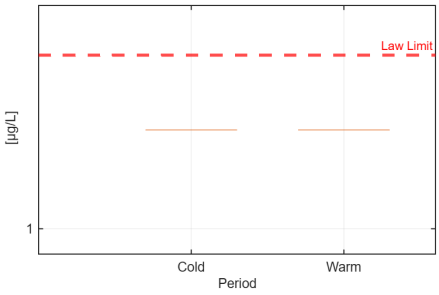

(c) Chromium (Log scale)

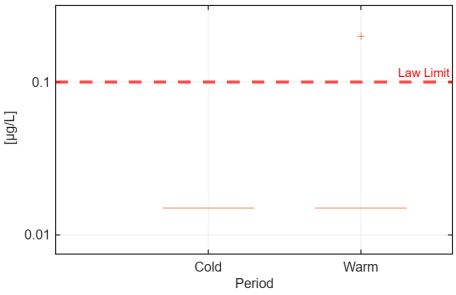

(d) Glyphosate (Log scale)

Figure B.5: Seasonal concentrations of heavy metals, trace elements, and specific pollutants.

Appendix C

Field monitoring data

This appendix presents the plots obtained from the two field monitoring campaigns conducted along the Río Sot (Reatillo) at Sot de Chera during autumn (November–December 2025) and spring (April 2026). Water quality parameters were analyzed along a longitudinal upstream-downstream gradient.

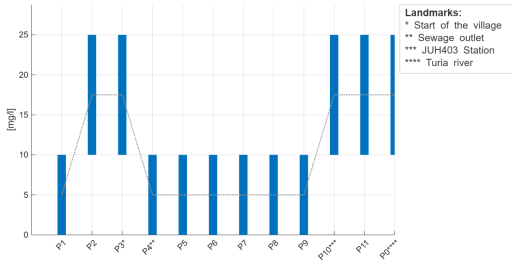

(a) Nitrates – Autumn 2025

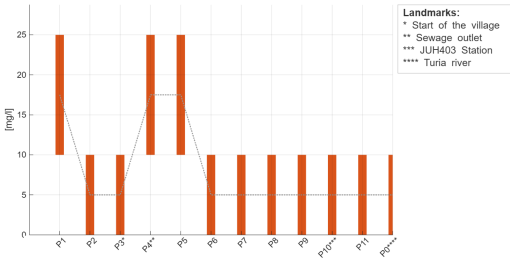

(b) Nitrates – Spring 2026

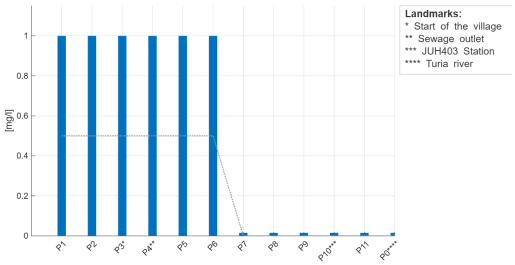

(c) Nitrites – Autumn 2025

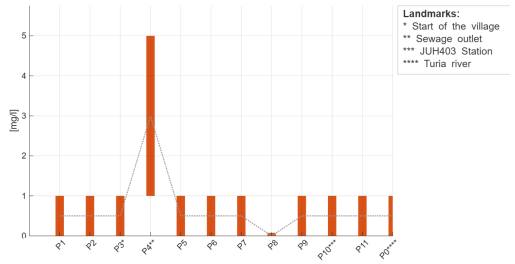

(d) Nitrites – Spring 2026

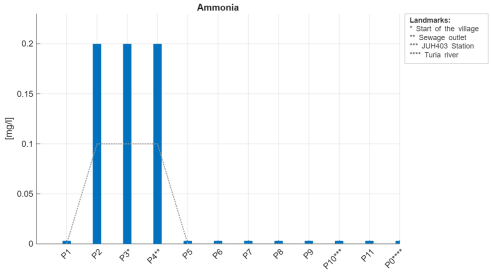

(e) Ammonium – Autumn 2025

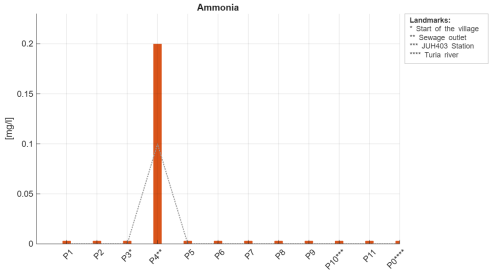

(f) Ammonium – Spring 2026

Figure C.1: Seasonal longitudinal concentrations of nutrients (nitrogen species) along the river sector: comparison between Autumn 2025 and Spring 2026 campaigns.

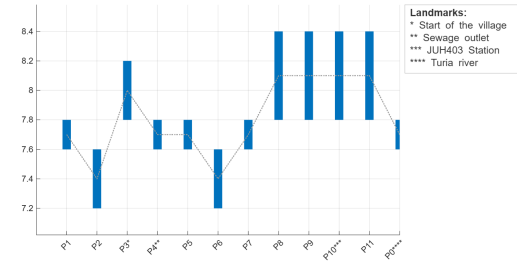

(a) pH – Autumn 2025

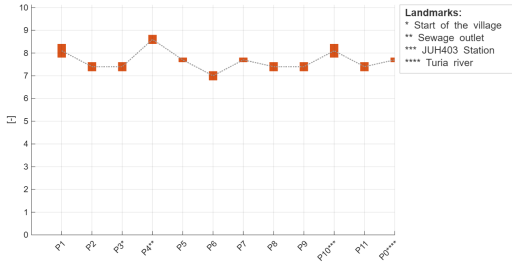

(b) pH – Spring 2026

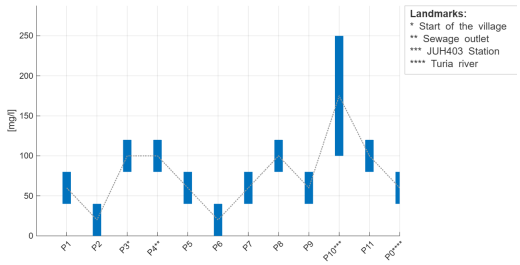

(c) KH – Autumn 2025

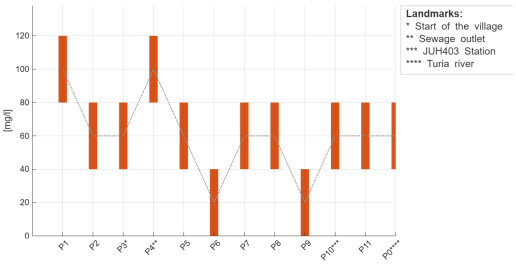

(d) KH – Spring 2026

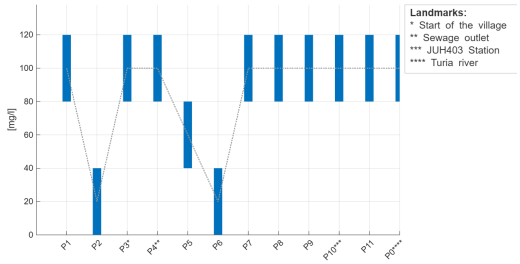

(e) Total Alkalinity – Autumn 2025

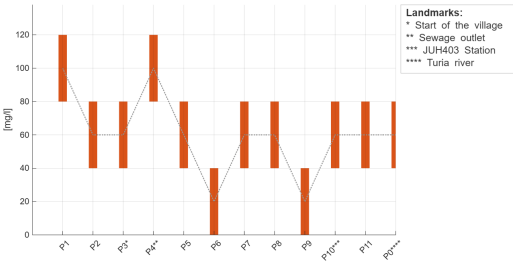

(f) Total Alkalinity – Spring 2026

Figure C.2: Seasonal longitudinal data of pH and carbonate system parameters (KH and Total Alkalinity) along the river sector: comparison between Autumn 2025 and Spring 2026 campaigns.

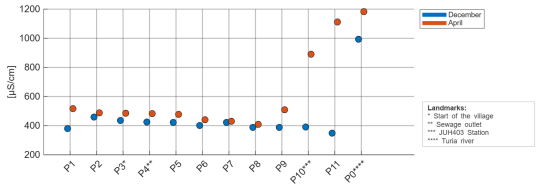

(a) Electrical Conductivity – Autumn vs Spring

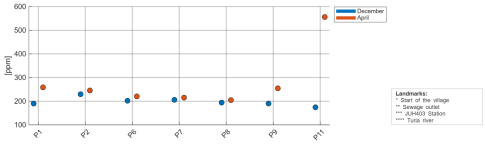

(b) Total Dissolved Solids – Autumn vs Spring

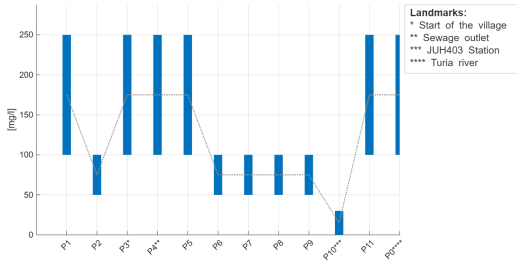

(c) Total Hardness (GH) – Autumn 2025

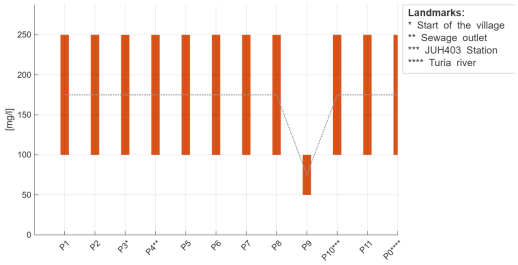

(d) Total Hardness (GH) – Spring 2026

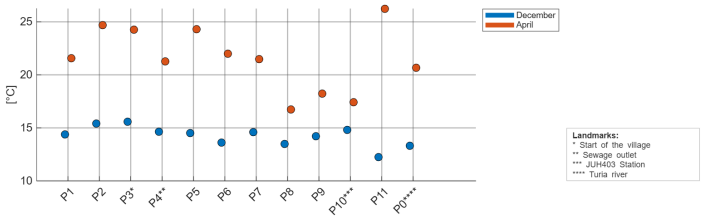

(e) Water Temperature – Autumn vs Spring

Figure C.3: Seasonal longitudinal data for physical and mineralization parameters: Electrical Conductivity (EC), Total Dissolved Solids (TDS), Total Hardness (GH), and Water Temperature (T) across Autumn 2025 and Spring 2026 campaigns.

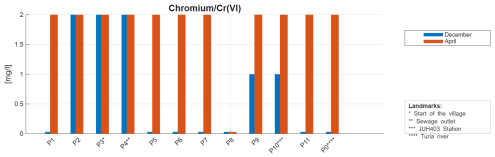

(a) Hexavalent Chromium (Cr VI) – Autumn vs Spring

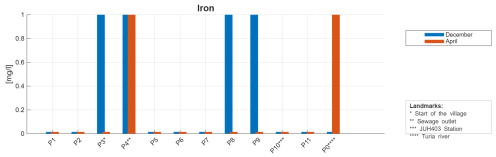

(b) Iron (Fe) – Autumn vs Spring

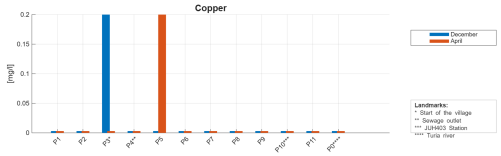

(c) Copper (Cu) – Autumn vs Spring

Figure C.4: Longitudinal concentration trends of heavy metals (Chromium VI, Iron, and Copper) along the river sector: comparison between Autumn 2025 and Spring 2026 campaigns.

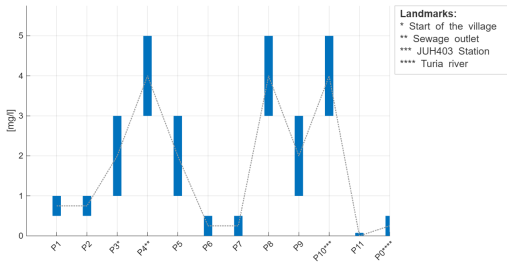

(a) Free Chlorine – Autumn 2025

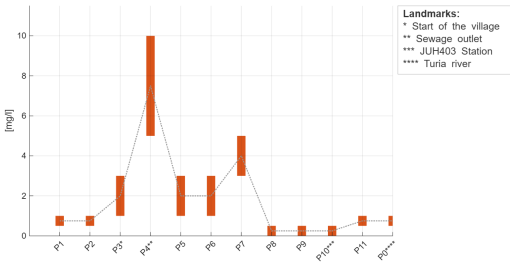

(b) Free Chlorine – Spring 2026

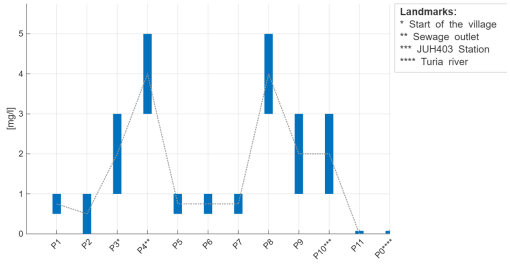

(c) Total Chlorine – Autumn 2025

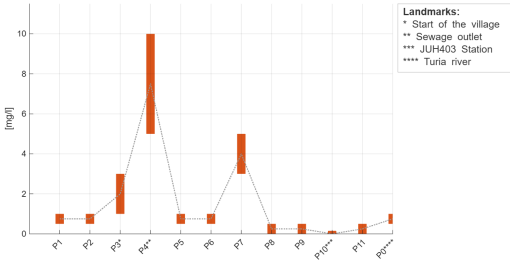

(d) Total Chlorine – Spring 2026

Figure C.5: Longitudinal concentration datasets for halogen species (Part 1: Free and Total Chlorine) along the river sector: comparison between Autumn 2025 and Spring 2026 campaigns.

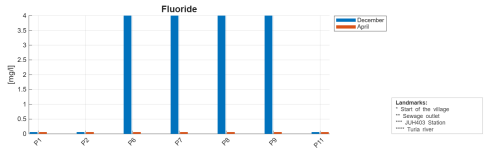

(a) Fluoride – Autumn vs Spring

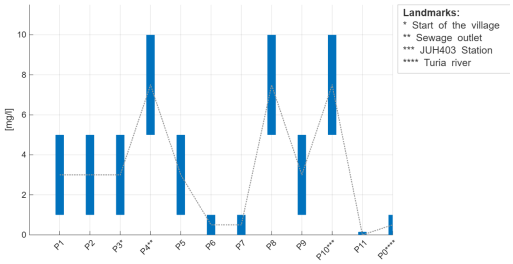

(b) Bromine – Autumn 2025

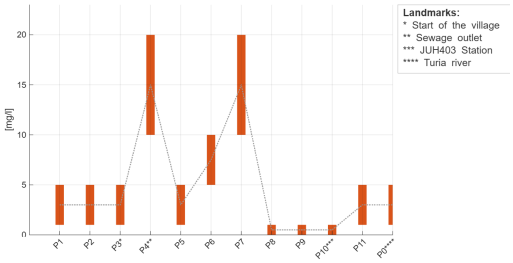

(c) Bromine – Spring 2026

Figure C.6: Longitudinal concentration datasets for halogen species (Part 2: Fluoride and Bromine) along the river sector: comparison between Autumn 2025 and Spring 2026 campaigns.

Appendix D

Comparison between field monitoring data and historical data

This appendix presents a comparison between the data collected during the recent field campaigns (Autumn 2025 and Spring 2026) and the long-term historical data provided by the CHJ.

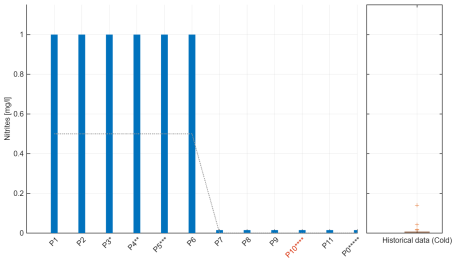

(a) Nitrites – Autumn 2025

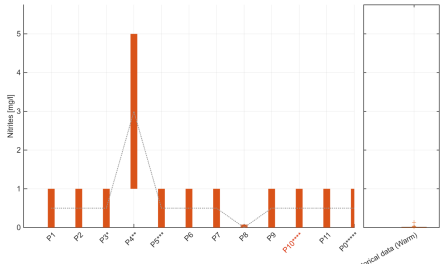

(b) Nitrites – Spring 2026

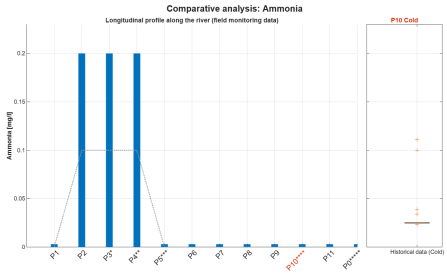

(c) Ammonia – Autumn 2025

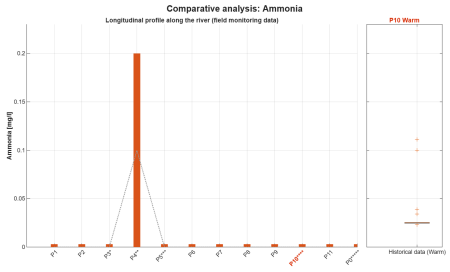

(d) Ammonia – Spring 2026

Figure D.1: Seasonal longitudinal trends of primary nutrient indicators (Nitrites and Ammonium) along the river sector: comparison between Autumn 2025 (blue) and Spring 2026 (orange) field campaigns and the respective seasonal boxplots at the JUH403 monitoring station (located near P10). Sampling points denote: P3 (start of the village), P4 (sewage outlet), P5 (end of the village), P10 (JUH403 station), and P0 (Turia river confluence).

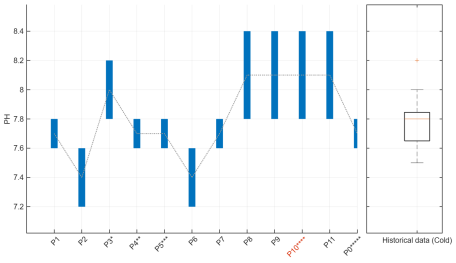

(a) pH – Autumn 2025

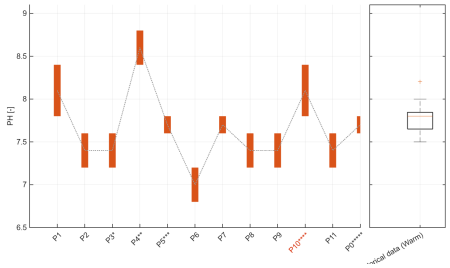

(b) pH – Spring 2026

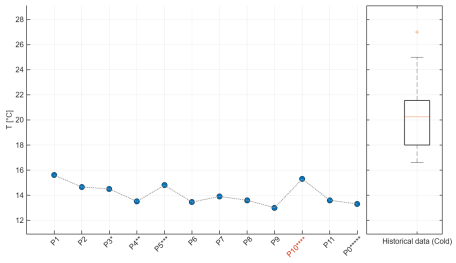

(c) Water Temperature – Autumn 2025

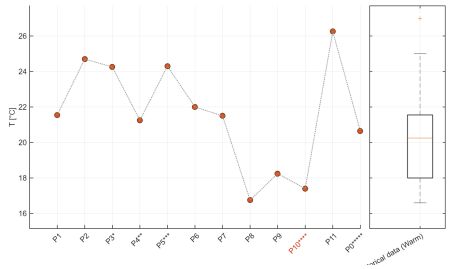

(d) Water Temperature – Spring 2026

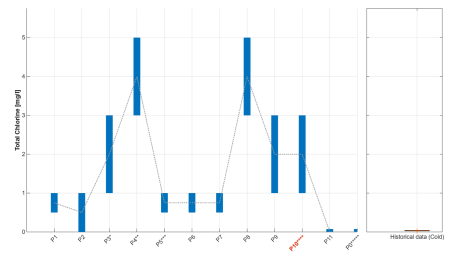

(e) Total Chlorine – Autumn 2025

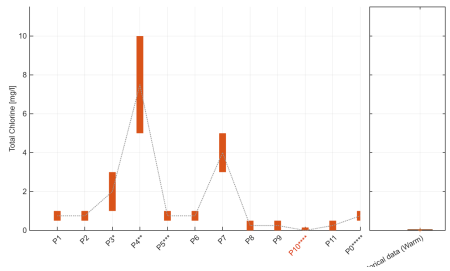

(f) Total Chlorine – Spring 2026

Figure D.2: Seasonal longitudinal trends of secondary hydrochemical indicators (pH, Water Temperature, and Total Chlorine) along the river sector: comparison between Autumn 2025 (blue) and Spring 2026 (orange) field campaigns and the respective seasonal boxplots at the JUH403 monitoring station (located near P10). Sampling points denote: P3 (start of the village), P4 (sewage outlet), P5 (end of the village), P10 (JUH403 station), and P0 (Turia river confluence).

Appendix E

Riparian Vegetation

This appendix present the spatial distribution maps for riparian vegetation resulting from the field survey of November-December 2025 in the municipality of Sot de Chera.

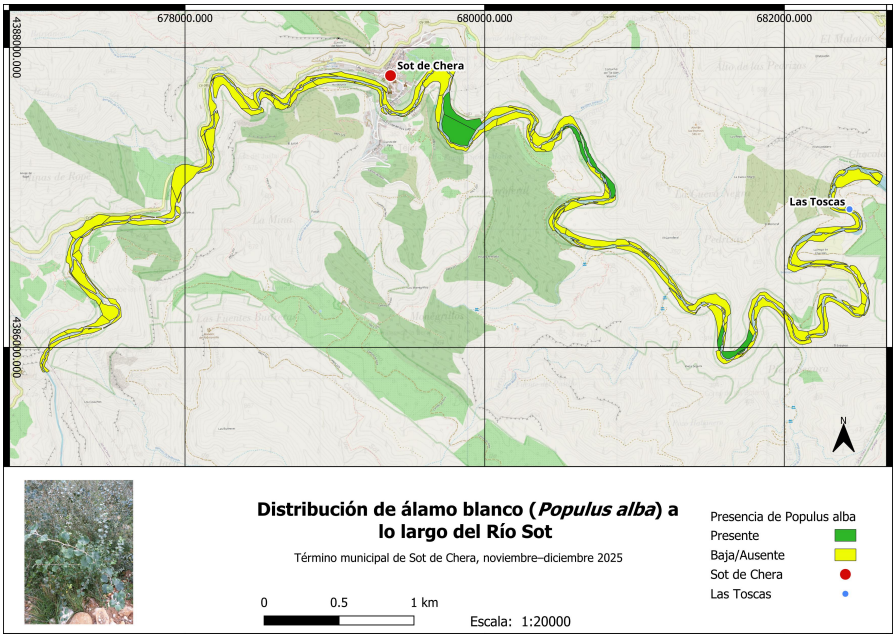

(a) *Populus alba* spatial distribution.

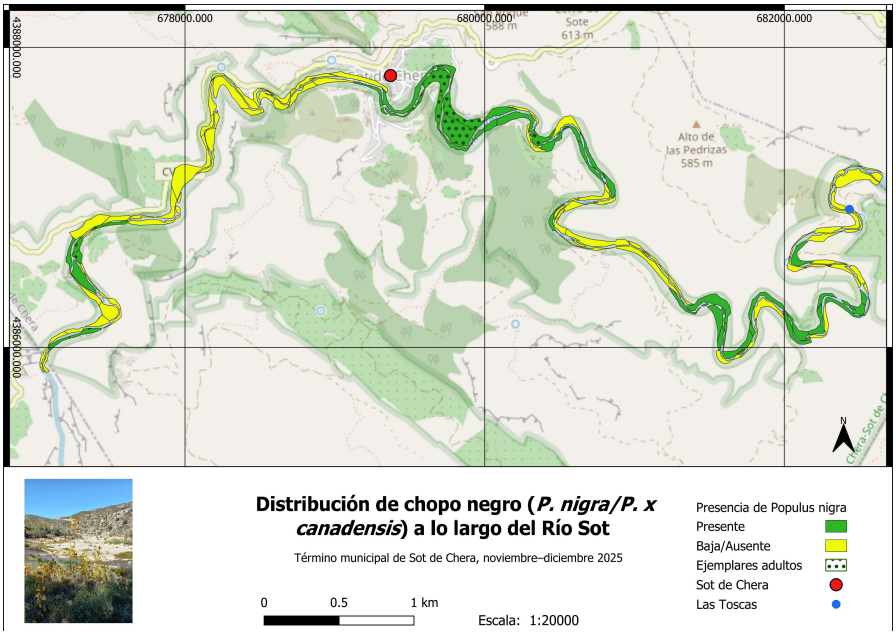

(b) *P. nigra* / *P.* × *canadensis* group spatial distribution.

Figure E.1: Spatial distribution of riparian poplar species (*Populus* spp.) along the Rio Sot in the municipal area of Sot de Chera, November-December 2025. The maps retains the original Spanish layout utilized during the local River Assemblies. Translation of key map terms: *Presente* = Present; *Baja/Ausente* = Low/Absent; *Ejemplares adultos* = Adult individuals.

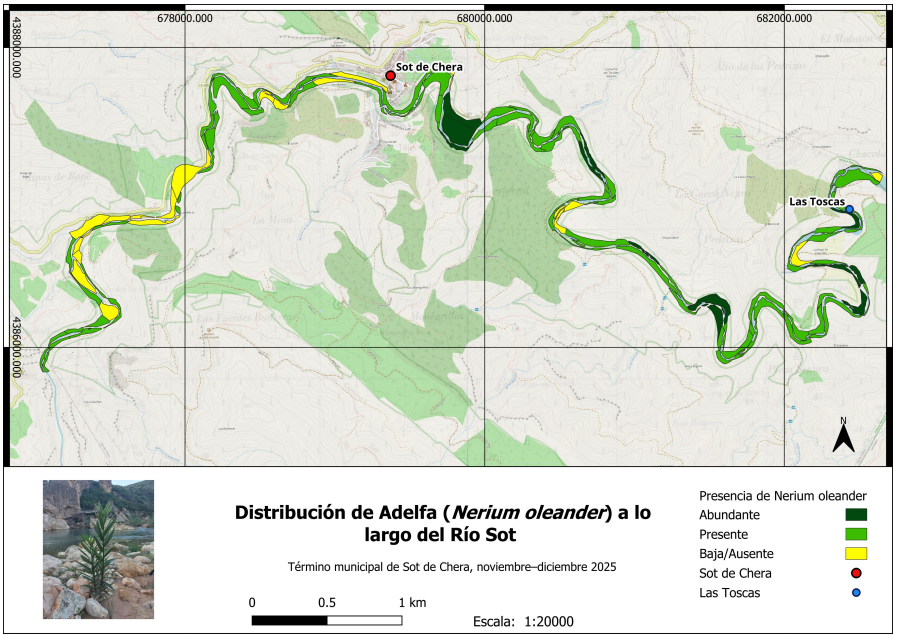

(a) *Nerium oleander* spatial distribution.

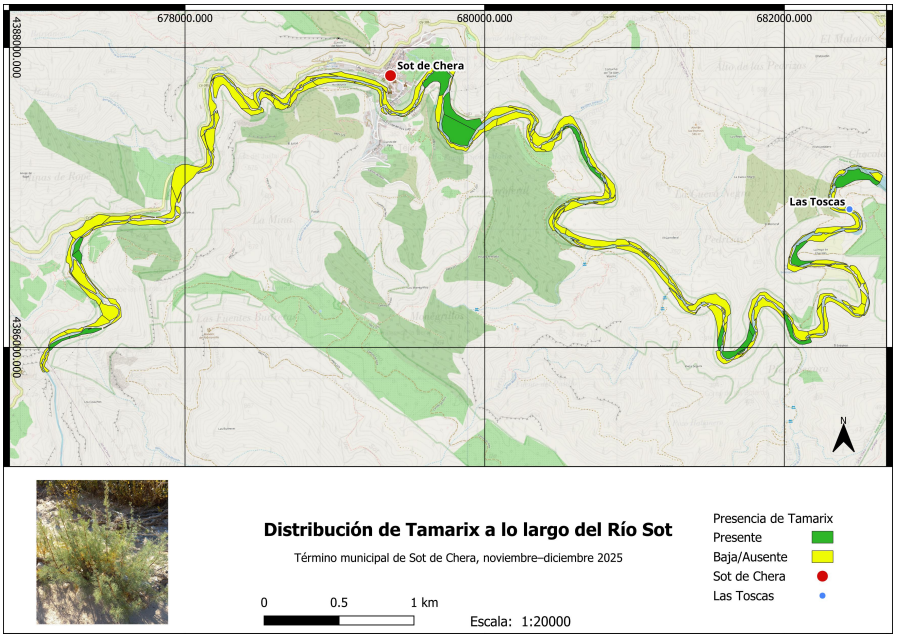

(b) *Tamarix* spp. spatial distribution.

Figure E.2: Spatial distribution of shrub riparian species along the Rio Sot in the municipal area of Sot de Chera, November-December 2025. The maps retains the original Spanish layout utilized during the local River Assemblies. Translation of key map terms: *Abundante* = Abundant; *Presente* = Present; *Baja/Ausente* = Low/Absent.

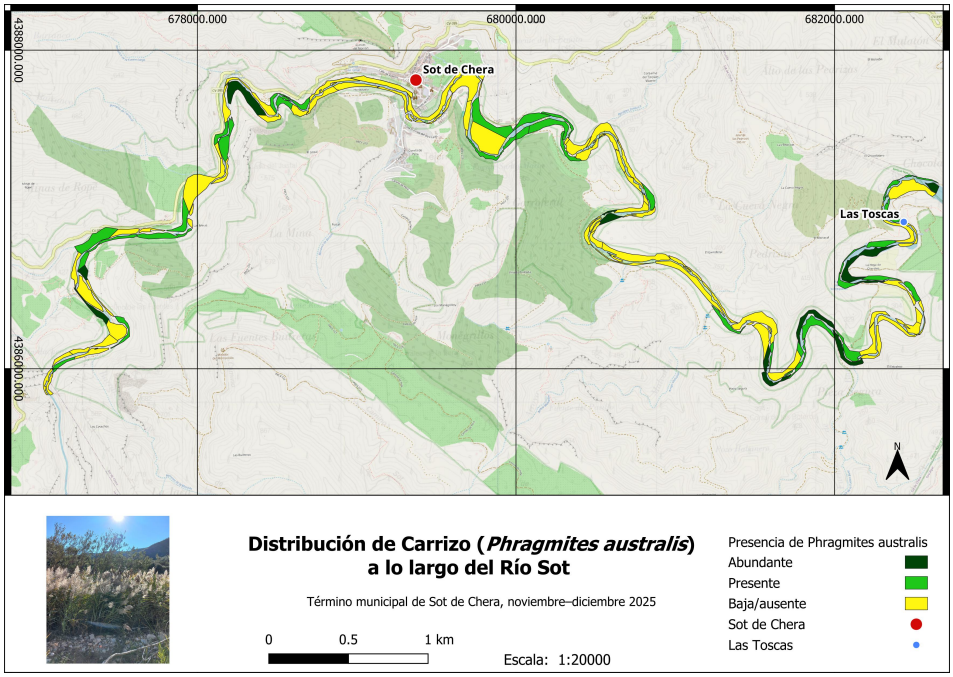

Figure E.3: Spatial distribution of *Phragmites australis* along the Rio Sot in the municipal area of Sot de Chera, November-December 2025. The map retains the original Spanish layout utilized during the local River Assemblies. Translation of key map terms: *Abundante* = Abundant; *Presente* = Present; *Baja/Ausente* = Low/Absent.

Bibliography

[1] C. Vörösmarty et al. «Global Threats to Human Water Security and River Biodiversity». In: *Nature* 468 (Nov. 2010), p. 334. DOI: 10.1038/nature09549.

[2] European Environment Agency (EEA). *Europe's State of Water 2024: The Need for Improved Water Resilience*. EEA Report 07/2024. Luxembourg: European Environment Agency, 2024. DOI: 10.2800/02236. URL: https://www.eea.europa.eu/en/analysis/publications/europes-state-of-water-2024 (visited on 06/23/2026).

[3] Jan U Lemm et al. «Multiple stressors determine river ecological status at the European scale: Towards an integrated understanding of river status deterioration». In: *Global change biology* 27.9 (2021), pp. 1962–1975.

[4] Maarten Wynants, Lukas Hallberg, Laura-Ainhoa Prischl, John Livsey, and Magdalena Bieroza. «Trends and purposes of European river monitoring and restoration». In: *Environmental Science & Policy* 170 (2025), p. 104130. ISSN: 1462-9011. DOI: 10.1016/j.envsci.2025.104130. URL: https://www.sciencedirect.com/science/article/pii/S1462901125001467 (visited on 06/23/2026).

[5] F. Magdaleno, F. Blanco-Garrido, N. Bonada, and T. Herrera-Grao. «How are riparian plants distributed along the riverbank topographic gradient in Mediterranean rivers? Application to minimally altered river stretches in Southern Spain». In: *Limnetica* 33.1 (2014), pp. 121–138. DOI: 10.23818/limn.33.10. URL: https://doi.org/10.23818/limn.33.10.

[6] IPCC. *Climate Change 2022: Impacts, Adaptation and Vulnerability*. Contribution of Working Group II to the Sixth Assessment Report. Intergovernmental Panel on Climate Change, 2022. URL: https://www.ipcc.ch/report/ar6/wg2/.

[7] European Commission. *EU Biodiversity Strategy for 2030: Bringing nature back into our lives*. European Commission, 2020. URL: https://environment.ec.europa.eu/strategy/biodiversity-strategy-2030_en.

[8] European Parliament and Council of the European Union. *Regulation (EU) 2024/1991 of the European Parliament and of the Council of 24 June 2024 on nature restoration and amending Regulation (EU) 2022/869*. 2024.

[9] M. A. Palmer et al. «Standards for ecologically successful river restoration». In: *Journal of Applied Ecology* 42.2 (2005), pp. 208–217. DOI: 10.1111/j.1365-2664.2005.01004x.

[10] E. Wohl, S. N. Lane, and A. C. Wilcox. «The management of sediment dynamics in river corridors». In: *Wiley Interdisciplinary Reviews: Water* 2.4 (2015), pp. 359–374. DOI: 10.1002/wat2.1021.

[11] W. Buytaert et al. «Citizen science in hydrology and water resources: opportunities for knowledge generation, ecosystem service management, and sustainable development». In: *Frontiers in Earth Science* 2 (2014), p. 26. DOI: 10.3384/feart.2014.00026.

[12] B. Büscher and R. Fletcher. «Towards convivial conservation». In: *Conservation and Society* 17.3 (2019), pp. 283–296. DOI: 10.4103/cs.cs_19_47.

[13] P. M. Edwards, G. Shaloum, and D. Bedell. «A unique role for citizen science in ecological restoration: a case study in streams». In: *Restoration Ecology* 26.1 (2018), pp. 29–35. DOI: 10.1111/rec.12531.

[14] RIVIVE Project. *Riverscape Conviviality: A framework for socio-ecological reconnection in Mediterranean river restoration*. Concept Note Deliverable 1.4. European Biodiversity Partnership (Biodiversa+), RIVIVE Consortium, 2024. URL: https://rivive.es/wp-content/uploads/D.1.4.-Riverscape-Conviviality-concept-note.pdf (visited on 06/22/2026).

[15] Biodiversa+. *Biodiversa+ European Biodiversity Partnership*. Consultato il 23 giugno 2026. 2026. URL: https://www.biodiversa.eu/.

[16] Ayuntamiento de Sot de Chera. *Información Municipal y Geografía Local*. 2025. URL: http://www.sotdechera.es (visited on 04/22/2025).

[17] Gran Enciclopedia. *Gran Enciclopedia de la Región Valenciana*. Vol. 11. Valencia: Gran Enciclopedia de la Región Valenciana, 1973, p. 86. ISBN: 84-300-5539-8.

[18] Confederación Hidrográfica del Júcar (CHJ). *Plan Hidrológico de la Demarcación Hidrográfica del Júcar (2022-2027)*. Technical Report Real Decreto 35/2023 framework. Valencia, Spain: Ministerio para la Transición Ecológica y el Reto Demográfico, Gobierno de España, 2022. URL: https://www.chj.es/es-es/medioambiente/planificacionhidrologica/Paginas/PHC-2022-2027-Plan-Hidrologico-cuenca.aspx (visited on 06/17/2026).

[19] Generalitat Valenciana. *Guía d'itineraris de fonts, paratges i senders: Parque Natural de Chera-Sot de Chera*. Conselleria de Medi Ambient, Aigua, Infrastructures i Territori. 2024. URL: https://parquesnaturales.gva.es.

[20] Generalitat Valenciana. *Geología del Parque Natural Chera-Sot de Chera*. 2025. URL: https://parquesnaturales.gva.es/va/web/pn-chera-sot-de-chera/geologia (visited on 11/15/2025).

[21] Ministerio para la Transición Ecológica y el Reto Demográfico (MITECO). *Descarga de Datos Geográficos: Cuencas y Subcuencas Hidrográficas de España*. Centro de Descargas del Centro Nacional de Información Geográfica. 2024. URL: https://www.miteco.gob.es.

[22] Sistema Automático de Información Hidrológico (SAIH). *Ficha técnica del Embalse de Buseo*. 2026. URL: https://saih.chj.es/embalses/295 (visited on 02/10/2026).

[23] J. García. «Las restricciones operativas y el plan de seguridad de la presa de Buseo tras el impacto de la DANA». In: *Levante-EMV* (Dec. 11, 2024). URL: https://www.levante-emv.com.

[24] Asociación Cultural de Chera. *El Embalse de Buseo: origen e historia hidráulica*. 2023. URL: https://www.encherate.com/info/buseo.php (visited on 05/10/2025).

[25] Ministerio para la Transición Ecológica y el Reto Demográfico (MITECO). *Anuario de Aforos de las Cuencas Hidrográficas de España: Datos históricos de caudales*. Tech. rep. Secretaría de Estado de Medio Ambiente, 2022. URL: https://www.miteco.gob.es.

[26] Consell de la Generalitat Valenciana. *Decret 86/2018, de 22 de juny, del Consell, pel qual es designen les zones vulnerables a la contaminació per nitrats procedents de fontes agràries en la Comunitat Valenciana*. Diari Oficial de la Generalitat Valenciana (DOGV) No. 8328. 2018. URL: https://dogv.gva.es.

[27] European Economic Community. «Council Directive 92/43/EEC of 21 May 1992 on the conservation of natural habitats and of wild fauna and flora». In: *Official Journal of the European Communities* L 206 (1992), pp. 7–50.

[28] Angela M. Gurnell, Walter Bertoldi, and Dov Corenblit. «Changing river channels: The roles of plant species, their growth forms and physical structures in modulating geomorphological processes». In: *Earth-Science Reviews* 111.1-2 (2012), pp. 1–16. DOI: 10.1016/j.earscirev.2011.11.005.

[29] A. Maceda-Veiga, P. Baskaran, C. Webster, and J. Cortina. «Impacts of the invasive giant reed (*Arundo donax*) on riparian plant communities and soil properties». In: *Scientific Reports* 6.1 (2016). PMID: 27666244; PMCID: PMC5611372, p. 34054. DOI: 10.1038/srep34054. URL: https://www.nature.com/articles/srep34054.

[30] H. L. Moggridge and A. M. Gurnell. «Controls on the sexual and asexual regeneration of *Salicaceae* along a highly dynamic, braided river system». In: *Aquatic Sciences* 71.3 (2009), pp. 305–317. DOI: 10.1007/s00027-009-9193-3. URL: https://doi.org/10.1007/s00027-009-9193-3.

[31] K. Seiwa, M. Tozawa, N. Ueno, M. Kimura, M. Yamasaki, and K. Maruyama. «Roles of cottony hairs in directed seed dispersal in riparian willows». In: *Plant Ecology* 198.1 (2008), pp. 27–35. URL: http://www.jstor.org/stable/40305530.

[32] I. Soriano. «*Phragmites* Adans.» In: *Flora Iberica: Plantas vasculares de la Península Ibérica e Islas Baleares*. Vol. 19. 2. Madrid, Spain: Real Jardín Botánico, CSIC, 2021, pp. 1289–1295.

[33] S. Lowe, M. Browne, S. Boudjelas, and M. De Poorter. *100 of the World's Worst Invasive Alien Species: A selection from the Global Invasive Species Database*. Technical Report. Auckland, New Zealand: Invasive Species Specialist Group (ISSG), IUCN, 2000.

[34] H. Kato-Noguchi and M. Kato. «The Invasive Mechanism and Impact of *Arundo donax*, One of the World's 100 Worst Invasive Alien Species». In: *Plants* 14.14 (2025), p. 2175. DOI: 10.3390/plants14142175. URL: https://doi.org/10.3390/plants14142175.

[35] D. A. Watts and G. W. Moore. «Water use by Arundo donax and native riparian vegetation under varying hydrological regimes». In: *Ecohydrology* 4.3 (2011), pp. 412–422.

[36] Generalitat Valenciana. *Plan de Prevención de Incendios Forestales del Parque Natural Chera-Sot de Chera (PPIF) - Revisión 2021*. Technical Report. Valencia, Spain: Conselleria de Agricultura, Desarrollo Rural, Emergencia Climática y Transición Ecológica, 2021.

[37] Instituto Nacional de Estadística (INE). *Cifras oficiales de población resultantes de la revisión del Padrón municipal a 1 de enero*. 2025. URL: https://www.ine.es (visited on 06/15/2026).

[38] Generalitat Valenciana. *Fitxes municipals: Sot de Chera. Portal Estadístico de la Generalitat Valenciana*. 2025. URL: https://pegv.gva.es (visited on 06/15/2026).

[39] Confederación Hidrográfica del Júcar (CHJ). *Plan Hidrológico de la Demarcación Hidrográfica del Júcar (2022-2027): Anejo 08 - Objetivos Ambientales y Deterioros Temporales*. Technical Report. Gobierno de España, 2023.

[40] Valencia Bonita. *El Charco del Gruñidor: la piscina natural de Sot de Chera*. Recreational archive database. 2018. URL: https://www.valenciabonita.es/2018/05/01/charco-el-grunidor-la-piscina-natural-de-sot-de-chera/ (visited on 06/03/2026).

[41] Agencia Estatal de Meteorología (AEMET). *ESTUDIO SOBRE LA SITUACIÓN DE LLUVIAS INTENSAS, LOCALMENTE TORRENCIALES Y PERSISTENTES, EN LA PENÍNSULA IBÉRICA Y BALEARES ENTRE LOS DÍAS 28 DE OCTUBRE Y 4 DE NOVIEMBRE DE 2024*. Technical Report. Ministerio para la Transición Ecológica y el Reto Demográfico, Gobierno de España, 2024. URL: https://www.aemet.es.

[42] Confederación Hidrográfica del Júcar (CHJ). *Informe del episodio de lluvias y avenidas del 28 de octubre al 4 de noviembre de 2024. Versión 2*. Tech. rep. Ministerio para la Transición Ecológica y el Reto Demográfico, 2024. URL: https://saih.chj.es/docs/20241029-1104Informe-Episodio-C-version2.pdf.

[43] Ministerio para la Transición Ecológica y el Reto Demográfico (MITECO). *Plan para la Recuperación y Mejora de la Resiliencia frente a las Inundaciones en el Territorio Afectado por la DANA en la Comunitat Valenciana*. Strategic Action Plan. Gobierno de España, 2024. URL: https://www.miteco.gob.es.

[44] Cámara de Comercio de Valencia. *Informe preliminar de daños en la actividad industrial y comercial afectada por la DANA en la provincia de Valencia*. Impact Assessment Report. Cámara Oficial de Comercio, Industria, Servicios y Navegación de Valencia, 2024. URL: https://www.camaravalencia.com.

[45] Alejandro Cueva, Rafael Serrano, Ghaleb Fansa, José Mora, and Adrián Ferrero. *Aportaciones pluviométricas y avenidas durante el episodio de lluvias intensas del 29/30-Oct-2024 en las cuencas del Magro, Turia y Poyo*. Tech. rep. Dec. 2025, pp. 27–59. DOI: 10.7203/CGUV.114-15.32041.

[46] J. García. «Sot de Chera: cincuenta días después de la DANA en Valencia». In: *Levante-EMV* (Dec. 18, 2024). URL: https://www.levante-emv.com.

[47] M. Seco. «Dios pasó de puntillas por Sot de Chera». In: *El País* (Nov. 7, 2024). URL: https://elpais.com.

[48] T. Cervera. «El impacto de la riada en el casco urbano de Sot de Chera y la pérdida de servicios esenciales». In: *Levante-EMV* (Nov. 1, 2024). URL: https://www.levante-emv.com.

[49] Confederación Hidrográfica del Júcar. *SIA Júcar: Water Information System. Surface water bodies quality control network - Quality data by monitoring station (Station JUH403)*. 2025. URL: https://aps.chj.es/siajucar/ (visited on 06/03/2026).

[50] European Parliament and Council of the European Union. «Directive 2000/60/EC of the European Parliament and of the Council of 23 October 2000 establishing a framework for Community action in the field of water policy». In: *Official Journal of the European Communities* L 327 (2000). URL: https://eur-lex.europa.eu/legal-content/EN/TXT/?uri=CELEX:32000L0060 (visited on 06/03/2026).

[51] Boletín Oficial del Estado. *Real Decreto 817/2015, de 11 de septiembre, por el que se establecen los criterios de seguimiento y evaluación del estado de las aguas superficiales y las normas de calidad ambiental*. BOE-A-2015-9806. 2015. URL: https://www.boe.es/buscar/doc.php?id=BOE-A-2015-9806 (visited on 06/03/2026).

[52] Boletín Oficial del Estado. *Real Decreto 665/2023, de 18 de julio, por el que se modifica el Reglamento del Dominio Público Hidráulico*. BOE-A-2023-16674. 2023. URL: https://www.boe.es/buscar/doc.php?id=BOE-A-2023-16674 (visited on 06/03/2026).

[53] European Parliament and Council of the European Union. «Directive 2008/105/EC of the European Parliament and of the Council of 16 December 2008 on environmental quality standards in the field of water policy». In: *Official Journal of the European Union* L 348 (2008). URL: https://eur-lex.europa.eu/legal-content/EN/TXT/?uri=CELEX:32008L0105 (visited on 06/03/2026).

[54] European Parliament and Council of the European Union. «Directive 2013/39/EU of the European Parliament and of the Council of 12 August 2013 amending Directives 2000/60/EC and 2008/105/EC as regards priority substances in the field of water policy». In: *Official Journal of the European Union* L 226 (2013). URL: https://eur-lex.europa.eu/legal-content/EN/TXT/?uri=CELEX:32013L0039 (visited on 06/03/2026).

[55] Dielmo 3D. *Datos LiDAR clasificados, ortofoto y Modelos Digitales de Terreno (MDT) - Aguas arriba y aguas abajo*. Dataset técnico interno (LiDAR + ortofoto + MDT). Vuelo con dron. Datos clasificados LiDAR, ortofoto derivada y MDT a 0.5 m de resolución. Bloques de 100x100 m. Material técnico no publicado. 2024.

[56] Gobierno de España. *Real Decreto 849/1986, de 11 de abril, por el que se aprueba el Reglamento del Dominio Público Hidráulico*. Boletín Oficial del Estado (BOE), núm. 103, 30 de abril de 1986. Texto consolidado. Consultato

il 3 luglio 2026. 1986. URL: https://www.boe.es/eli/es/rd/1986/04/11/849/con.

[57] Boletín Oficial del Estado. *Real Decreto Legislativo 1/2001, de 20 de julio, por el que se aprueba el texto refundido de la Ley de Aguas*. BOE-A-2001-14276, updated consolidated version. 2001. URL: https://www.boe.es/buscar/doc.php?id=BOE-A-2001-14276.

[58] Confederación Hidrográfica del Júcar and Ministerio para la Transición Ecológica y el Reto Demográfico. *Sistema de Información Ambiental del Júcar (SIA Júcar): Cartografía del Dominio Público Hidráulico (DPH) - Tercer Ciclo SNCZI (Cod. DPH_ARPS_0022-12_SOT_DE_CHERA)*. 2026. URL: https://www.chj.es/es-es/ciudadano/SIAJucar/Paginas/SIAJucar.aspx (visited on 06/03/2026).

[59] *Sistema Nacional de Cartografía de Zonas Inundables (SNCZI): Deslinde del Dominio Público Hidráulico (DPH) - Primer Ciclo (Cod. ES080-Z0099-T40.25-DPH)*. 2026. URL: https://www.miteco.gob.es/es/cartografia-y-sig/ide/descargas/agua/snczi.html (visited on 06/03/2026).

[60] Dirección General del Catastro. *Servicios INSPIRE de la Dirección General del Catastro: Descarga de datos catastrales*. n.d. URL: https://www.sedecatastro.gob.es/Accesos/SECAccDirecto.aspx?Suplemento=inspire (visited on 06/02/2026).

[61] L. Tshapa, K. Naidoo, and G. Naidoo. «Morphological and physiological responses of *Arundo donax* and *Phragmites australis* to waterlogging stress». In: *Flora* 279 (2021), p. 151816. DOI: 10.1016/j.flora.2021.151816. URL: https://doi.org/10.1016/j.flora.2021.151816.

[62] Levante-EMV. «El desastre ambiental de l'Albufera: la caña invasora avanza sin freno tras el daño de la DANA». In: *Levante-EMV* (Apr. 2025). URL: https://www.levante-emv.com/comunitat-valenciana/2025/04/22/desastre-ambiental-albufera-cana-invasora-avanza-freno-vez-dano-116591729.html (visited on 06/18/2026).

[63] Ministerio para la Transición Ecológica y el Reto Demográfico. *Bases para el manejo y control de Arundo donax (Caña común)*. Tech. rep. Madrid, Spain: Centro Nacional de Educación Ambiental (CENEAM), Organismo Autónomo Parques Nacionales, 2021. URL: https://www.miteco.gob.es/content/dam/miteco/es/ceneam/grupos-de-trabajo-y-seminarios/red-parques-nacionales/Bases%20para%20el%20manejo%20y%20control%20de%20Arundo%20donax_tcm30-169319.pdf (visited on 06/18/2026).